RSP-0294

PU/NE-13-11

Canadian Nuclear Safety Commission

Assessment of Leak Rates through Steam Generator Tubes

Final Report

S. T. Revankar, Brian Wolf and Anand Vadlamani

PURDUE UNIVERSITY

SCHOOL OF NUCLEAR ENGINEERING

PU/NE-13-11

Canadian Nuclear Safety Commission

Assessment of Leak Rates through Steam Generator Tubes

Final Report

October 8, 2010 to July 15, 2013

PRINCIPAL INVESTIGATOR:
SHRIPAD T. REVANKAR
PURDUE UNIVERSITY
School of Nuclear Engineering
West Lafayette, IN 47906-1290
765-496-1782
shripad@ecn.purdue.edu

Contributing Authors:

S. T. Revankar, Brian Wolf and Anand Vadlamani

PURDUE UNIVERSITY
School of Nuclear Engineering
West Lafayette, IN 47906-1290

July 2013

ACKNOWLEDGEMENT

The project was sponsored by the Canadian Nuclear Safety Commission (CNSC). The authors are grateful for the kind support by CNSC. We are thankful for the discussions and advice by the CNSC staff and particularly to Dr. Jovica R. Riznic of CNSC for helpful technical comments in achieving project milestones.

DISCLAIMER

The Canadian Nuclear Safety Commission is not responsible for the accuracy of the statements made or opinions expressed in this publication and do not assume liability with respect to any damage or loss incurred as a results of the use made of the information contained in this publications.

TABLE OF CONTENTS

LIST OF FIGURES

LIST OF TABLES

ACRONYMS

ANL	Argonne National Laboratory
B&W	Babcock & Wilcox
BCL	Battelle Columbus Laboratories
BWR	Boiling Water Reactor
AECL	Atomic Energy Of Canada Limited
CANDU	Canadian Natural Uranium Deuterium
CNSC	Canadian Nuclear Safety Commission
COA	Crack Opening Area
COD	Crack Opening Displacement
CSA	Canadian Standards Association
DOE	Department Of Energy
DW	Dry Well
EPRI	Electrical Power Research Institute
GE	General Electric
IAEA	International Atomic Energy Agency
ICS	Isolation Condensation System
IGSCC	Intergranular Stress Corrosion Cracks
LBB	Leak Before Break
LCM	Life Cycle Management
LOCA	Loss Of Coolant Accident
LWR	Light Water Reactor
NDE	Non-Destructive Examination
NEI	Nuclear Energy Institute
NRC	Nuclear Regulatory Commission
ODSCC	Outside Diameter Stress Corrosion Cracking
PWR	Pressurized Water Reactor
PWSCC	Pressurized Water Stress Corrosion Cracks
RPV	Reactor Pressure Vessel
SCC	Stress Corrosion Cracking
SG	Steam Generator
T/C	Thermocouple
TS	Test Section
TW	Through Wall

NOMENCLATURE

A	area [m^2]
C_p	specific heat [j/kg·C]
C_d	discharge coefficient
d,D	diameter [m]
f	friction factor
g	gravitational acceleration [m/s^2]
G	mass flux (kg/m^2s)
h	enthalpy [J/kg]
h_{fg}	latent heat of vaporization [J/kg]
k	conductivity [$W/m^2·C$]
L	crack length [m]
m	mass flow rate [kg/s]
m_{cond}	condensed mass
P, p	pressure [Pa]
P	Perimeter [m]
q''	heat flux [W/m^2]
Q	heat Transfer Rate [W]
R	radius [m]
Re	Reynolds number
t	time [s]
T	temperature [K or C]
v	velocity [m/s]
x	thermodynamic quality
z	axial coordinate [m]

a	Speed of Sound
N	Experimental parameter
s	Entropy i
S	Slip ratio
u	velocity
U	velocity

Subscripts

0	Stagnation
a	Speed of Sound
b	Back Pressure
c	Critical
e	Entrance
E	Equilibrium
eq	Equilibrium
ex	Exit
exp	Experimental
f	Fluid
f l	Flashing
g	Vapor phase
h	hydraulic
HE	Homogeneous Equilibrium
i	Index

s	Isentropic
sat	Saturation
t	Throat
up	Upstream

Greek Symbols

α	Void fraction
γ	Isentropic exponent
η	Pressure ratio
ρ	Density
ν	Specific Volume
Σ	Depressurization rate
τ	Relaxation time
μ	Dynamic viscosity [kg/m·s]
v_f	liquid specific volume [m^3/kg]
v_g	vapor or gas specific volume [m^3/kg]
v_l	liquid specific volume [m^3/kg]
ρ	Density [kg/m^3]
σ	Surface tension [N/m]
τ	Shear stress [Pa]

Subscripts

ave	average
cond	condensation
f	liquid
g	gas or vapor
i	i-th component, i-th node, inside
l	liquid
o	outside, stagnation
out	outlet
sat	saturation
v	vapor

EXECUTIVE SUMMARY

The main goal of the project was to develop a comprehensive database and models on the steam generator tube degradation process and resulting leak rates that permit the CNSC to independently evaluate the integrity of steam generator tubes as plants age and degradation proceeds, new forms of degradation appear, and thus new defect-specific management schemes should be implemented. The scope of the present research includes consolidation of data on CANDU and PWR steam generator tube degradation mechanisms (Primary Water Stress Corrosion Cracking (PWSCC), pitting and fretting) and the development of flaw and their growth based on fracture mechanics models. An experiment and modeling program was initiated. Experimental data on leakage rates for CANDU SG relevant tube cracks was collected and a Homogeneous Equilibrium Model (HEM) and Homogeneous Non-Equilibrium Model (HNEM) were derived from the conservation equations, providing a physical basis for prediction. Several tasks were carried out under this project

- An experimental program was created which includes: the design and building of a experimental test facility; development of a test matrix; the design and manufacture of simulated crack test specimens; conduction of experiments for various operating conditions.
- A consolidated database on choked flow for small length to diameter cracks was compiled by running tests on the Facility for Leak Rate Testing (FLRT) at the Multiphase Flows and Fuel Cell Research Labs (MFRL) at Purdue University by simulating the pressure difference of a steam generator tube across crack samples conducting a constant area leak rate tests.
- Development of a new choking flow model and validation against experimental data.
- Application of the RELAP5 code model for predicting choking flow and assessing it's predictive capabilities.
- Recommendation of an optimal choked flow modeling approach for application for SG tube integrity assessments.

1. INTRODUCTION

1.1 Significance of the Problem

Steam generators (SG) are considered primary heavy components in CANDU reactors and in PWR. During the design and construction phases of the reactors, these components were not meant to be replaced over the lifetime of the power plant. However due to failure of some steam generator tubes, maintenance and replacement of the steam generators is required. Each steam generator contains between 3200 and 15,500 tubes depending on the manufacturer, and each tube acts as a primary pressure boundary. The steam generator tubes together account for a majority of the primary pressure boundary surface of both CANDU and PWRs, and ultimately determines if radiation is leaked to the environment under normal operating conditions. Steam generator tubes as well as many other components of a CANDU and PWR use Monel 400, Inconel 600 (Alloy 600), Alloy 690, and Alloy 800 which have experienced in-service corrosion and mechanical degradation of various forms (ANL, 2010, Staehle and Gorman 2003).

There is the potential that if a tube bursts while a plant is operating, radioactivity from the primary coolant system - the system that pumps water through the reactor core - could escape directly to the atmosphere in the form of steam. However, failure of a single steam generator tube, or even a few tubes, would not be a serious safety-related event in a CANDU reactor. The leakage from a ruptured tube is within makeup capacity of the primary heat transport system, so that as long as the operator takes the correct actions, the off-site consequences will be negligible. The Alloy 600 mill annealed steam generator tubes in PWR may serve as a good example of allowable continued operation with limited leakage. A sufficient safety margin against tube rupture used to be the basis for a variety of maintenance strategies developed to maintain a suitable level of plant safety and reliability. Several through-wall flaws may remain in operation and potentially contribute to the total primary-to-secondary leak rate. However, assurance that no tubes deteriorate to the point where their integrity could be seriously breached as result of a potential event, and that any leakage caused by such an accident will be small enough to be inconsequential, can only be obtained through detailed monitoring and management of steam generator conditions in practice (IAEA 2007, IAEA 2011).

1.2 Steam Generator Degradation

While many of the current nuclear power reactors in the United States have shown great integrity and allowed to be relicensed for a period beyond their originally predicted lifetime, the safety of these plants is an integral part of the future of safe, environmentally friendly, nuclear power. Steam generator (SG) tubes constitute a large fraction of the reactor primary coolant loop pressure boundary surface area in both CANDU and PWR. The SG tubes play an important safety role because they act as a main barrier for radiation or fission products between the primary and secondary side of a power plant. This means that any leakage of coolant through the wall of a SG tube will allow radiation to escape into the non-radioactive side of the plant, which then has the potential to leak to the atmosphere. Therefore, the integrity of the SG tubes is an essential part of the overall safety of a plant and the public.

Damage to a steam generator tube impairs its ability to perform its required safety function in terms of both structural integrity and leakage integrity. There are many different degradation mechanisms that can occur related to SG tubes. They are susceptible to corrosion and mechanical damage, while at the same time must maintain more than 6.9

MPa (1000 psi) pressure differential between the inside and outside tube wall during normal operation. In the event of a main steam-line break (MSLB) in a pressurized water reactor where the secondary side drops to atmospheric pressure, the tube wall differential pressure can be as high as 18 MPa (2560 psi). Traditionally, steam generators were designed with a sufficient safety margin against rupture. The design requirements of ASME code and the Nuclear Regulatory Commission (NRC) for steam generator tubes is $1.4 \cdot \Delta P_{MSLB} \simeq 25$ MP a (3660 psi) (Majumdar, 1999). These safety margins are based on the rupture or burst pressure of unflawed tubes. A typical unflawed Alloy 600 tube has an industry expected burst pressure of $\simeq 86$ MP a (12500 psi) (Vaia et al, 2005). Some of the main tube degradation mechanisms that have been identified are due to corrosion, mechanical wear, and fatigue. Table 1.1 explains only a small portion of the potential degradation mechanisms. The definitions are adapted from EPRI (Fuller et al., 2006).

Table 1.1 Steam Generator Degradation (Adapted from Wade 1995)

Type of Degradation	Description
Denting	The physical deformation of the Inconel Alloy 600 tubes as they pass through the support plate. Caused by a buildup of corrosive material in the space between the tube and the plate.
Fatigue cracking	Caused by tube vibration.
Fretting	The wearing of tubes in their supports due to flow induced vibration.
Intergranular attack/stress-corrosion cracking (outside diameter)	Caused when tube material is attacked by chemical impurities from the secondary-loop water. It occurs primarily within tube sheet crevices and other areas where impurities concentrate.
Pitting	The result of local breakdown in the protective film on the tube. Active corrosion occurs at the site of breakdown.
Stress-corrosion cracking (inside diameter)	Cracking of steam generator tubes occurring at the tangent point and apex of U-bend tubes, at the tube sheet roll transition, and in tube dents. It occurs when Inconel Alloy 600 tubing is exposed to primary-loop water.
Tube wear	A thinning of tubes caused by contact with support structures as the tubes vibrate or as feed water entering the vessel impinges on the tube bundle at that location.
Wastage	A general corrosion caused by chemical attack from acid phosphate residues in areas of low water flow.

Current and past studies point to intergranular attack/stress-corrosion cracking as the most common mode of failure. This form of failure accounted for 60 to 80 percent of all tube defects that required plugging up to the year 2007. While, fretting and pitting combined to account for another 15 to 20 percent of all tube defects. The remaining failures were due to mechanical damage, wastage, denting, and fatigue cracking (Karwoski et al, 2007). Most all SGs in the U.S. were originally built using mill annealed Alloy 600. Past research has shown that thermal treatment of Alloy 600 makes it less vulnerable to degradation, and even more promising is thermally treated Alloy 690 which has even further improved mechanical properties and corrosion resistance. As of 2009, 51 of the 69 PWRs in operation in the U.S. have replaced their tubing material: 42 units

switched to thermally treated Alloy 690; 8 units switched to thermally treated Alloy 600 and the remaining unit stayed with the original mill annealed Alloy 600 tubing (H. Rathbun et al, 2009). In just two years (2008-2009), the number of power plants using Alloy 690 SG tubing increased by 25%, with approximately 69% using Alloy 690, 25% using thermally treated Alloy 600, and the remaining using mill annealed Alloy 600 tubes. It must be acknowledged that while any one of these defined mechanisms may cause a SG tube defect, they do not inherently lead to leak rates across the primary radiation boundary. They must of course, grow to become through-wall flaws. Also, it is beyond the scope of this study to introduce or define the mechanistic behavior of crack growth. Actual cracks may have a very complex morphology, which can be difficult to define. This study is focused on the leak rate behavior of well-defined crack geometries, as crack opening area will highly affect the choking flow rates and must be well known. If one were able to accurately predict the crack growth and opening area, this would not necessarily lead to accurate prediction of the thermo-hydraulic path. For instance, in actual reactor environments, corrosion products are transported throughout the reactor loops by the coolant. The origin of such products cannot be well established. However they may concentrate to form deposits. These deposits are referred to by the acronym CRUD in the nuclear industry, with the origin of such terminology difficult to determine. Three different acronyms have been used in literature which are; Chalk River Unidentified Deposits, Canadian Reactor Unidentified Deposits, and Corrosion Related Unidentified Deposits. While these deposits may in fact be the source or cause of a SG tube defect, they also will likely influence the thermal-hydraulic flow path of such defect. Not only may they partially plug a through-wall flaw, they also may extend from the tube wall effectively lengthening the flow channel.

1.3 **Leak before Break Approach**

Assessment of the conditional probabilities of tube failures, leak rates, and ultimately risk of exceeding licensing dose limits is an approach to steam generator tube fitness-for-service assessment that has begun to be used increasingly in recent years throughout the nuclear power industry. The advantage of this type of analysis is that it avoids the excessive conservatism typically present in deterministic methodologies. However, it requires considerable effort and expense to develop all of the failure, leakage, probability of detection, and flaw growth distributions and models necessary to obtain meaningful results from a probabilistic model. The Canadian Nuclear Safety Commission (CNSC) recently developed the CANTIA methodology for probabilistic assessment of inspection strategies for steam generator tubes as a direct effect on the probability of tube failure and primary-to-secondary leak rate.

The probabilistic approach largely depends on the models and data for crack detection, crack growth, failure probability, and two-phase critical flow. Recently there are several advances made on crack initial growth, and detection methodology as given in the following review. There is almost no data on two-phase critical flow in crack that has well defined entrance condition (sharp entrance or smooth entrance), flow turns (45^o or 22^o turn) and roughness. Also, there is limited data on the actual simulated cracks for steam generator tubes. In order to verify the critical flow model and estimate the performance of the thermalhydraulic model in assessment of leak rates through the steam generator tubes experimental data is needed in well-defined crack geometry.

Thus, there is a need for improvement of existing probability assessment methodology for the leak rates through SG tubes. In view of this, the present work addresses these issues by providing experimental data and models on two-phase critical flow for well-

defined crack geometry and then develop an improved probability assessment methodology for the leak rates through SG tubes.

1.4 **Scope and Objectives**

The scope of the project was to provide the experimental data and the predictive correlations and models needed to permit the CNSC to independently evaluate the integrity of steam generator tubes as plants age and degradation proceeds, new forms of degradation appear, and as new defect-specific management, schemes are implemented.

The following objectives were defined for the research project.

i. To develop experimental program which includes: the design and building of a experimental test facility; development of a test matrix; the design and manufacture of simulated crack test specimens; conduction of experiments for various operating conditions;
ii. To consolidated database on choked flow for small length to diameter cracks;
iii. To development of a new choking flow model and validate against experimental data;
iv. To apply RELAP5 code model for predicting choking flow and assessing it's predictive capabilities; and
v. To recommend an optimal choked flow modeling approach for application for SG tube integrity assessments

There have been many studies both theoretical and experimental on choking flow. Very few studies however have the same geometric setup. Some focus on slits, some large pipe breaks, and some converging or diverging nozzles. It is therefore difficult to translate these results to the specific problem of steam generator tube cracks. It is theorized that with such small length to diameter ratio in steam generator tube cracks, that non-equilibrium effects will play a significant role in the flow. There will be a very large pressure gradient at the choking plane and there will not be a sufficient amount of time for thermal equilibrium to take place. This will show that the homogeneous equilibrium model will under predict such flow and non-equilibrium models may too be insufficient

2. LITERATURE REVIEW

2.1 Steam Generator Characteristics

Steam Generators are heat exchangers between the primary and secondary loops of a PWR and CANDU nuclear reactors. The inlet from the primary loop is referred to as the 'hot-leg' and the secondary loop portion is referred to as the 'cold-leg'. In CANDU reactors, the primary side operates between 9.3 MPa and 10.2 MPa (1350 psi-1480 psi) at 305°C (579°F) while the secondary side operates between 4.5 MPa and 5.7 MPa (650 psi-830 psi) at around 265°C (509°F) . In case of PWR the primary side operates at a pressure of about 15.51 MPa (2,250 psi) or about at an average temperature of 315°C (600° F) and is subcooled while the secondary loop operates at pressure of 6.89 MPa (1000 psi) or and an average temperature of 260°C (500° F). This indicates a pressure difference of about 1000 psi between the inner and outer walls of the steam generator tubes since the water from the primary loop flows through the tubes and the water in the power loop outside them. The steam generated is then sent to the turbines to produce power and then condensed in the condensers before looping back to the SG via a feed pump.

CANDU Steam Generator designs are of a U-bend type and are manufactured by Babcock & Wilcox. Existing PWR SGs in the United States are manufactured by 2 vendors – Westinghouse, and Babcock & Wilcox (Combustion Engineering has stopped manufacturing Steam generators). Most of Combustion engineering and all of Babcock & Wilcox's designs are 2 loop reactors while the Westinghouse designs range from 2 to 4 loops. While all of Babcock & Wilcox's SGs are once-through designs, Westinghouse and Combustion Engineering utilize a recirculating "U-bend" design. Most tube diameters range from 19 to 25 millimeters while their thicknesses vary from 1.3 to 2 mm.

The tube materials for SGs built in the early 1950s was Inconel 600 (Alloy 600) but its susceptibility to Primary Water Stress Corrosion Cracking (PWSCC) and the subsequent problems and costs involved with replacements caused researchers to search for better materials and the solution lay in the use of Inconel 690 (Alloy 690), which over extensive testing shows a marked reduction in susceptibility to SCC after testing for over 10000 hours (Norring & Engstrom, 2008).This reduced susceptibility is due to the increase in Chromium content from 15% in Alloy 600 to almost 30% in Alloy 690. This is because any grain boundary segregation causing the formation of chromium carbides along grain boundaries and surface films will not succeed in thoroughly depleting surrounding regions of chromium (due to the high content), resulting in a reduction in crack formation and growth due to stress corrosion cracking (SCC) (Rios et al, 1995).

Thus, it is clear that switching to Alloy 690 or Alloy 800 tubes in SGs significantly reduces the risk of SCC. However, of the 69 steam generators in the United States, 10 still use mill-annealed Alloy 600 and 42 still use thermally treated Alloy 600 in their SGs, the former of which is more susceptible to SCC. This makes it important and still relevant to study both SCC and subcooled choking flow of Alloy 600 tubes, as they are still in service. CANDU steam generators use Monel 400, Alloy 600 and Alloy 800 as tubing material. Alloy 800 have been very successful for CANDU steam generators.

Some steam generators have operated with a minimum of problems while other designs have experienced a variety of corrosion and mechanically induced problems. Corrosion problems include denting, wastage, intergranular attack, stress corrosion cracking, corrosion fatigue, pitting on the outside surfaces of the tubes and stress corrosion cracking on the inner surfaces of the tubes. Mechanical concerns have included water hammer, thermal stratification in feed water pipes, fretting and wear of the tubes caused by excessive tube vibration and erosion-corrosion. These problems have caused unscheduled outages and expensive repairs. Where most extensively affected, steam generators have been replaced after 8-12 years of operation, far short of the expected plant operating period of 40 years. The International Atomic Energy Agency (IAEA) reports that over the last 10 years unplanned steam generator outages have resulted in over 60 billion kilowatt hours of lost generation (IAEA 2007). The economic consequences of these unplanned outages are enormous.

2.2 **Steam Generator Tube Degradation**

Steam generator tubes undergo a variety of degradations and this affects their ability to function while increasing the chances of a Loss of Coolant Accident (LOCA) or radiation leak. Though the tubes are designed to withstand operating conditions of 1000 psi (6.89 MPa) pressure differential, in the event that the primary loop is compromised vis-à-vis a rupture of the main steam line (Main Steam Line Break) then the tube wall differential can be as high as 2500 psi (18 MPa) as per the NRC's strict guidelines for the design and use of tubes and thus they have a very high factor of safety. Some of the methods of failure of SG tubes are listed below and have been classified by the Electric Power Research Institute (EPRI, 1994) and Staehle and Gorman (2003).

i. Denting

Tube degradation near the connection with the support plate which occurs due to a buildup of corrosive materials between the tube and plate.

ii. Fatigue Cracking

Cyclical stresses acting on the tubes due to vibrations or impact stresses over time that cause crack growth.

iii. Pitting

The creation of micro cracks due to an electrochemical reduction of the surface after films breakdown. Turnbull et al., (2006) proposed a model that a series of 'pits' or micro cracks would grow at the point of active corrosion and the rate of growth of the pits would be exceeded by the crack growth rate due to the coalescence of various pits over time.

iv. Wastage

Phosphate and sulfur residues causing chemical corrosion in 'wet' areas with low fluid flow rates.

v. **Vibration** induced wearing of tubes at the point of contact with the support plates.

vi. Wear

Thinning and eventual failure of tubes caused either by vibratory contact with the support plates or constant wear from water impact.

vii. Stress-Corrosion cracking

The cracking of steam generator tubes that can occur from the secondary side or primary side and is occurs due to a combination of corrosive environment, susceptible material and a constant tensile stress on the material.

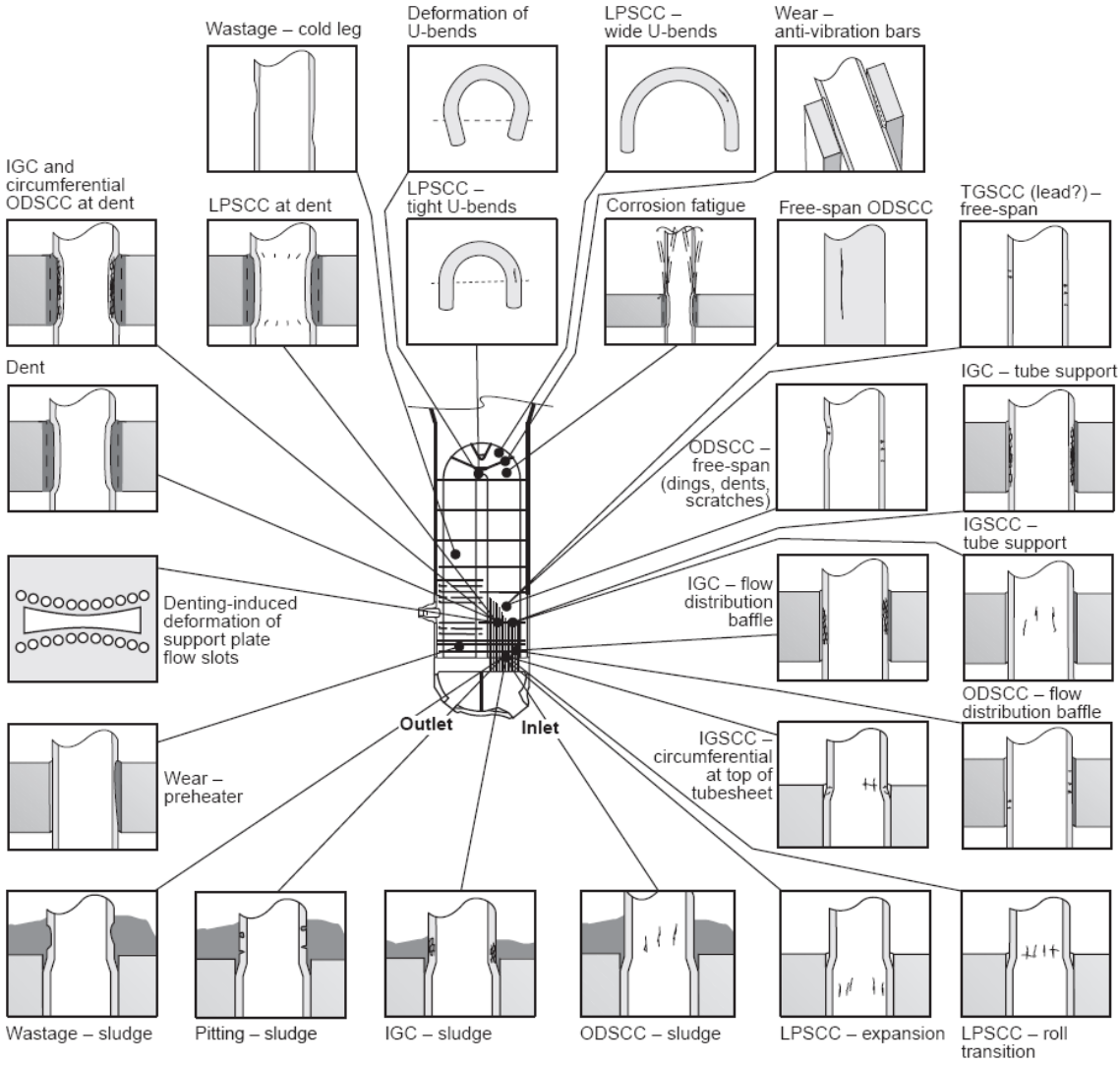

Figure 2.1: Summary of the various modes of failure at various locations (mode-location cases) that have occurred in recirculating steam generators (Staehle and Gorman 2003)

Of the various reasons for failure listed above, the most likely mode of failure to occur is Stress Corrosion Cracking (SCC) which accounts for about 60 to 80% of all damage in steam generator tubing. Stress Corrosion Cracking is a delayed cracking mechanism that occurs only when the 3 conditions mentioned above are achieved and any crack formation or defect growth that occurs when one of those conditions is not achieved cannot be classified as SCC but as corrosion, fatigue failure etc.

There are various submodes of SCC including alkaline stress corrosion cracking (AkSCC), low potential stress corrosion cracking (LPSCC), acidic stress corrosion cracking (AcSCC), high-potential stress corrosion cracking (HPSCC), lead stress corrosion cracking (PbSCC), low-valence stress corrosion cracking (Sy–SCC), organic stress corrosion cracking (OgSCC), doped steam stress corrosion cracking (DSSCC), and low-temperature stress corrosion cracking (LTSCC). The occurrence of these SCC generally depend on the seven primary variables: pH, potential, species, alloy composition, alloy structure, temperature, and stress. The detailed discussion of SCC on

designs of steam generators as they affect corrosion, bulk water chemistry as it relates to chemistry in heat-transfer crevices, and the chemistry of heat-transfer crevices are given in reviews by Staehle and Gorman (2003, 2004a, 2004b) . At the end of each section, the state of present knowledge is summarized including the lessons learned from service and laboratory experience. In addition, possible problems for future reliable performance as affected by corrosion are identified.

SCC depends on several factors which can be classified into primary and secondary factors. Primary factors include the nature of the environment (Rios et al, 1995), the tensile stresses acting on the material (Rebak, 1996), the film forming ability of that material Anderson and Ford (1988), grain boundary sensitization (Was, 1990) and the nature of the material (in terms of the composition and alloying elements present within) along with the manufacturing technique utilized (for example, mill-annealed Alloy 600 tubes are more susceptible to SCC than Thermally Treated Alloy 600). Secondary factors would be the degree of cold working, the location of the component within the reactor, operating temperatures, nature of grain boundaries, impurity levels within the environment and material (here the impurity being the major component that forms the surface films, Ru and Staehle 2013), the expansion of the materials and the actual films themselves.

SCC is a phenomenon with great historical significance. The first recorded instance of SCC was by Moore et al, (1921) in 1921 who were examining the cracking of brass cartridges and determined that ammonia from the urine of horses pulling the ammunition carts combined with residual stresses from manufacture caused the cracking, whereby the ammonia reacted with the copper to desensitize the material. At the time it was referred to as ‘season’ cracking and annealing resolved this problem, which was of critical priority to the British army since 63 years earlier, a mutiny by Indian soldiers against the British army, widely considered to be the starting point for the Indian independence movement was in protest of having to utilize pig fat to grease the brass cartridges in order to prevent stress corrosion cracking.

There have been several reviews in literature (Rebak, 1996, Van Rooyen, 1975) that have examined SCC over the decades since the beginning of the use of Ni-alloys in SGs and an extensive review and report of various phenomena, models of initiation and growth and conservative estimates to ensure prediction on actual data compiled at reactor operating conditions from 3 different sources was compiled by this author but is beyond the scope of this thesis to report in detail. A conclusion was drawn that SCC is a complex phenomenon that is a combination of various factors and while most models assume a single mode of failure, in reality it is likely a combination of all these factors combined.

The most likely method of SCC leading to failure in Alloy 600 tubes can be described in the following manner:

An Inconel 600 Tube is extruded during manufacturing and thus possesses residual stresses, which when coupled with an environment of distilled, sub-cooled water at high temperatures, the conditions are primed for SCC.

While the stress intensity within the material contributes to an increase of the electrochemical dissolution rate as described by the Coupled Environment Fracture Model (MacDonald and Urquidi-MacDonald, 1991), pits may form at the surface and when the growth rate of the pits exceeds the crack pit coalescence rate (or crack growth rate), a stress corrosion crack has initiated. This crack’s growth is then determined by the conditions at the crack tip such as the stress intensity (Andresen and Ford, 1988), the pH within the crack tip environment (MacDonald and Urquidi-MacDonald, 1991) and the melting temperature of the surface films (Galvele, 1987).

The stress intensity is in turn dependent on the formation of carbides and segregation at the grain boundaries. The movement of grain boundaries due to the formation of vacancies and the existing tensile stress within the material causes the grains to spread apart as vacancies coalesce into voids leading to crack growth. At the same time, the formation of films on the surface and their subsequent breakdown due to the movement of a dissolution plane to the surface causes the exposure of a bare surface, causing electrochemical dissolution that is cyclical in nature, as the film tends to repassivate from the chief impurities (in this case the chief constituents like Nickel, Ferrous and Chromium) within Alloy 600.

Any probabilistic Risk assessment code must keep in mind that failures within a steam generator occur due to fatigue and SCC. However, SCC is not such a major problem for Alloy 690 tubes due to the increase in Chromium, reinforcing the importance of Chromium in keeping corrosion at bay.

Thus it is apparent the a knowledge of SCC is mandatory for reactor designers and Steam Generator design, but any description of crack growth, initiation and geometries are beyond the scope of this study, which focuses on the study and analysis of leaking of a subcooled liquid through these cracks, and the influence of crack areas, L/D, flow channel length, roughness and subcooling on the critical flow rates.

3. CRITICAL FLOW LITERATURE AND MODELS

3.1 Choking Flow in Literature

Choking flow is a phenomenon which occurs in a wide range of industrial systems. It is especially important in a nuclear reactor; where high pressure subcooled water in the case of a PWR is used to generate steam. In the instance of a loss of coolant accident (LOCA), choking flow determines the coolant inventory of the reactor vessel. If choking were not to occur, the reactor water inventory would be depleted rapidly. This is not the case however because as the pressurized subcooled water nears the break, it flashes to vapor which limits the mass flow rate due to choking. Therefore, the integrity of the core during a LOCA is dependent upon this choking phenomenon.

A LOCA from a small break or large break in the main steam line or valve is not the only place in a reactor where coolant could be escaping the primary side of the reactor. Steam generator tubes have a history of small cracks and even ruptures, which lead to a loss of coolant from the primary side to the secondary side under the previously explained leak before break approach to steam generator tube integrity. Therefore, choking flow plays an integral part not only in the engineered safeguards of a nuclear power plant, but also to everyday operation. In the case of leakage through SG tubes to the secondary side of the plant, radiation detection measurements of the secondary flow are taken and calibrated to predict and increase or decrease of leakage through the SG tubes. If excessive leakage occurs, the plant must shut down or the operator must take appropriate action. It is therefore of great interest to not only qualitatively, but quantitatively be able to predict such flow rate with great accuracy.

Most of the recent research related to steam generator tubes is in characterizing defects as well as predicting burst pressures for tubes with defects. There is a plethora of information related to the material behavior under such conditions (Pagan et al, 2009, Kichirka et al, 1997). While some studies do experimentally determine leak rates from steam generator tube defects, they are concentrated on the leak rates after burst. Burst is associated with a very large opening in the side of a tube. The overall prediction of leak rates through cracks is very dependent on the crack opening area, thus the future of leak rate prediction will be the coupling of crack morphology and leak rate models. The work presented here is concentrated on the leak before break, or leak before burst and does not allow for crack growth during leakage.

There is very limited data on the steam generator tube leak rate measurement. Most studies of subcooled choking flow are related to long tubes with large L/D and nozzles (Henry, 1970, Henry and Fauske, 1971). A literature survey performed list the limited sets of data that focus on crack and simulated crack geometries, and can be seen in Table 3.1. (Wolf and Revankar, 2012). The survey shows that this geometry has been studied over a large range of pressures and liquid subcoolings however, as can be seen, these data focus on L/D geometries greater than 15. Also, all of those data have a channel length greater than 10 mm, which is not indicative of steam generator tubing. Steam generator tubes have a wall thickness typically less than 3 mm.

From available tabulated data on crack geometries, the parameter range associated with the current study can further be realized by Figures 3.1 and 3.2. From Figure 3.2, it can be seen that most data points fall at the higher L/D ratios than that of the current study. Also, in the smallest range of L/D very few data exist at lower choking mass flux. From figure 1.3, it can be seen that of those data points that fall at the smallest L/D seen in red, no data points fall in subcoolings below 50 °C. In view of this an experimental program was carried out where the simulated steam generator tube crack geometry were well characterized and choking flow of subcooled water tests were performed.

Table 3.1: Summary of Studies conducted on two-phase choked flow with MFRL Data included (Wolf and Revankar 2012) at Purdue University

Authors	Geometry |fluid	L [mm]	t X w [mm] x [mm]	Dh [mm]	Area [mm^2]	L/D	R roughness [μm]	P [Mpa]	ΔTsub [K]
Agostinelli et al. (1958)	annulus (slit) |steam-water	152-254	(0.15-0.43) X (78.4-79.3)	0.3-0.86	12-38	176-840	(----)	3.5-20.51	10-67
Ryley & Parker (1968)	slits |steam	35.6	(1.27) X (25.4)	2.42	32.3	14.7	(----)	0.008-0.017	0-
Simoneau (1974)	slits |cryogenic N_2	25.4	(25.4)X (0.284-0.3)	0.58	7.42	43.5	(----)	P_{max}=6.8	(----)
Collier et al. (1980)	slits |steam-water	60-75	(0.2-1.12) X (57.2)	0.4-2.2	11.4-64	27-187	0.3-10.2	P_{max}=11.5	33-120
Abdollahian, Levy, Chexal (1983)	cracks |steam-water	18.6-57.2	(0.74-63.5) X (0.0183-1.12)	0.03-1.9	0.015-71.1	30-634	0.3-10.2	3.26-11.53	1-119
Amos & Schrock (1983)	slits |steam-water	63.5	(0.127-0.381) X (14.8-20.5)	0.16-0.77	2.6-7.8	83-400	(----)	4.1-16.2	0-65
Collier et al. (1984)	cracks |steam-water	20	(0.02-0.22) X (0.74-27.9)	0.04-0.44	0.015-6.55	45-500	1.78	P_{max}=11.5	0-72
Kefer et al. (1986)	slits/cracks |steam-water	10-33	(0.097-0.325) X (19-108)	0.26-0.64	5.89-13.93	15-127	20-40	P_{max}=16.0	0-60
John et al. (1987)	slits |steam-water	46	(80)X (0.2-0.6)	0.4	20.0-51.2	115	5-240	4.0-14.0	3-60
Bandyopadhyay et al. (2007)	slits/cracks |steam-water	8	(0.27-0.50) X (15-43.73)	0.54-0.97	5.7-11.8	8.3-14.8	(----)	1.14-8.66	58-264
Wolf & Revankar, (2012)	slit | steam-water	3.175	(0.25-0.50) X (2.4-3.2)	0.55-0.84	0.86-1.92	4.48-6.94	30	6.89	24-46
Samples tested in This Study	slit | steam-water	1.3	(0.83-2.6) X (0.285-0.648)	0.61-1.04	0.513-4.59	1.2-2.1	5-30	6.895	14.1-49.1

It is evident from literature (table) that except for the findings of Wolf, most research was conducted for crack L/Ds (Flow channel length over Hydraulic Diameter) over 14.7 and flow channel lengths of over 8 mm. The most recent work by Wolf and Revankar (2012) was conducted on laser cut (therefore rough) samples with L/Ds ranging between 4.8 and 6.2 and flow channel length of 3.175 mm for 5 samples and additional testing on a pinhole. Steam generator tubes thicknesses however range between 1 to 2 mm depending on the material, design and manufacturer and between 12.5 and 19 mm in diameter (Outer diameter OD). Also, L/D ratios are generally on the order of between 0.8 and 2 since the thickness is small but the crack can propagate over time thereby increasing its hydraulic diameter. Thus further studies are being conducted on cracks of 1.3mm thickness with L/D ratios varying from 1.1 to 2.1

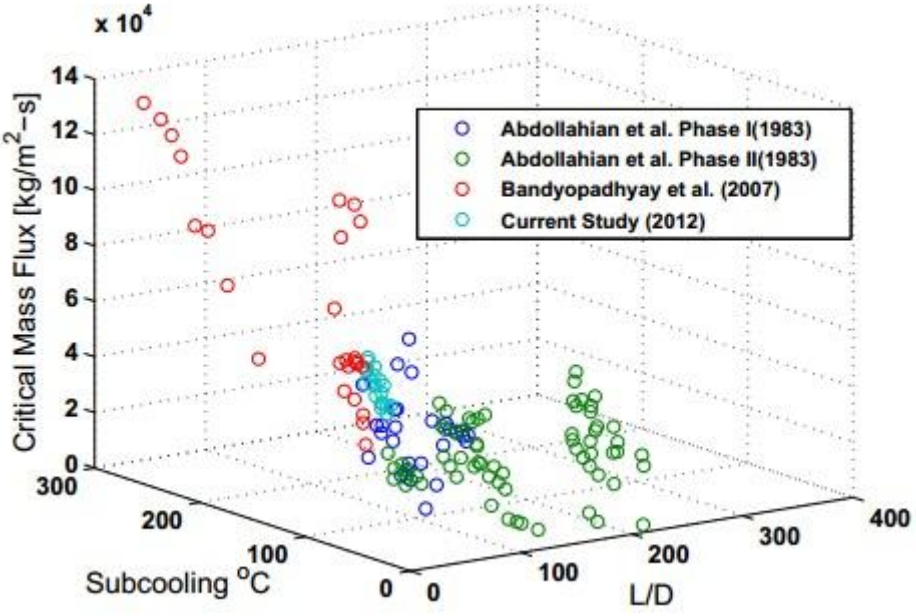

Figure 3.1: Comparison of current experimental data with relevant data in literature as a function of mass flux, L/D ratio and Subcooling

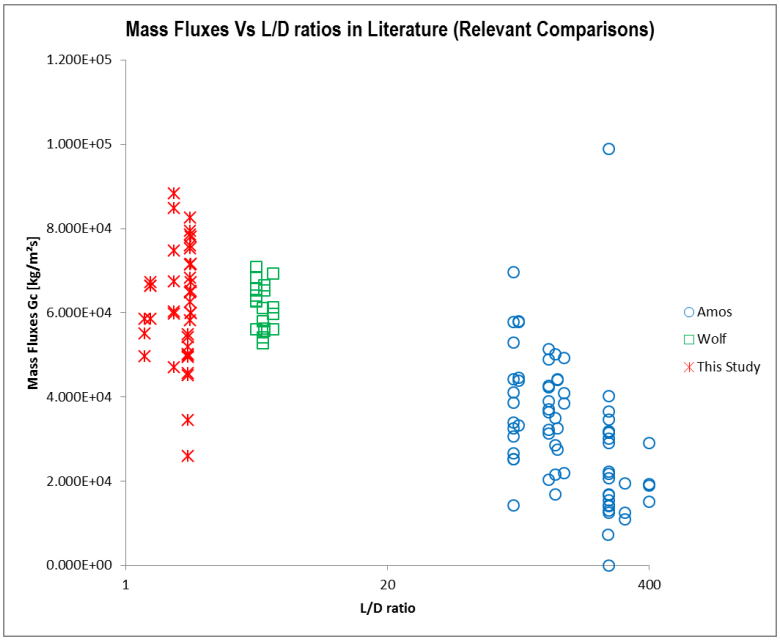

Figure 3.2: The L/D ratios of this study compared with those the most widely accepted work in literature (Amos and Schrock, 1983)

3.2 **Modeling Efforts on Choked Flows**

The next four sections will briefly outline various choking flow models such as the homogeneous equilibrium model, homogeneous non-equilibrium models, nonhomogeneous equilibrium models, and non-homogeneous non-equilibrium models. In the context of these categories, equilibrium models are describing the thermal equilibrium in which the temperature of each phase is the same. The flow is considered in non-equilibrium if there is a temperature discontinuity between phases. If homogeneous flow

is considered, then the assumption is made that both the gas and liquid velocities of a two-phase one-component flow are equal. In the case of nonhomogeneous flow, two different criteria may be met. One case is that the gas and liquid velocities are different, however the relative velocity is constant. That is that $(V_g - V_f)$ is at steady state. This type of flow is considered to be in mechanical equilibrium, but non-homogeneous. There also exists mechanical non-equilibrium, non-homogeneous flow in which the acceleration rates of each phase are different.

3.2.1 **Homogenous Equilibrium Models (HEM)**

The homogenous equilibrium model assumes the fluid is homogenous by treating it as a pseudo-fluid whereby both the phases are in equilibrium, thus enabling the simplification of a two-fluid mixture as a single phase (Wallis, 1969). In this assumption, the fluid's phases are assumed to be in both thermal and mechanical equilibrium meaning that there is no slip between the two phases (both are travelling with the same velocity) and both of them are at the same temperature. This allows the properties such as thermodynamic quality to be calculated easily from steam tables and simplifies the calculation since any equations of state have to applied to a single fluid, since the assumption is that temperature and pressure of both phases follow the saturation curve with isentropic expansion of the fluid (Amos and Schrock 1983).

Wallis (1980) studied the influence of changing parameters such as geometries and pressures and its effect on the critical mass flux with respect to quality and found that long channels allowed or establishment of equilibrium but not for short pipes since there isn't enough time for equilibrium conditions to be established. Thus, the assumption made by many authors (Henry 1970, Wolf and Revankar 2012), for a liquid at low subcooling under high pressures for small channels like steam generator tubes is that flashing will occur at the exit or outlet of the flow channel where a large pressure gradient exists over a very small distance and the flow is also critical. The assumption is that the first bubbles are nucleated at this point (Wallis 1980).

The HEM is essentially a simple representation of the concept of critical flow, whereby any change or increase in pressure has no effect on the mass flux G_c, thus

$$\frac{dG}{dP} = 0 \tag{3.1}$$

And applying the mixture conservation equations allows for the sound velocity to be represented in terms of the fluid's critical flow velocity since

$$P = \rho UA \tag{3.2}$$

Now the mass conservation equation for HEM assumptions and a constant area of flow would be

$$\frac{du}{dz} = \left(\frac{1}{\mu}\left[(1-x)\frac{d\mu_f}{dP} + x.\frac{d\mu_g}{dP}\right]\frac{dP}{dz} + \frac{\mu_{gf}}{dz}\frac{dx}{dz}\right)u \tag{3.3}$$

And the equation for conservation of momentum is

$$\frac{dP}{dz} = \left(-\frac{dP}{dz}\right)_f - \frac{u}{\mu}\frac{du}{dz} \tag{3.4}$$

Thus combining these two equations with the boundary conditions of saturation temperature at flow channel exit and exit speed Mach 1 when applied to the critical flow criterion (Amos and Schrock, 1983),

$$u = a = \frac{dP}{d\rho}^{\frac{1}{2}} \tag{3.5}$$

Now combining this with (4.1) and rewriting ρ as $\frac{1}{\mu}$ gives us

$$a^2 = -\mu^2 \frac{dP}{d\mu} \tag{3.6}$$

Thus, (4.5) and (4.6) can be combined with equations (4.3) and (4.4) to give us the sound speed criterion for choking under a Homogenous Equilibrium assumption as

$$U_a = \mu[-((1-x)\frac{d\mu_f}{dP} + x\frac{d\mu_g}{dP} + \mu_{fg}(\frac{dx}{dp})_s)]^{\frac{1}{2}} \tag{3.7}$$

Where $(\frac{dx}{dP})_s$ is the equilibrium mass transfer rate defined by (Schrock et al., 1982) as

$$(\frac{dx}{dP})_s = \frac{(1-x)\frac{ds_f}{dP} + x\frac{ds_g}{dP}}{s_{fg}} \tag{3.8}$$

In other words, for short channel lengths, the HEM is a 'frozen flow' model that assumes that there is no quality change over flow length and the expansion is isentropic with equal phase velocities (Henry and Fauske, 1971).

Since the HEM ignores many of the non-equilibrium phenomena along with an isentropic assumption, it has a tendency to under predict the mass flow rate. A simple explanation for this in terms of the isentropic assumption is because for a subcooled stagnation state, the velocity of the mixture could exceed the velocity of the homogenous fluid calculated at zero quality and since supersonic flow cannot occur in a straight duct, this means the HEM will under predict the flow rate.

The HEM assumptions for a straight duct also disregards area change, friction and energy addition along the length of the channel, instead assuming the liquid undergoes no changes between the entrance and exit (since it is isentropic, and only area change will be isentropic, Amos and Schrock, 1983) and since these are the only processes that can cause phase change, for an isentropic assumption it is mandatory that friction loss and energy addition in the channel be disregarded. Then the phase change would make no sense in straight ducts, thus this is useful only if choking and flashing are occurring at the exit.

3.2.2 **Non Homogenous Equilibrium Models (NHEM)**

The NHEMs assume that both phases are in thermal equilibrium but that there is slip between the phases and they flow at different velocities. Thus solving it will involve incorporation of the Drift flux model with a velocity difference factor.

In this scenario, knowledge of the quality factor becomes important since that allows determination of the velocities of the individual phases (Wallis 1980) and from this, the velocity ratio (slip)

$$S = \frac{V_g}{V_l},$$

the ratio of mean vapor velocity to the mean liquid velocity can be found. This is helpful since there are 3 major models explained in detail in (Wallis, 1980 Moody 1965, Fauske 1962) that attempt to model the interphase slip as a function of ratios of the specific volumes of the fluids.

These models are essentially simplifications that allow for the slip to be calculated if the quality and therefore the specific volumes or densities of the individual phases are known. The shortcomings of these assumptions is that the Moody model fails to consider momentum conservation and thus knowledge of the energy balance allows Moody's criterion to be used, whereas the Fauske and Levy model disregard energy balance and they can be utilized only if the momentum flux at the exit is known. Levy took the void fraction into consideration in his model, however all 3 of these models tend to overpredict the slip ratios from experimentally observed values. This also means that the mass fluxes they predict would be higher than the HEM.

The inherent problem with these assumptions is that two-phase flow will have transition regimes and bubble nucleation, while the slip assumption only regards two perfect phases of fluid and vapor.

The advantage then, of the HEM and NHEMs is that they are simple, easy to calculate and can be used as references to predict experiments and easily modified to match data (empirical).

3.2.3 **Homogenous Non-Equilibrium Models (HNEMs)**

A subcooled liquid which flashes at the choking plane experiences thermal non-equilibrium conditions since the two-phase depressurization could occur over a very short distance and could be greater than the thermal exchange rate between the two phases and disregarding these phenomena is why most researchers believe the equilibrium models under predict the flow rates.

The non-equilibrium phenomena that have to be considered are bubble nucleation and mass, momentum and heat transfer through the interphase between the two phases. There are many phenomena occurring that influence the two-phase flow formation and the more effects are considered in models, the more complex they become and some of the assumptions that researchers are forced to assume for the models predictions to match experimental data are far from observed values. Thus, all of the HNEMs contain a certain degree of empiricism (Wallis 1980).

These models account for the non-equilibrium phenomena like bubble formation by utilizing parameters such as the pressure undershoot ΔP developed by Alamgir and Lienhard (1981) which is a pressure drop correction to a frozen flow, thereby resulting in the saturation temperature of the fluid being higher than the actual temperature of the fluid, resulting in a degree of superheat. In other words, the correlations attempt to correct the deviation noticed in the HEMs and provide a theoretical justification for the correlations.

Fauske (1985) modeled the flow of subcooled fluid for different relaxation times for samples of varying geometries (varying L/Ds) and found that the relaxation times and

lengths, or the time or distance required for the establishment of an interphase and nucleation sites, were too large and long respectively with regards to steam generators tube wall thicknesses. For extremely small L/Ds (L/D < 3), he stated that flow rate could be modeled using a simple orifice equation for a given critical pressure.

$$G_c = 0.61\sqrt{2\rho_f(p_0 - p_c)} \tag{3.9}$$

In this study, the L/D ratios range from 0.98 to 2.1 and thus this equation becomes relevant. Thus by Fauske's conclusions, the flow rate should be higher since there isn't enough time for a subcooled liquid to flash thereby reducing the critical flow rate.

Other models that have attempted to study non-equilibrium phenomena are like the empirical models of Henry and Fauske that utilized a coefficient which indicates fractional vapor generation at equilibrium which when combined with a simple assumption of mechanical equilibrium (both phases are at the same velocity) allows correlation of the model and data, by controlling the exit quality. This is extremely simplified since only stagnation states are relevant and processes within the flow channel are ignored. However, Wallis (1980) in his study of critical two-phase flows observed that these empirical models did match experimental data and in some cases offered a slight over prediction depending on the stagnation pressures, than the HEMs could. These models are simple, have been utilized by the researcher and can be represented in terms of the critical mass fluxes as,

Henry-Fauske model:

$$G_c^2 = \left[\frac{x_0 \nu_g}{nP} + (\nu_g - \nu_{f0}) \left\{ \frac{(1-x_0)N}{s_{gE} - s_{fE}} \frac{ds_{fE}}{dP} - \frac{x_0 c_{pg} \left(\frac{1}{n} - \frac{1}{\mathrm{Y}} \right)}{P(s_{gE} - s_{fE})} \right\} \right]_t^{-1} \tag{3.10}$$

where N is the parameter discussed above and is equal to zero for frozen flows and when unity is close to the HEM and thus describes partial phase change. This model was found to be relevant for crack L/Ds > 12.

Henry Model (Henry, 1970):

$$\begin{aligned} G_c &= 0.61\ 2\rho_l P_0 (1-\eta)^{0.5} \\ \text{Where } \eta &= 0.1(L/D)\ \ if\ \ 0 < L/D < 7 \\ \eta &= 0.7\ \ when\ L/D > 7 \end{aligned} \tag{3.11}$$

A major empirical model that has been utilized by several researchers attempting to model non-equilibrium choked flow (Amos and Schrock 1983, Wolf and Revankar 2012) is the pressure undershoot correlation of Alamgir and Lienhard (1981) mentioned earlier, which allows for the development of the superheat needed for bubble formation as,

$$\Delta P_d = \frac{0.258\sigma^{1.5}T_r^{13.76}(0.49+13.25\Sigma^{0.8})^{0.5}}{(k_s T_c)^{0.5}\left(1-\frac{\nu_f}{\nu_g}\right)} \tag{3.12}$$

thus the pressure at the point of flashing would be

$$P_{fl} = P_{sat}\ \ T_{f0}\ \ - \Delta P_d \tag{3.13}$$

Thus for the required amount of superheat to be achieved, the explanation for this phenomenon would be that the fluid is at a vapor at its saturation pressure of P_{sat} and the liquid is at its saturation value of $P + \Delta P_d$ just upstream of the flashing location. The averaged depressurization rate is the integral of the momentum equation over the length 'L' of the channel. For very long ducts however, the authors found that this model overpredicts the flow rates when the liquid is subcooled, perhaps because the model doesn't factor in friction and energy transfer from the walls, which would cause a larger pressure drop and further reduce actual flow rate.

There have been other models in literature that attempted to model specific physical phenomena like bubble nucleation, interphase transfer and entrainment. These parameters can have a significant effect on the location of flashing for longer channel lengths and larger L/D values but at the cost of accuracy. Many of the assumptions made are very different from values that are measured in literature and cast doubts on their accuracy.

Thus we have looked at empirical and physical phenomena based models. The last category is those models that attempt to model each phase of the fluid and therefore can be called a Non Homogenous Non-Equilibrium Models

3.2.4 **Non Homogenous Non-Equilibrium Models (NHNEMs)**

These models assume a lack of mechanical equilibrium, (the phases move at different velocities), non-homogeneous flows (wherein the effect of transition regimes and interphase conservation equations have to be considered) where the 2 phases are not in thermal equilibrium. Thus each phase is modeled as a separate entity with its own mass, momentum and energy equations and interaction terms must also be considered.

Since critical flow involves shock formation and breaks down at the point of shock formation (mathematically, refer to Strang, 2007 for further details) in case of the two-fluid model it becomes important to solve the equations of flow upstream and downstream till the point where the equation breaks down, indicating the shock formation. If this was to be integrated into an iterative code, it would be infinitely complex and use up a large amount of computational resources. Just trying to model the formation of a bubble, then consider the number of bubbles formed, which in turn affects the surface area and void fraction calculations must be considered. Then, the flow regime must be taken into consideration and the viscous forces, drag forces and inertial forces on each bubble have to be considered and when combined with velocity of bubble and interfacial transfer phenomena, the complexity of these calculations can be understood.

Until a justification of the costs and resources required for utilizing such a method can be made or computational methods and technology catch up to models, it is safer from the point of view of an experimentalist to stick to semi-empirical models with a physical basis such as the HNEM model by Wolf and Revankar (2012) for larger L/Ds and Fauske model (1985) for smaller L/Ds.

Another class of models as mentioned earlier in this review is the integral analysis model which averages and integrates the fluid property under consideration over the flow length. It is relevant mentioning here earlier experiments that were tested in this author's lab by Wolf and Revankar (2012) were done to gather data which was then fitted to a modified, integral model based on an empirical correlation by (Burnell, 1946) proposed in 1946 to calculate the critical mass flux of an orifice (L/D < 3) on the basis of the surface tension and the stagnation temperature of the fluid, which can be listed as

$$G_c = 2\rho_l (P - kP_{sat})^{0.5} \tag{3.14}$$

where k indicates the critical pressure as

$$k = 1 - 0.264 \frac{\sigma(T_0)}{\sigma_{(12.1bar)}} \tag{3.15}$$

Wolf's (4) modified Burnell model makes use of Burnell model and modified it via an empirical correlation by utilizing the k factor as a function of the subcooled temperature as

$$k = 1 + 11.6 \left(\frac{\Delta T_{sub}}{T_{sat}} \right)^{1.7} \tag{3.16}$$

which he found better predicted his data and similar efforts were made to compare this model to critical flows through channels with SG thickness by this author.

4. EXPERIMENTAL TEST FACILITY

4.1 Introduction

The purpose of the experimental program was to develop database on critical flow through crack geometries with subcooled liquid flow at the entrance. These database are then used in validating critical flow models that can be used in assessing leak rates from steam generator tube cracks. In the previous chapter the crack opening area (COA) models were studied. With a validated critical flow model and COA model the leak rates from the steam generator tube cracks can be evaluated. Crack growth models enable the leakage expected in future. All this information is useful to assess the steam generator tube integrity and for maintenance scheduling. In view of this, an experimental test program was developed to develop database on and new data on critical flow in tubes.

4.2 Experimental Test Facility

4.2.1 Test Facility Design

Design of a test facility to measure leak rates of through wall cracks was based on the following goals. (1) The test facility should be modular so that various crack geometries can be studied. (2) The pressure differential across the break should be similar to the prototype about 6.8 MPa (1000 psi). (3) Facility should be such that tests can be easily repeated. Based on these goals a test facility is designed. Figure 4.1 shows a schematic of the test facility design. It consists of a vertical pressure vessel, which serve as the blowdown tank, a water tank where steam condenses and the discharge from crack is collected and measured, a nitrogen supply line to pressurize the vessel with control valve, instrumentation and data acquisition system.

The volume of the vessel was based on the maximum discharge rate expected from the crack. In designing the test facility the most important aspect is the volume of the pressure vessel as this will determine what leak rates can be measured and for how long. Also, the size of the condensing tank will affect this as well. Therefore, calculating the ratio of the pressure vessel and condensing tank size is useful. The leak rates with different sizes cracks using ANL leak rate model for PWSCC have shown that at normal operating conditions are of the order of 50 l/m for a one inch crack as shown in Figure 4.2. This indicates that one needs a very large pressure vessel to perform the experiments with crack size of the order of 25 mm. Equating the mass specific heat of the condensing volume with change introduced by leak rate allows us to calculate the ratio of the mass required in the collection tank to that of the pressure vessel.

Using h_{fg} ~ 2000 KJ/kg and Cp ~ 4.18 KJ/kg K if we allow the condensing tank to rise 20^{o}C in temperature then the mass accumulated in the condensing tank to the mass held in the pressure vessel is equal to ~24.

Given this limitation it has been determined that appropriate crack sizes to be studied are between 2 and 8 mm in length. The given leak rates for different crack size at pressure difference of 10 MPa (1450 psi) are shown in Table 4.1. A typical crack size of 2-10 mm seems reasonable design size. For 10 mm crack size a 3" O.D. Schedule 80 or higher piping as the pressure vessel and allowing 2/3 of the volume to be occupied by pressurized nitrogen, a minimum of 0.9 m (3 ft) in length is required for the pressure vessel. The design of the pressure vessel is shown in Figure 4.3. It has several inlet/outlet ports including one for liquid discharge through the test section at the bottom, one inlet port at the top for supply of nitrogen from nitrogen bottles, and six ports for thermocouples and pressure sense lines.

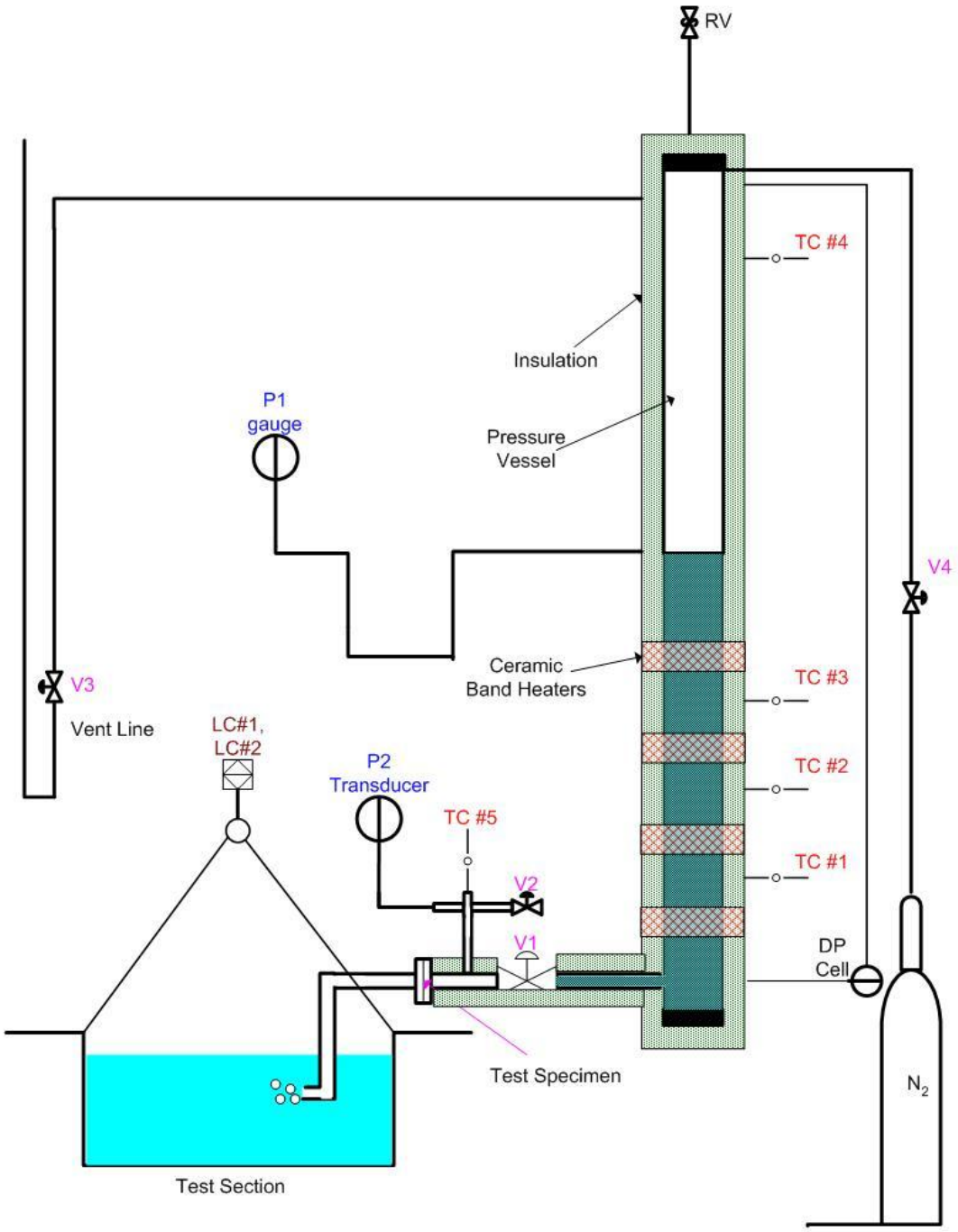

Figure 4.1: Schematic of test facility

$$m_{cond} C_p \Delta T_{cond} = \dot{m}_{leak} h_{fg} \Delta t \tag{4.1}$$

$$\frac{m_{cond}}{\dot{m}_{leak} \Delta t} = \frac{h_{fg}}{C_p \Delta T_{cond}} \tag{4.2}$$

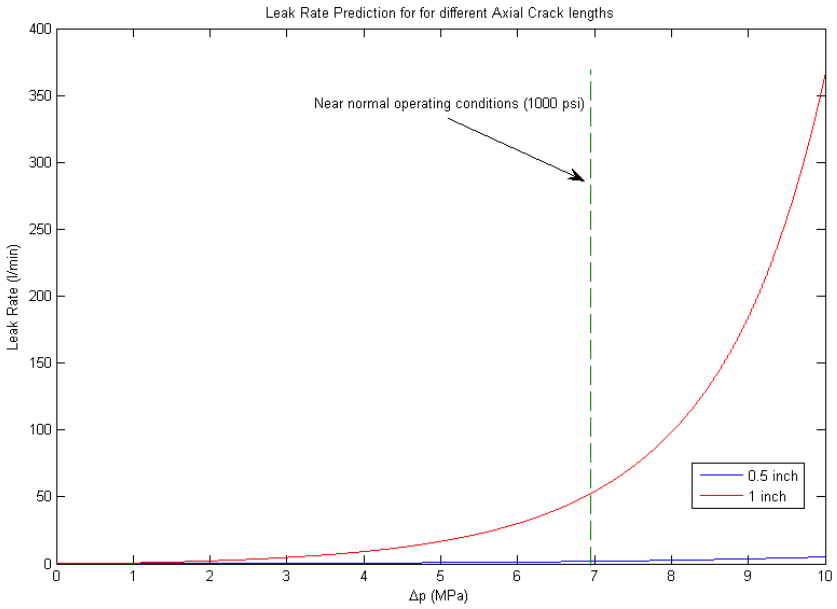

Figure 4.2: Leak rate predictions for 0.5 and 1 inch length cracks using the ANL leak rate model for PWSCC

Table 4.1: Leak rates for a given crack length at Δp=10 MPa.

Crack Length (mm)	Crack Width (mm)	Leak Rate (L/min)
1	0.0016	0.0082
2	0.0033	0.0339
3	0.0053	0.0815
4	0.0078	0.1586
5	0.0109	0.2776
6	0.0150	0.4579
7	0.0204	0.7285
8	0.0278	1.1322
9	0.0378	1.7315
10	0.0514	2.6162

4.2.2 **Test Facility**

The pressure vessel was first hydrostatic tested at 10.3MPa (1500 psig). Then another hydro test was completed at 14 MPa (2000 psig), which is over 200% of the operating pressure. The hydrostatic test was successful with no leaks or complications. The vessel has one pressure relief valve (Kunkle brand) with pressure preset to 8.3 MPa (1150 psi) and is mounted with a half inch NPT connection.

The pressure vessel is connected via 3/8 inch stainless steel tubing to the compressed nitrogen bottles. Ceramic band heaters are used for heating the pressure vessel contents. The band heaters of interests are 4.5 inches in inner diameter and vary between 800 and 1800 watts. They are placed in parallel for operation at 240 volts. Pressure and temperature are measured and a relief valve is placed at the top of the tank. Pressure and temperature are also measured just before the test section. A valve is used to initiate the experiment. As the subcooled water is discharged it flashes and a two-phase critical flow ensues. The discharge steam is condensed by the cooler water bath where the outlet of test section is submerged. The condensed steam and discharged water are collected in the bath volume. This allows for a time averaged mass flow rate to be measured.

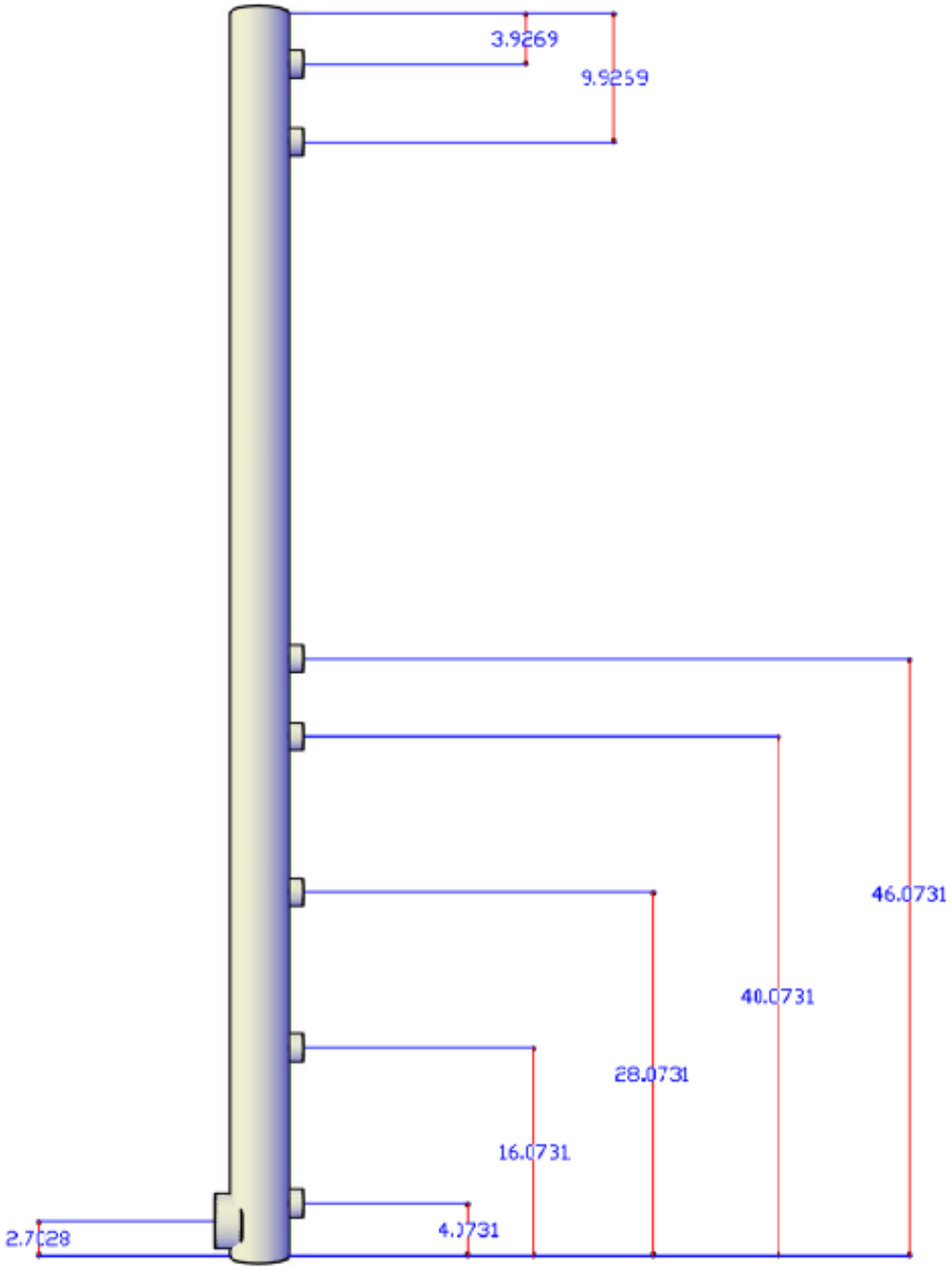

Figure 4.3: The pressure vessel design

The design of the condensing tank hanging system involves cable supporting the tank with two load cells, which are strain gage type. The tank was suspended using steel wire rope and eyebolts from channel struts spanning the test section support structure. The load cells signal need to be amplified before measuring using the data acquisition system. The load cells range is 0-300 lbs. and puts an output in the range of 0-23mV. These have a maximum error of 0.15 lb. at any load. Figure 4.4 shows the picture of the two load cells.

An instrument amplifier with a gain of 100 was built in order to accomplish this. The amplifier consist of a 15 volt DC power supply wired to two separate high precision instrumentation op amps as seen in Figure 4.5. The calibration of the load is cell carried out with known mass of the water in the tank. The test facility without insulation is shown in Figure 4.6.

Figure 4.4: Strain gage load cells

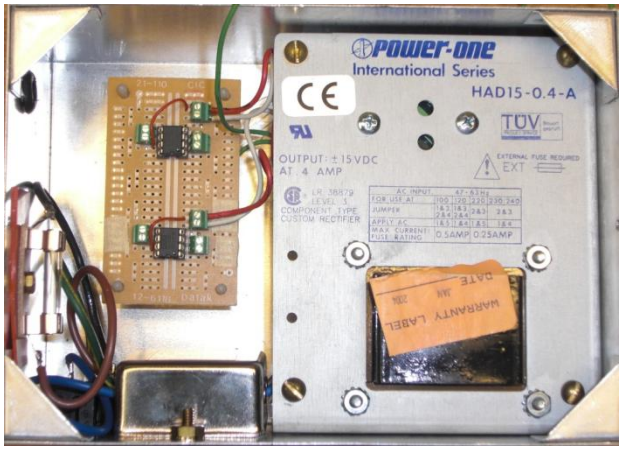

Figure 4.5: Precision instrumentation amplifiers, Gain=100.

The water level in the vessel is measured with Honeywell DP transducers. Detailed heat transfer calculations on heat loss from the pressure vessel were done and it was found that a thickness of 2 inches in insulation is required for the pressure vessel. This insulation is of the mineral wool variety, which has temperature tolerance up to 600^{o}C. Its thermal conductivity is lower than fiber glass. The DP cells were calibrated with NIST standard pressure calibrator unit for the range of water level in the pressure tank. The load cells, differential pressure cell and thermocouples were wired to the data acquisition system for testing. The load cells, differential pressure cell and thermocouples were wired to the data acquisition system and were tested. A Labview program was developed for data acquisition and real time data display and monitoring.

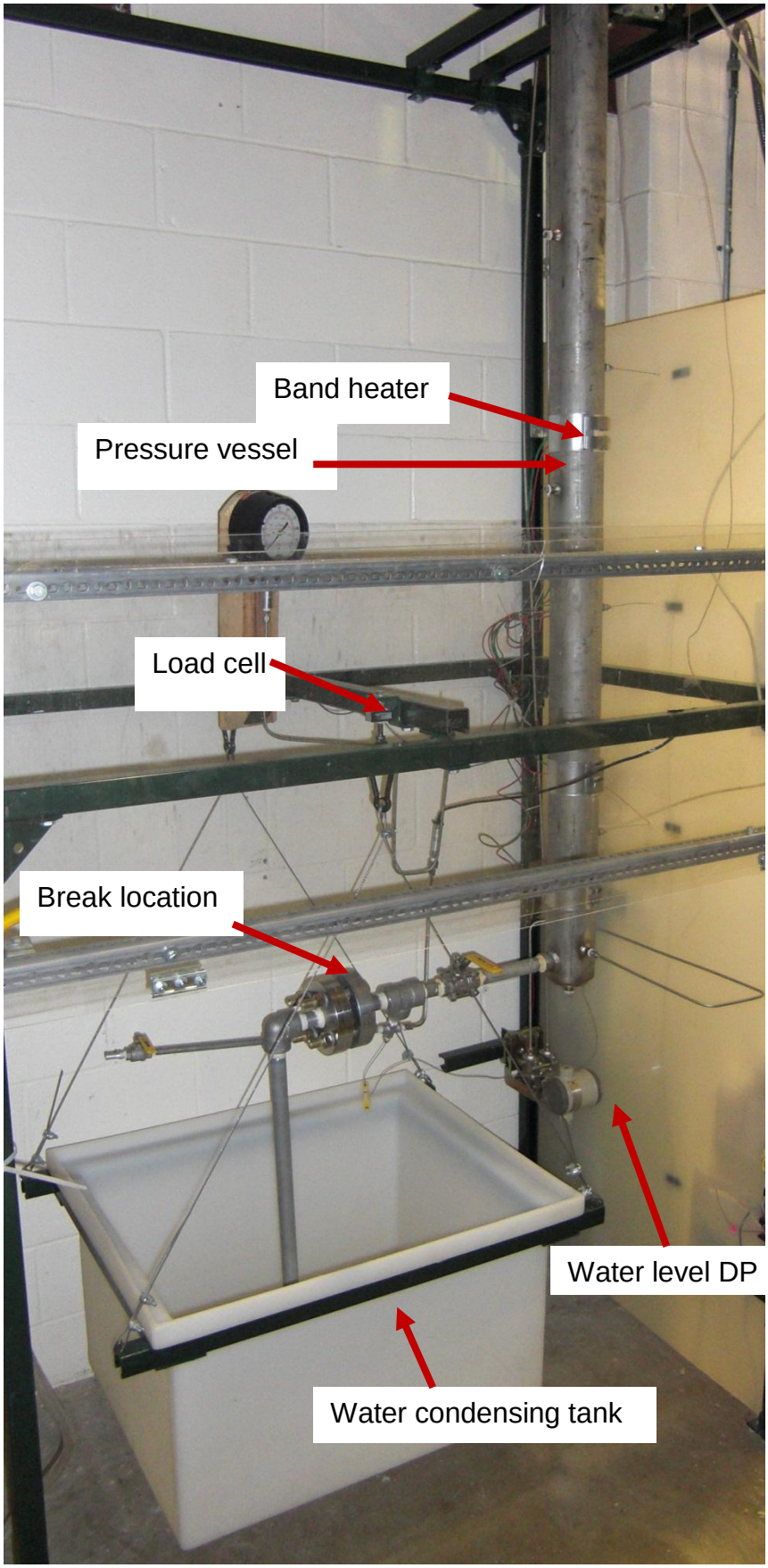

Figure 4.6: Steam generator tube crack leak rate test facility assembly

4.2.3 **Crack Specimens**

Two types of test crack specimens split into two batches were used. Samples were manufactured by laser cutting, drilling and welding semicircular discs together over a stainless steel nipple with the faces milled. This enabled the study of different geometries and surface roughness's. The hole was drilled with a drill bit and the slits were laser machined on stainless steel SS 316 plates of thickness 3.175 mm. In Figure 4.7(a), the orifice hole is shown. There is roughness in the hole and the average hole diameter was estimated as 475.5 micrometer (μm). By measuring the valleys and peaks the roughness was estimated at 25 μm. The slit test specimen number 2, 3, 4, 5 and 6 are shown in Figures 4.8, 4.9, 4.10, 4.11, and 4.12 respectively. Since slits were cut with laser, the sizes at front (downstream) and back (upstream) side of slit are not same as shown in Figures 4.8 to 4.12. The measured slit dimensions are indicated on the figures.

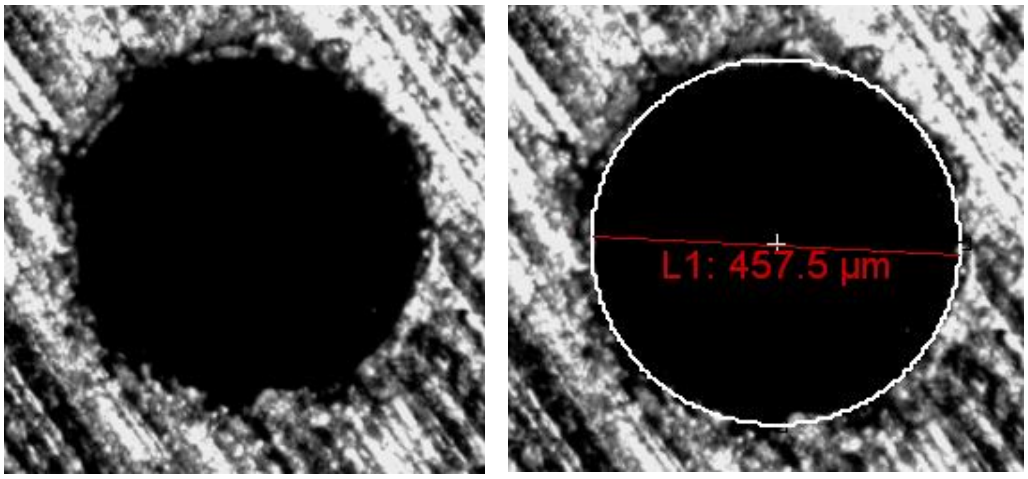

(a) **(b)**

Figure 4.7: Pin-hole crack test specimen #1

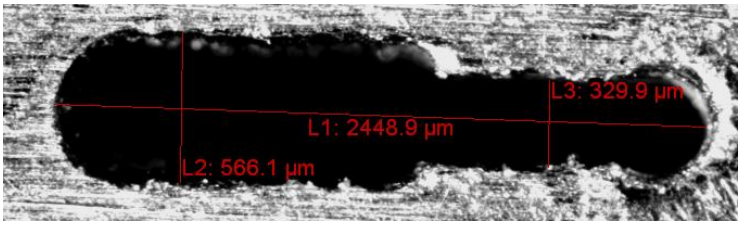

Slit front

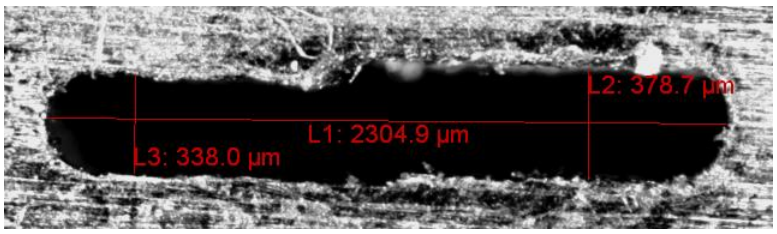

Slit Back

Figure 4.8: Slit crack test specimen # 2

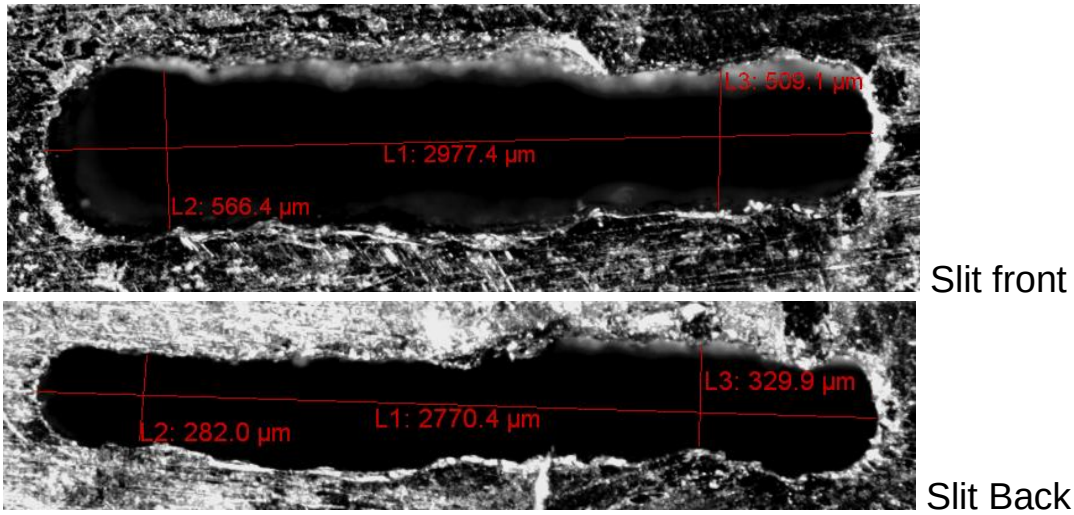

Figure 4.9: Slit crack test specimen #3

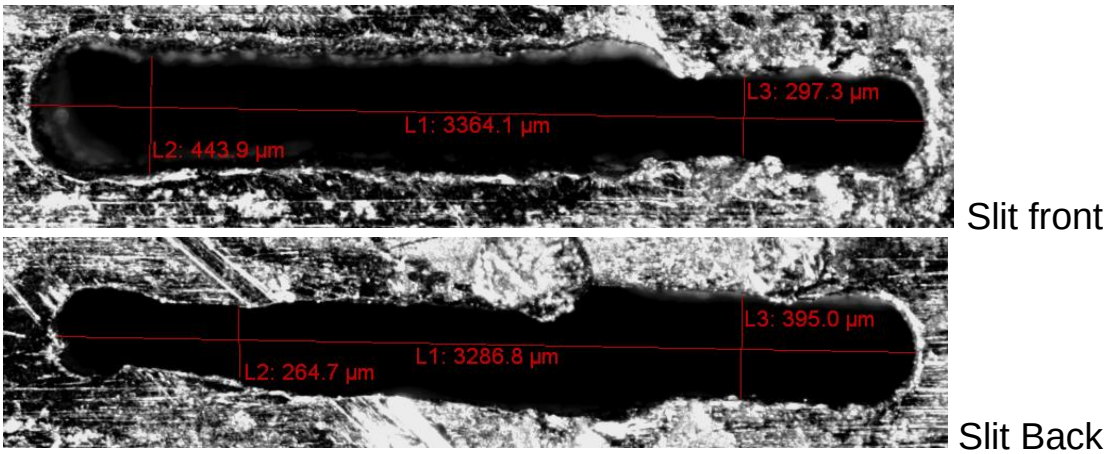

Figure 4.10: Slit crack test specimen #4

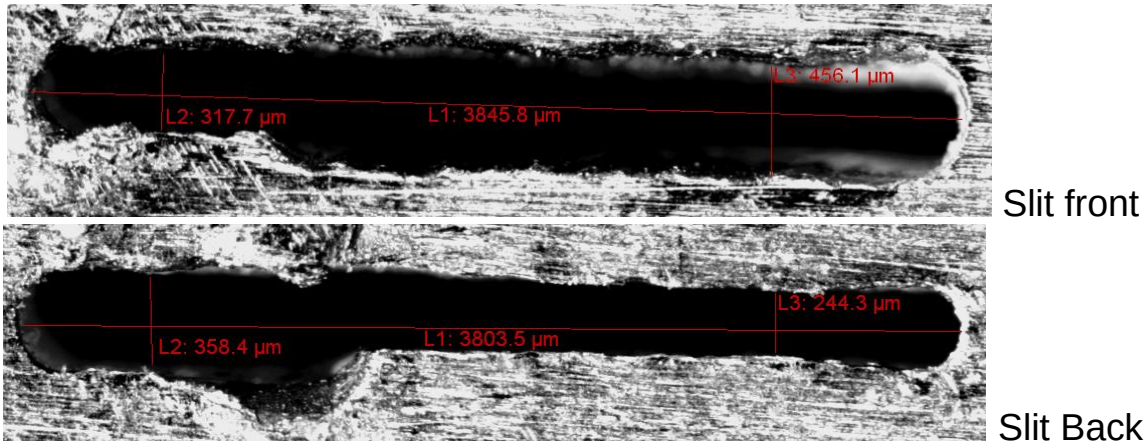

Figure 4.11: Slit crack test specimen #5

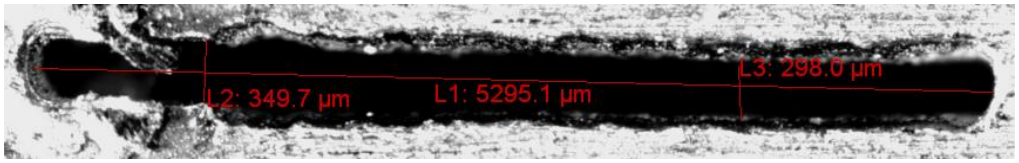

Slit front

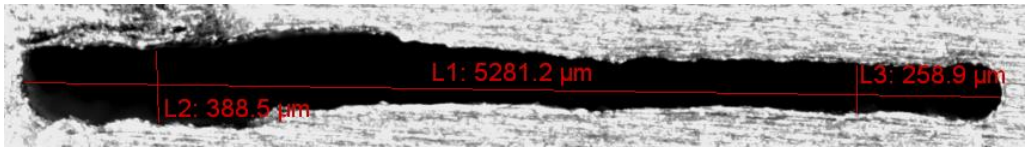

Slit Back

Figure 4.12: Slit crack test specimen #6

The effective cross sectional flow area was calculated by averaging the front and back cross section of the slit. In Table 4.2 and 4.3 dimensional characteristics of the pin hole and slit cracks respectively. In Figures 4.13 to 4.19, the laser machined and welded slit test specimens with L/D =1.7 to 2.1 are shown and in Table 4.4, the dimensional characteristics for these specimens are given.

Table 4.2: Dimensions and flow area of the pinhole test specimen # 1

Test Specimen	**Diameter (m)**	**Roughness (m)**	**Relative roughness**	**Flow area (m2)**
Pin Hole #1	4.57500E-04	2.50000E-05	5.46448E-02	1.64389E-07

Table 4.3: Dimensions and flow area of the slit test specimen # 2 to #6 (Batch 1)

Test Specimen	**Dimension (m)**		**Hydraulic Diameter (m)**	**Wall Roughness (m)**	**Relative roughness**	**Flow area**
	Length	Width				
Slit #2						
Upstream	2.4489E-03	4.7162E-04	7.9092E-04	3.5000E-05	4.4252E-02	1.1550E-06
Downstream	2.3049E-03	3.6242E-04	6.2635E-04	4.0000E-05	6.3862E-02	8.3534E-07
Slit #3						
Upstream	2.9774E-03	4.9457E-04	8.4824E-04	3.5000E-05	4.1262E-02	1.4725E-06
Downstream	2.7704E-03	3.0595E-04	5.5105E-04	4.0000E-05	7.2589E-02	8.4760E-07
Slit #4						
Upstream	3.3641E-03	4.0201E-04	7.1820E-04	3.5000E-05	4.8733E-02	1.3524E-06
Downstream	3.2868E-03	3.2985E-04	5.9953E-04	4.0000E-05	6.6719E-02	1.0842E-06
Slit #5						
Upstream	3.8458E-03	4.2150E-04	7.5973E-04	3.5000E-05	4.6069E-02	1.6210E-06
Downstream	3.8035E-03	2.8709E-04	5.3388E-04	4.0000E-05	7.4923E-02	1.0919E-06
Slit #6						
Upstream	5.2951E-03	3.1277E-04	5.9065E-04	3.5000E-05	5.9256E-02	1.6562E-06
Downstream	5.2812E-03	3.0750E-04	5.8116E-04	4.0000E-05	6.8828E-02	1.6240E-06

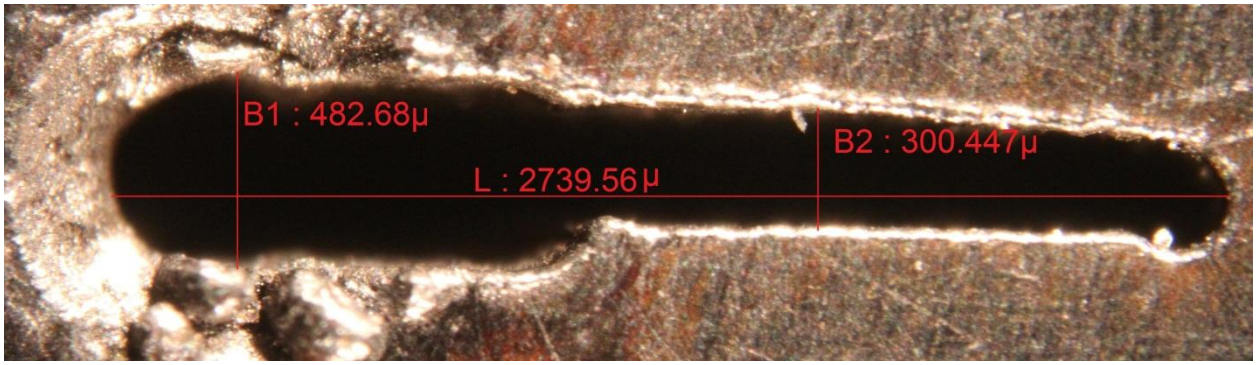

Figure 4.13: Laser 7 with dimensions that shrunk 40%, image taken post-weld, L/D of 2.1

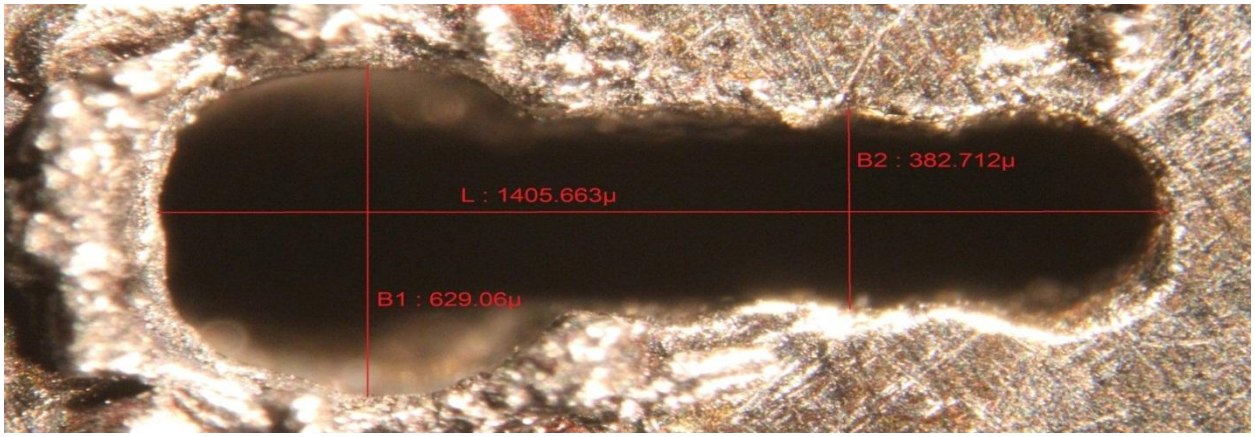

Figure 4.14: Laser8 with dimensions and L/D of 2.0

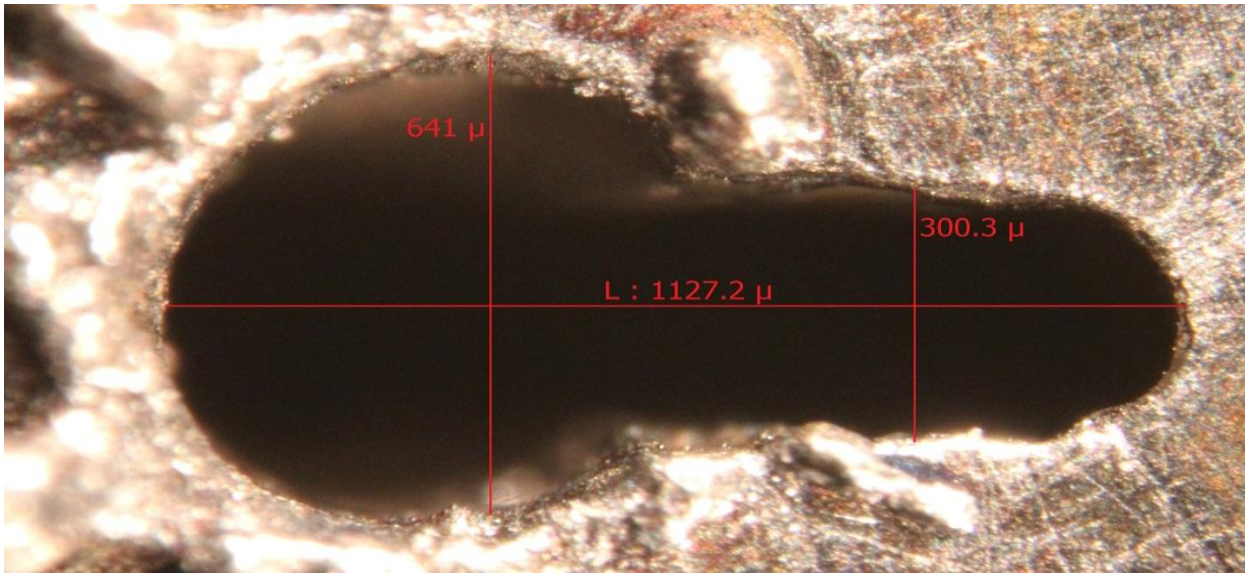

Figure 4.15: Laser9 with L/D of 2.1

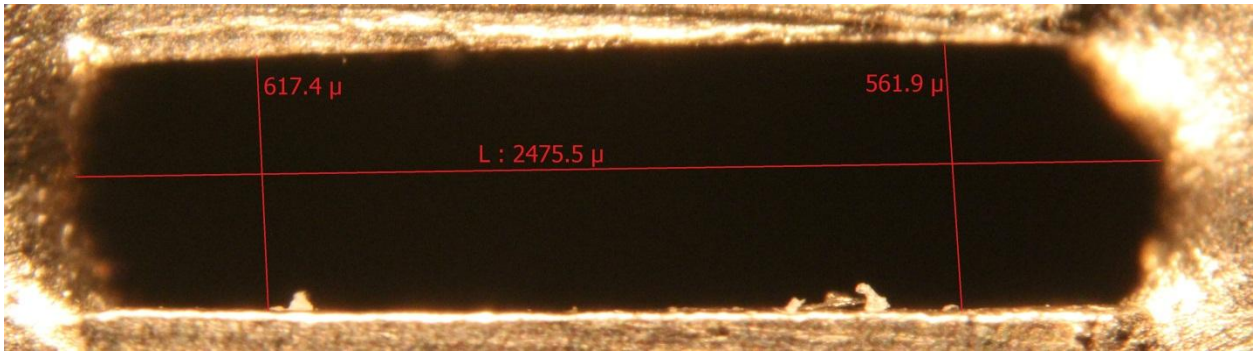

Figure 4.16: Weld10 with L/D of 1.3

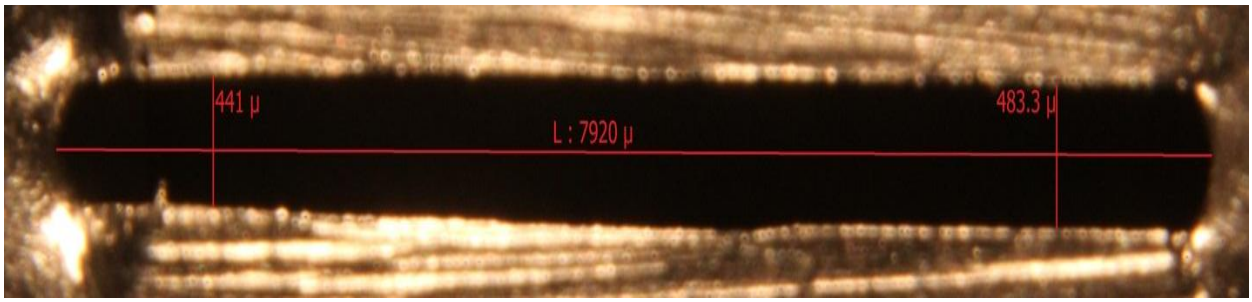

Figure 4.17: Weld11 with L/D of 1.2

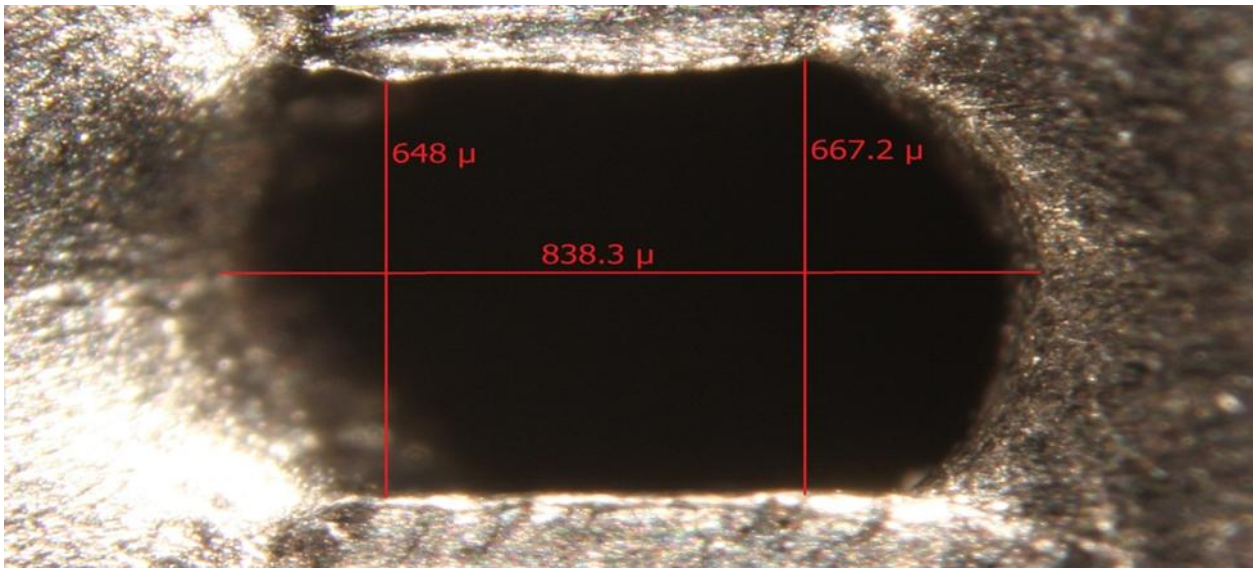

Figure 4.18: Weld13 with L/D of 1.7

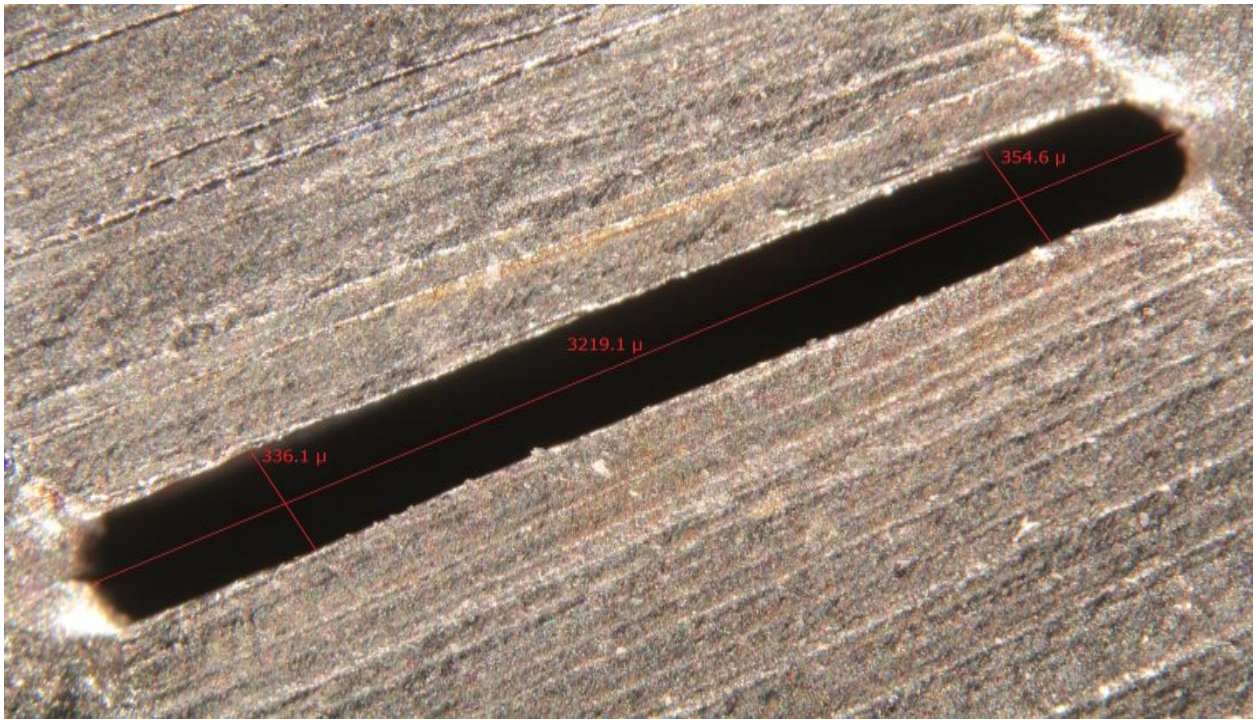

Figure 4.19: Weld12 with L/D of 2.1

Table 4.4: Sample Specimens tested in Batch 2

Sample	Area [m²]	Hydraulic Diameter Dh [m]	Channel Length L [m]	L/Dh
Laser7	9.060E-07	6.220E-04	1.300E-03	2.1
Laser8	5.769E-07	6.355E-04	1.300E-03	2.0
Laser9	4.639E-07	6.172E-04	1.300E-03	2.1
Weld10	1.404E-06	9.755E-04	1.300E-03	1.3
Weld11	4.594E-06	1.043E-03	1.300E-03	1.2
Weld12	1.110E-06	6.214E-04	1.300E-03	2.1
Weld13	5.132E-07	7.483E-04	1.300E-03	1.7

4.2.4 **Reduction of Raw Data**

In order to calculate the mass flow rates into the collecting tank in this experiment, load cells are utilized while data is also recorded from thermocouples at various points of the facility and a pressure transmitter to measure pressure upstream of the gauge and a differential Pressure Cell to record the water level change within the pressure vessel.
The data stored within the text file is imported to the Microsoft EXCEL® file and is reduced to find out:

i. The average Temperature of the water flowing through the choking plane in °C taken at a frequency of 1 Hz.

ii. The average temperature of the Nitrogen gas in the cylinder above the water in °C taken at a frequency of 1 Hz.

iii. The mass flow rate of water/steam into the collecting tank as measured by the load cells which is averaged for every 10 data points and is recorded at a frequency of 20 Hz.

iv. The mass flow rate as computed by the changing of water levels and nitrogen from the pressure vessel, factoring in the change of densities of both the nitrogen and water at different pressures and densities.

v. The average pressure as calculated by the pressure transmitter for the duration of flow, since the variation is very small and the inlet of nitrogen as water level is reduced causes the pressure vessel to behave at stagnation conditions.

The start and end points of this test are taken on the basis of the data from the pressure transducer just before the crack. The instant the valve is opened, the pressure reading spikes and the portion of the test considered relevant for calculating mass flow rate is while the pressure profile is constant. Figure 4.20 shows the plot of pressure versus time to determine the steady state condition for the data. The plot of averaged mass data (for every 10 data points) is shown with time in Figure 4.21 which shows a linear profile. The slope of this line gives the mass flow rate.

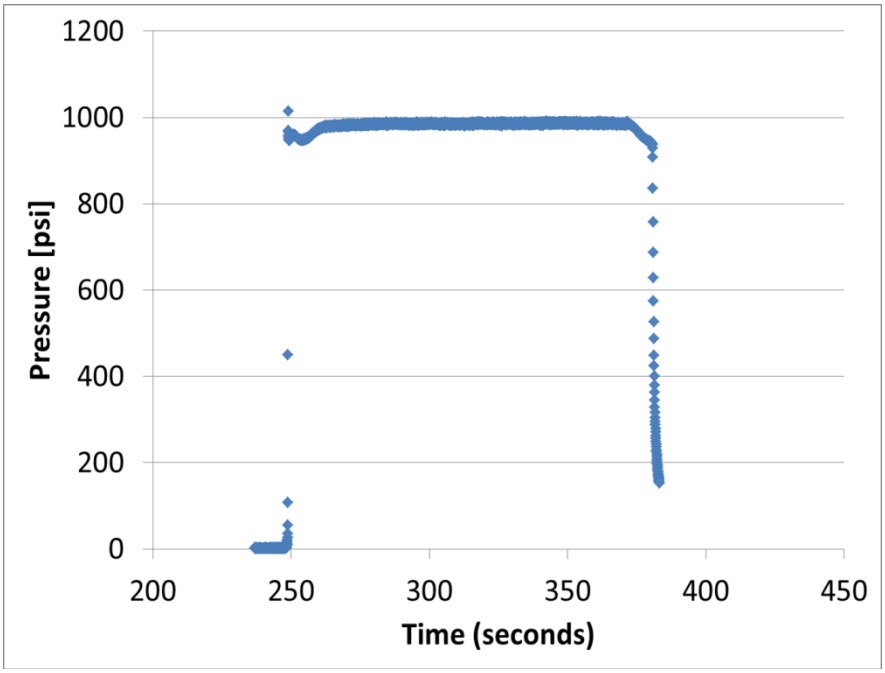

Figure 4.20: Figure of Pressure Profile vs. Time that is used to find the steady state condition after the opening of the valve

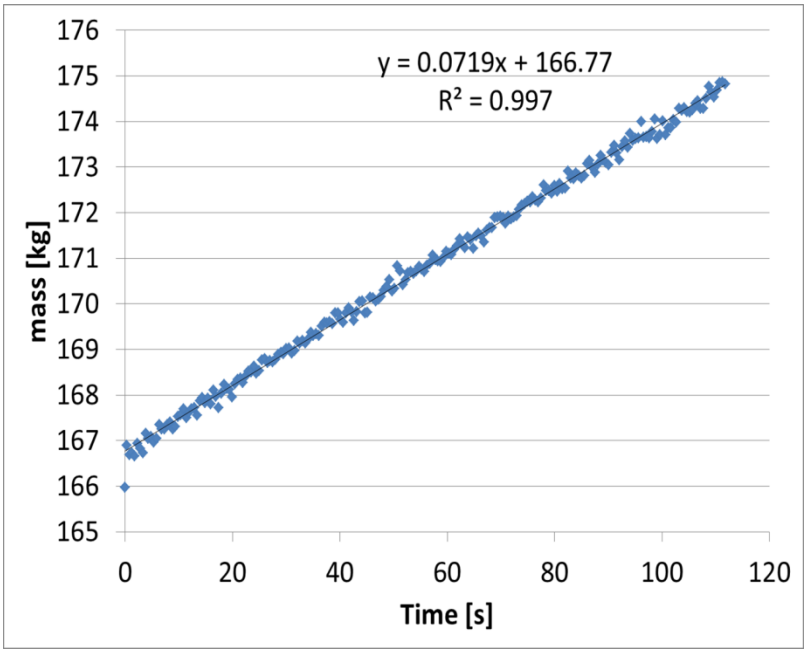

Figure 4.21: Plot of Mass Vs Time averaged every 10 data points used to find the mass flow rate, where initial mass is weight of tank and water combined

The time of the tests varies to a small extent with different stagnation conditions for the same sample but varies to a great degree with changing crack geometry. As recorded by this study, tests have lasted between an 80 seconds and 12 minutes, the latter time being for pinhole geometry with 457 micron size hole. Typical tests lasted between 80 and 300 seconds of measurement depending on the size of the crack and upstream pressure. For sample WELD11, whose crack length is on the order of about 0.0079 m gives an extremely rapid blowdown and high flow rate, draining the pressure vessel in about 30 seconds for 8 MPa pressure tests. Hence for this sample repeated tests were conducted to get average mass flow rate..

Prior to the start of experimentation, calibration of the instruments was done. The Load cells were calibrated by measuring the voltage readings for individual pours of 3 liters each and plotting the measured voltages Vs weight and compared to the manufacturer's ratings for highest and lowest readings, including the weight of the tank.

4.3 **Test Procedures:**

The following outlines the experimental procedures for operation of the leak rate facility.

i. Water used for the experiments was de-ionized and filtered prior to all tests.

ii. For each test the condensing tank was filled with DI water to an acceptable level above the flange exit.

iii. All electronic data acquisition tools are turned on or plugged in well before the test to allow all components to warm up. These include the data acquisition computer, the differential pressure (DP) cell power supply (~24.5 V), the load cell power supply (10 V), the load cell signal amplifier, and the digital thermocouple temperature display.

iv. Before filling the vent line (V3) is opened to allow air in the vessel to escape.

v. Using the DP cell signal, the pressure vessel is filled to half height using the fill line pump and opening V2 and V1.

vi. V1 and V2 are both closed when desired water level is reached.

vii. For non-heating experiments, V3 is closed and the Nitrogen regulator (V4) is opened to obtain the desired test pressure. For heating experiments, the vessel is pressurized to 50 psi and the heaters are plugged in. The water is allowed to reach saturation temperature and then V3 is opened to vent off to help de-gas the water and also allow better mixing for heating. V3 is then closed again.

viii. During heating the data acquisition system is turned on to help characterize the heating characteristics of the test, and to systematically watch the heating up parameters.

ix. Before the test begins, the pressure is double checked using the precision pressure gauge P1.

x. Once the desired temperature is met, the main valve V1 is opened using gloves and safety glasses. The safety shield is then lowered and the test is watched via the data acquisition computer.

xi. Once the water level is near the bottom of the pressure vessel (checked by DP cell) the test is stopped by closing V1 and stopping the data acquisition.

xii. The supply pressure valve V4 is then closed and V3 is opened to depressurize the vessel.

xiii. Doors to the facility are then opened to allow adequate air ventilation in the area.

4.4 **Test Results**

4.4.1 **Cold Water Discharge Tests**

Flow discharge tests were carried out with water at room temperature (20C). In Table 4.5, 4.6 and 4.7, the mass flow rate data, corresponding Reynolds number and discharge coefficient for pinhole specimen #1, slit #2 and slit #6, are shown. For slit geometry, the equivalent hydraulic diameter was used while calculating the Reynolds number. For pinhole #1, the mass flux as function of upstream pressure it is shown in Figure 4.22. Since the water is discharged to atmospheric pressure, the upstream pressure represent total pressure drop across the slit. In Figures 4.23, 4.24, the mass flux is shown as function of pressure are shown for slit #2 and slit#6 respectively. The trend lines show square root fit to the pressure –showing that, in both cases, the mass flux increases as a square root of pressure. In Table 4.8, and 4.9, the cold water mass flow rate data, the corresponding Reynolds number and discharge coefficient for specimen Laser8, and Weld10, are shown and in Figures 4.25 and 4.26, the corresponding mass fluxes as function of pressure are shown.

Table 4.5: Cold Water discharge characteristics for Pinhole #1

P [kPa]	m [kg/s]	Temperature [C]	G [kg/m^{2}s]	Re	Cd
137.80	1.30000E-03	22.1	7.90810E+03	3.61790E+03	4.79240E-01
689.00	2.76670E-03	23.4	1.68300E+04	7.69970E+03	4.56120E-01
1378.00	4.10000E-03	22.0	2.49410E+04	1.14100E+04	4.77960E-01
2067.00	4.90000E-03	21.1	2.98070E+04	1.36370E+04	4.66400E-01
2756.00	5.60000E-03	20.8	3.40660E+04	1.55850E+04	4.61620E-01
3445.00	6.40000E-03	23.1	3.89320E+04	1.78110E+04	4.71870E-01
4134.00	6.80000E-03	22.6	4.13650E+04	1.89250E+04	4.57680E-01
4823.00	7.70000E-03	23.3	4.68400E+04	2.14290E+04	4.79810E-01
5512.00	8.30000E-03	23.2	5.04900E+04	2.30990E+04	4.83790E-01

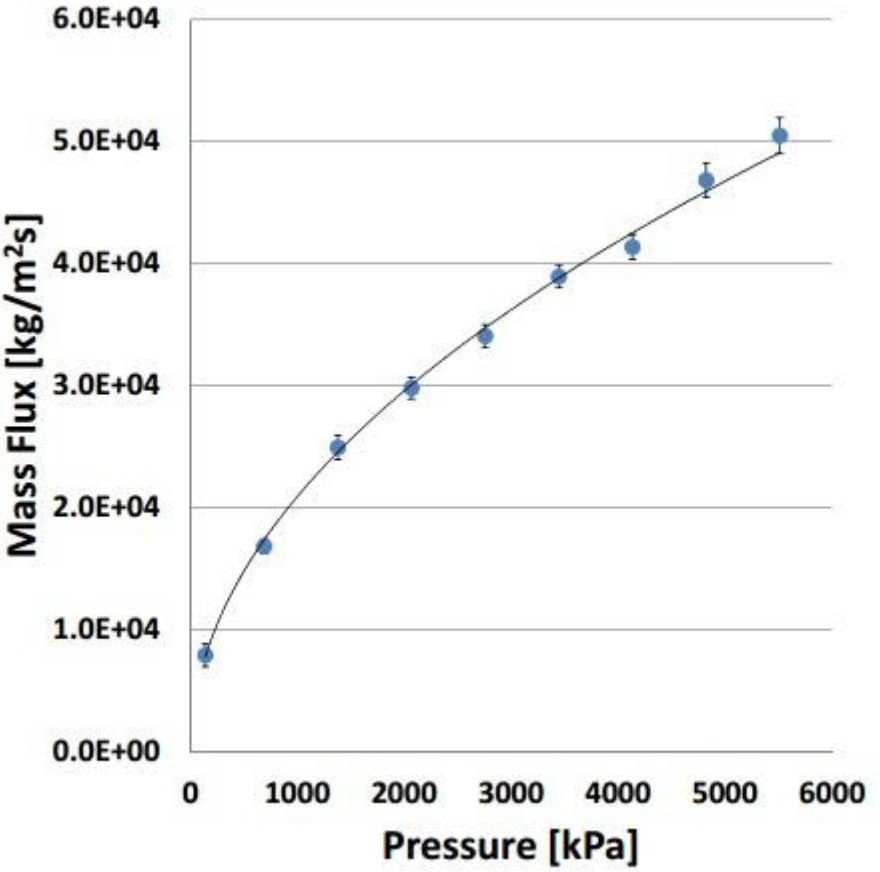

Figure 4.22: Cold Water Discharge Mass Flux for Pinhole #1

Table 4.6: Cold Water Discharge Characteristics for Slit# 2

P [kPa]	M [kg/s]	Temperature [C]	G [kg/m^{2}s]	Re	Cd
646.97	2.1300E-02	24.1	2.5499E+04	1.5971E+04	7.1315E-01
1455.17	3.2300E-02	23.2	3.8667E+04	2.4219E+04	7.2109E-01
2636.80	4.3700E-02	23.4	5.2314E+04	3.2767E+04	7.2475E-01
4168.45	5.6000E-02	23.1	6.7039E+04	4.1990E+04	7.3866E-01
5414.16	6.3600E-02	20.8	7.6137E+04	4.7688E+04	7.3610E-01
6657.81	7.1400E-02	20.1	8.5474E+04	5.3537E+04	7.4521E-01

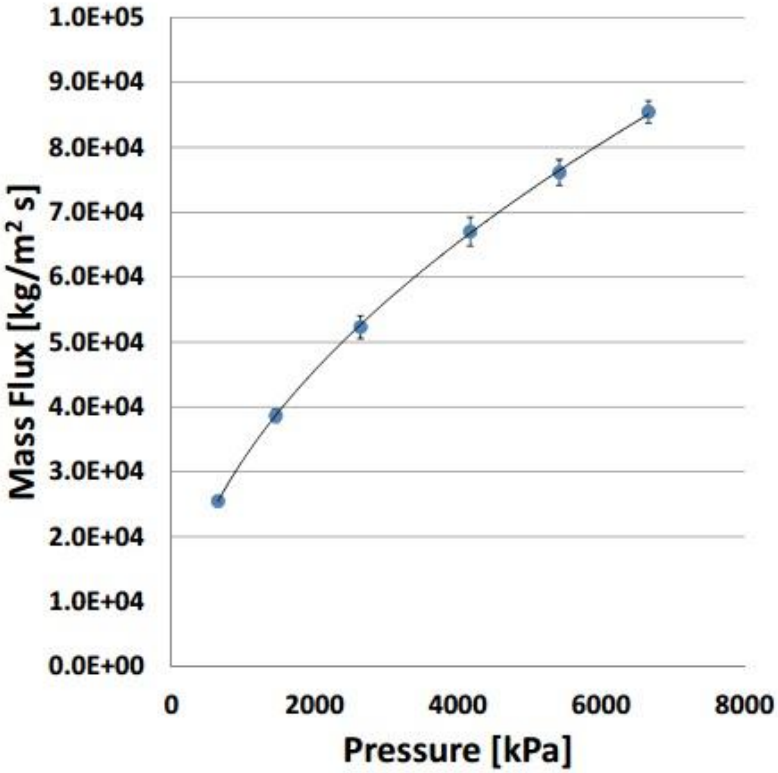

Figure 4.23: Cold Water Discharge Mass Flux for Slit #2

Table 4.7: Cold Water Discharge Characteristics for Slit# 6

Pressure [kPa]	m [kg/s]	Temperature [C]	G [kg/m^{2}s]	Re	Cd
704.85	3.25E-02	25.9	2.00E+04	1.40E+04	5.34E-01
1417.96	5.49E-02	29.2	3.38E+04	2.55E+04	6.36E-01
3083.96	9.76E-02	23.5	6.01E+04	3.84E+04	7.66E-01
4083.7	1.20E-01	25.8	7.41E+04	5.17E+04	8.22E-01
5551.96	1.34E-01	20.8	8.27E+04	4.81E+04	7.86E-01
6850.04	1.52E-01	20.1	9.34E+04	5.43E+04	7.99E-01

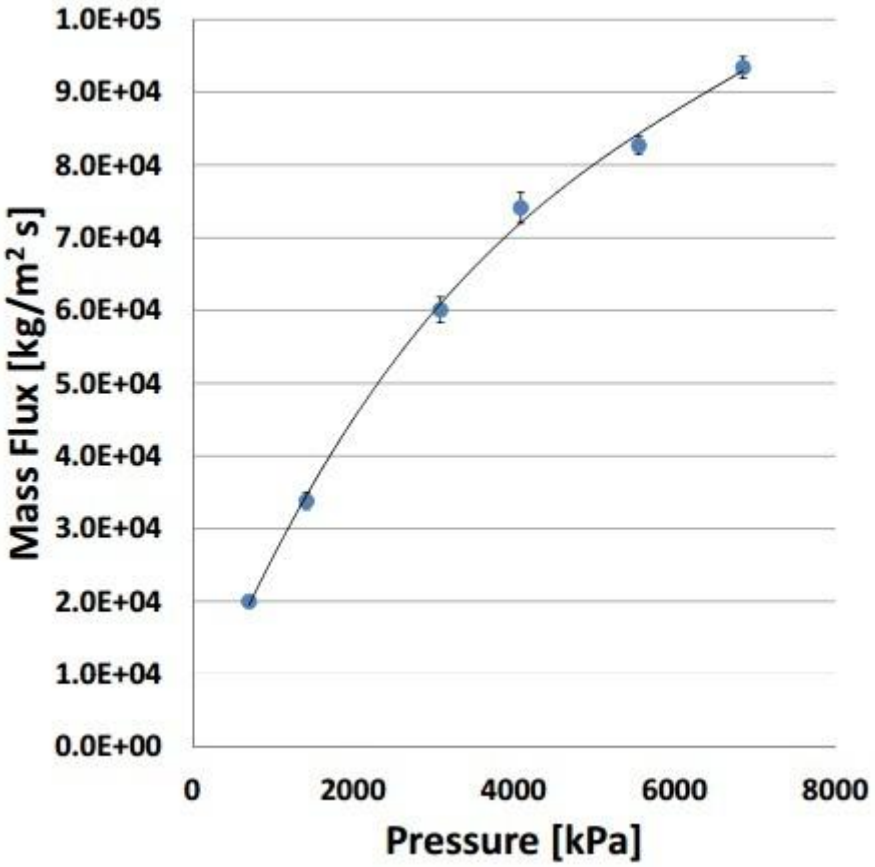

Figure 4.24: Cold Water Discharge Mass Flux for Slit# 6

Table 4.8: Cold Water Discharge Characteristics for Sample Laser8

Pressure [Kpa]	Subcooling ΔT [°C]	Area [m²]	Dh [m]	G [kg/m²s]	Re
638	139.2	5.7688E-07	6.3554E-04	1.898E+04	12682
1469	175.1	5.7688E-07	6.3554E-04	2.985E+04	20008
2736	206.6	5.7688E-07	6.3554E-04	4.037E+04	27611
5399	245.9	5.7688E-07	6.3554E-04	5.366E+04	37361
6636	259.6	5.7688E-07	6.3554E-04	6.229E+04	39506

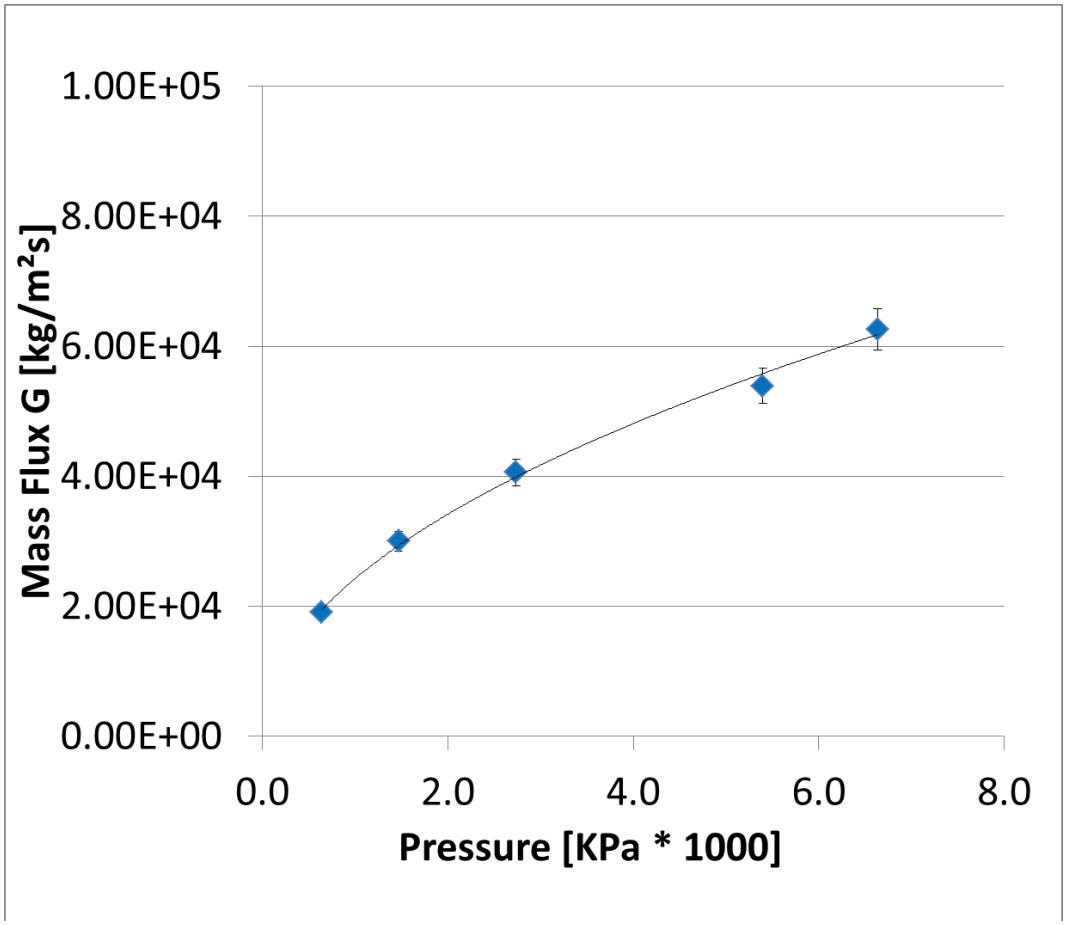

Figure 4.25: Cold Water Discharge Mass Flux for Sample Laser8

Table 4.9: Cold Water Discharge Characteristics for Sample Weld10

Pressure [Kpa]	Subcooling ΔT [°C]	Area [m²]	Dh [m]	G [kg/m²s]	Re
606	137.6	1.4039E-06	9.7550E-04	2.158E+04	21795
1315	170.7	1.4039E-06	9.7550E-04	3.134E+04	31518
2704	206.7	1.4039E-06	9.7550E-04	4.416E+04	44412
4017	228.7	1.4039E-06	9.7550E-04	5.271E+04	53063
5444	247.6	1.4039E-06	9.7550E-04	6.268E+04	63429
6497	259.5	1.4039E-06	9.7550E-04	6.909E+04	69916

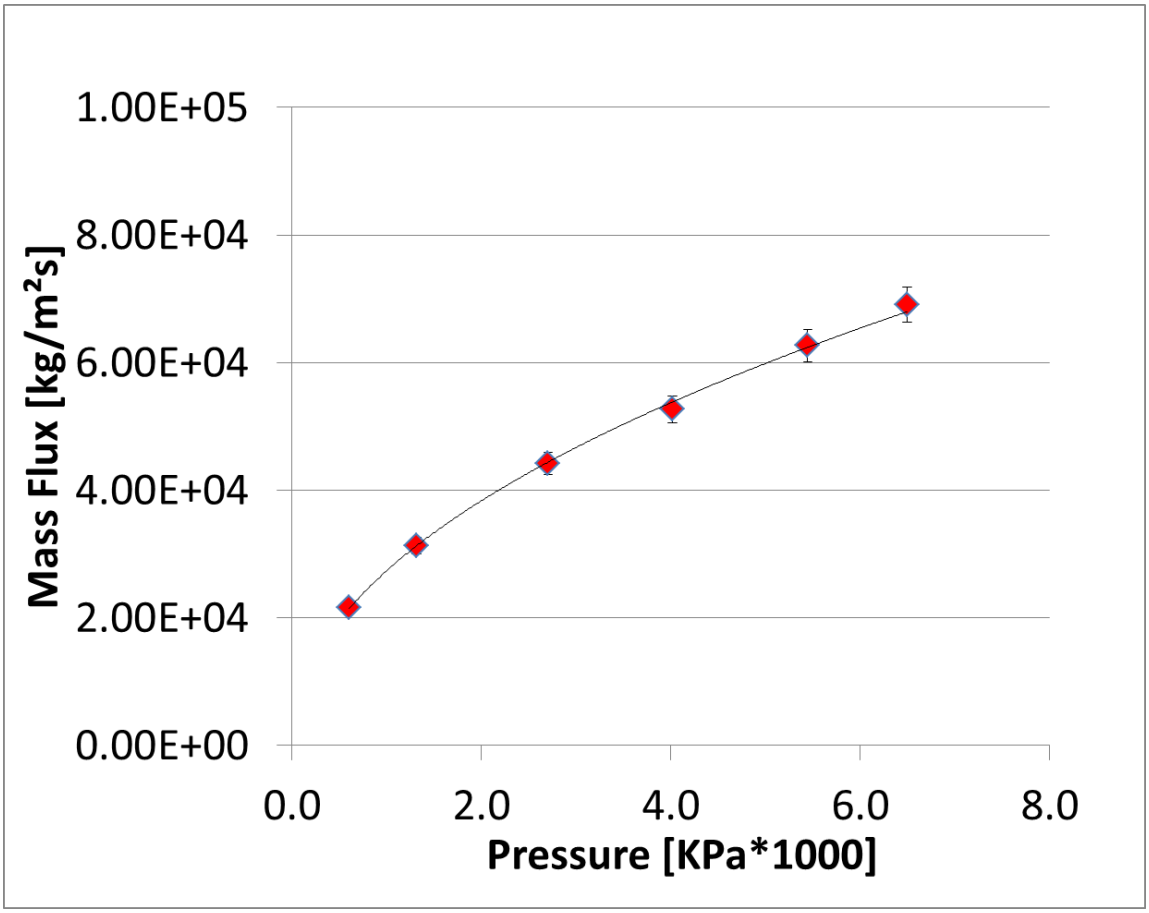

Figure 4.26: Cold Water Discharge Mass Flux for Sample Weld10

4.4.2 **Subcooled Flashing Discharge Tests**

Test of flashing choked flow with heated water were carried out up to a vessel pressure of 6.89 MPa (1000 psi). As the experimental program was designed around testing choking flow through steam generator tube cracks, the most valuable data are those at the highest pressures. The tests carried out at approximately 6.89 MPa, have a pressure differential across the choking plane of near equal value. This is approaching the same pressure differential across the walls of steam generator tubes. However, the differential in actual steam generators is from approximately 14 MPa to 4.5 MPa, not from 7 MPa to 0.1 MPa. Complete scaling of choking flow is not possible within the

constraints of this project however, a scaling method is proposed in Chapter 8. The tests carried out were varied with subcooling at near the same pressures.

The tests carried out were varied with subcooling at near the same pressures. A list of subcooled choking flow measurements for various specimens can be seen in Table 3.9. Pressures for the tests ranged from 6.87 MPa to 6.60 MPa, with a range of subcooling between 48.1 and 24.7. The highest mass flux for each specimen was obtained at the highest subcoolings, along with the lowest mass flux for the lowest subcoolings as expected. A representation of the mass flux data with respect to subcooling can be seen in Fig. 4.27. The vertical bars are given as a reference to the error involved in each measurement. As the subcooling increased for each specimen the mass flux increased. In general as the mass flux also increased as the area of the specimens increased. The hydraulic diameter however of specimens #2 and #3 are nearly identical.

Table 4.10 Summary of flashing flow discharge results for specimens Slit#2- Slit#6 near 6.8 MPa

Spec. #	Pressure [Mpa]	Temp. [°C]	ΔT_{sub} [°C]	M [kg/s]	Gc [kg/m2 s]
2	6.7277	237.0	46.1	5.430E-02	6.571E+04
	6.7348	241.2	42.1	5.180E-02	6.268E+04
	6.8737	252.1	32.5	4.630E-02	5.603E+04
3	6.7346	237.9	45.3	6.740E-02	7.090E+04
	6.7280	244.2	38.9	6.500E-02	6.837E+04
	6.7585	249.4	34.1	6.090E-02	6.406E+04
	6.8659	254.7	29.9	5.970E-02	6.280E+04
4	6.7698	235.5	48.1	7.540E-02	6.111E+04
	6.7760	245.4	38.2	7.150E-02	5.795E+04
	6.8310	251.4	32.8	6.680E-02	5.414E+04
	6.8178	256.4	27.7	6.500E-02	5.268E+04
5	6.6980	235.9	46.9	9.040E-02	6.652E+04
	6.7703	243.5	40.0	8.860E-02	6.520E+04
	6.7860	251.7	31.9	7.630E-02	5.615E+04
	6.8487	257.0	27.4	7.570E-02	5.571E+04
6	6.6810	236.4	46.3	1.205E-01	6.934E+04
	6.5970	243.3	38.5	1.066E-01	6.134E+04
	6.7672	250.2	33.4	1.038E-01	5.973E+04
	6.7367	258.6	24.7	9.730E-02	5.599E+04

The tests carried out for slit #2 at various pressures shown in Table 4.11 indicate that the flow rate is dependent on subcooling. Subcooling for the tests varied from 15 C to 29 C. The heated water flashes as it is discharged from the cracks and hence the mass flux discharge decreases with the heated tests. The comparison between cold water tests discharge and heated tests discharge for slit #2 can be seen in Figure 4.28 as a function of pressure. There is a slight offset in the third data point for flashing flow for slit #2 near 5.3 MPa. This lower flow rate than expected could not be explained until the test section was taken apart. It was found that a tiny piece of metal from the steel threads of a recently installed valve had come loose and lodged into the choking area. While studying flow in small channels this type of interruption can be common, as particles in the stagnant fluid can easily wedge into the flow channel. This lead to the additional step in the test procedure of dismantling the test section before each run, checking and reinstallation.

Data for measured mass discharge rate for slit #6 at different pressures is shown in Table 4.12. It can be seen from the data that tests were carried out at four different

subcoolings near the same pressure of 3.6MPa. This allows for the dependence of mass discharge rate on subcooling to be examined. The variance in pressure for these runs was less than 0.08 MPa (11 psi). The critical mass flux as a function of subcooling can be seen in Figure 4.29. As expected, the mass flux increases as subcooling increases.

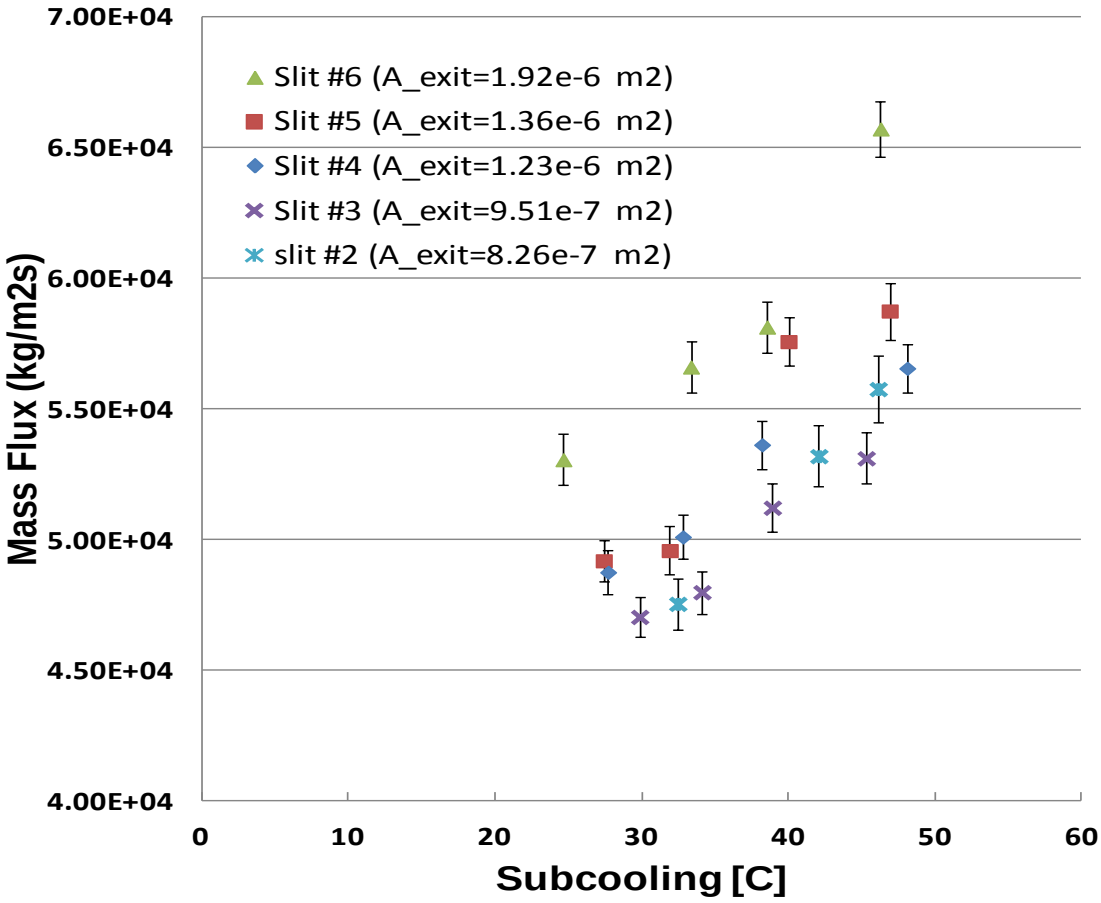

Figure 4.27. Critical mass flux as a function of subcooling for specimens Slit#2- Slit#6 at about 6.8 MPa

Table 4.11: Subcooled Discharge Characteristics for Slit# 2

P [kPa]	Temp [C]	Subcooling [C]	M [kg/s]	G [kg/m^{2}s]
1491.69	183	15.02	2.53E-02	3.03E+04
3376.1	218	22.49	3.34E-02	4.00E+04
5374.2	248	20.49	4.03E-02	4.82E+04
6814.21	255	29.01	5.31E-02	6.36E+04

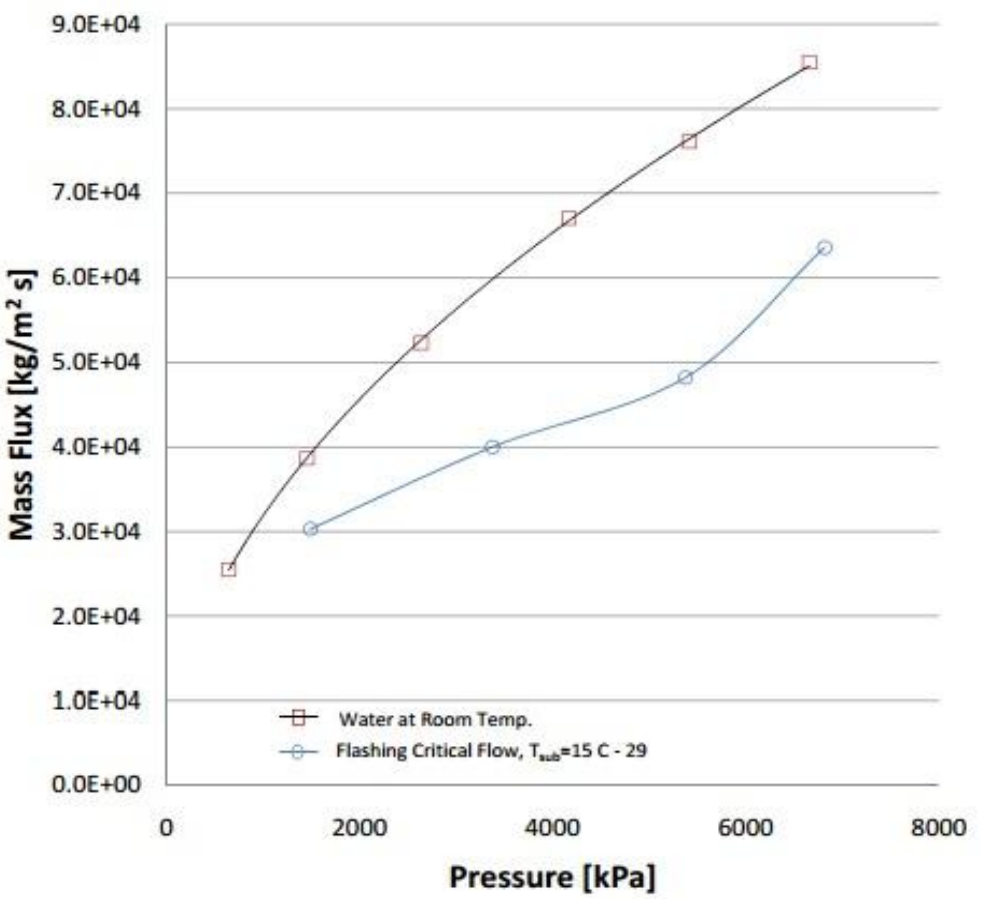

Figure 4.28: Subcooled Discharge Mass Fluxes compared to Cold Water Discharge for Slit# 2.

Table 4.12 Flashing flow discharge from slit #6 for different subcooling at near constant pressure of P ≈ 3.6 MPa.

P [kPa]	Temp. [°C]	Subcooling [°C]	M [kg/s]	Gc [kg/m² s]
3550.8	203.6	39.7	9.52E-02	5.8621E+04
3552.1	211.7	31.6	8.77E-02	5.4002E+04
3610.7	220.5	22.8	7.60E-02	4.6798E+04
3630.9	224	19.3	6.95E-02	4.2796E+04

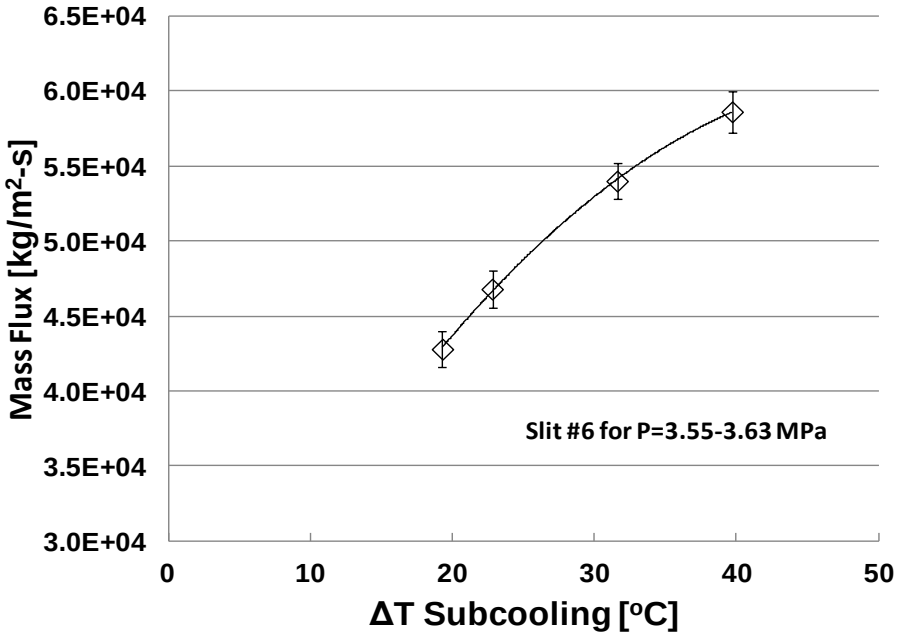

Figure 4.29. Critical mass flux for slit #6 for different subcooling at near constant pressure of P ≈ 3.6MPa.

Using the test specimens from Batch 2, listed in Table 4.4, low subcooling tests were conducted whose flow/channel lengths L/D equaled that of Westinghouse and Combustion Engineering‟s steam generator tubes, i.e., L/D = 1.2- 2.1. These tests attempted to CANDU and PWR SG crack channel conditions as close as possible and the important parameters that affect mass flux are the pressure differential across the crack channel and the degree of subcooling of the fluid. Thus tests were conducted up to maximum pressure differentials of approximately 6.89 MPa (1000 psi) while a variety of subcoolings were studied ranging from 15 °C to 50 °C. In Table 4.13 the measured mass flux for test specimen Laser7, Laser8, Laser9, Weld10, Weld11, Weld 12 and Weld13 are given for various subcooling and upstream pressures. These data are compared with Batch 1 test specimen data in Figure 4.30, where the choking mass flux data are shown for various subcoolings and pressure conditions. Data shows similar trend as seen from Batch 1 test specimen given in Figure 4.27, where the choked flow increases with increase in subcooling.

In Table 4.14, the Subcooled mass flux measured with Laser8 specimen is shown for subcooling ranging from 19.5C to 46C at upstream pressure between 1.5 MPa to 6.8 MPa. In Figure 4.31, the subcooled choked flow is compared with cold water discharge for this Laser8 specimen. Table 4.14 and Table 4.8 show the data used in Figure 4.31. The highest mass flux for each specimen was obtained at the highest subcoolings, along with the lowest mass flux for the lowest subcoolings as expected. As the subcooling increased for each specimen the mass flux increased. In general as the mass flux also increased as the area of the specimens increased. The hydraulic diameters however of specimens #2 and #3 are nearly identical.

Table 4.13: Summary of flashing flow discharge results for specimens Laser7-9 and Weld10-13 near 6.8 MPa

Sample	Pressure	Temperature T [°C]	Subcooling ΔT [°C]	m LC [kg/s]	G [kg/m²s]
Laser7	6756	239.8	43.6	0.0711	7.8476E+04
	6877	234.3	50.3	0.0719	7.9359E+04
	6764	245.5	38.0	0.0618	6.8211E+04
	6708	250.7	32.2	0.0566	6.2472E+04
	6806	260.9	23.0	0.0688	7.5938E+04
	6583	267.4	14.1	0.0527	5.8167E+04
Laser8	6641	235.5	46.8	0.0289	5.0097E+04
	6746	232.8	50.5	0.0287	4.9751E+04
	6741	243.4	40.0	0.0299	5.1831E+04
	6649	243.9	39.0	0.0285	4.9404E+04
	6821	248.8	35.3	0.0312	5.4084E+04
	6933	256.7	28.2	0.026	4.5070E+04
	1518	171.7	27.1	0.015	2.6002E+04
	3537	223.7	19.5	0.0199	3.4496E+04
	5683	241.9	30.1	0.0263	4.5590E+04
	6776	253.3	30.3	0.0316	5.4778E+04
Laser9	6768	233.1	50.4	0.0278	5.9001E+04
	6761	232.3	51.1	0.0362	7.6828E+04
	6845	244.4	39.9	0.0332	7.0461E+04
	6826	240.1	44.0	0.0278	5.9001E+04
	6787	247.9	35.8	0.0312	6.6217E+04
	6900	255.6	28.8	0.0302	6.4094E+04
Weld10	6715	236.3	46.7	0.093	6.6243E+04
	6853	243.0	41.3	0.093	6.6243E+04
	6851	251.6	32.7	0.0943	6.7169E+04
	6852	258.8	25.5	0.082	5.8407E+04
Weld12	6799	234.8	49.1	0.0792	7.1330E+04
	6932	242.4	42.7	0.0917	8.2588E+04
	6856	249.6	34.8	0.0835	7.5203E+04
	6788	259.5	24.2	0.0719	6.4755E+04
Weld11	6847	256.3	28.0	0.2283	4.9697E+04
	6758	246.3	37.1	0.2527	5.5008E+04
	6702	237.7	45.2	0.2685	5.8448E+04
Weld13	6798	235.9	48.0	0.0435	8.4766E+04
	6853	241.5	42.9	0.0383	7.4633E+04
	6840	248.5	35.7	0.0453	8.8273E+04
	6918	256.8	28.2	0.0346	6.7423E+04
	1440	172.1	24.3	0.0241	4.6962E+04
	3514	226.3	16.5	0.0306	5.9628E+04
	5592	244.2	26.8	0.0309	6.0213E+04

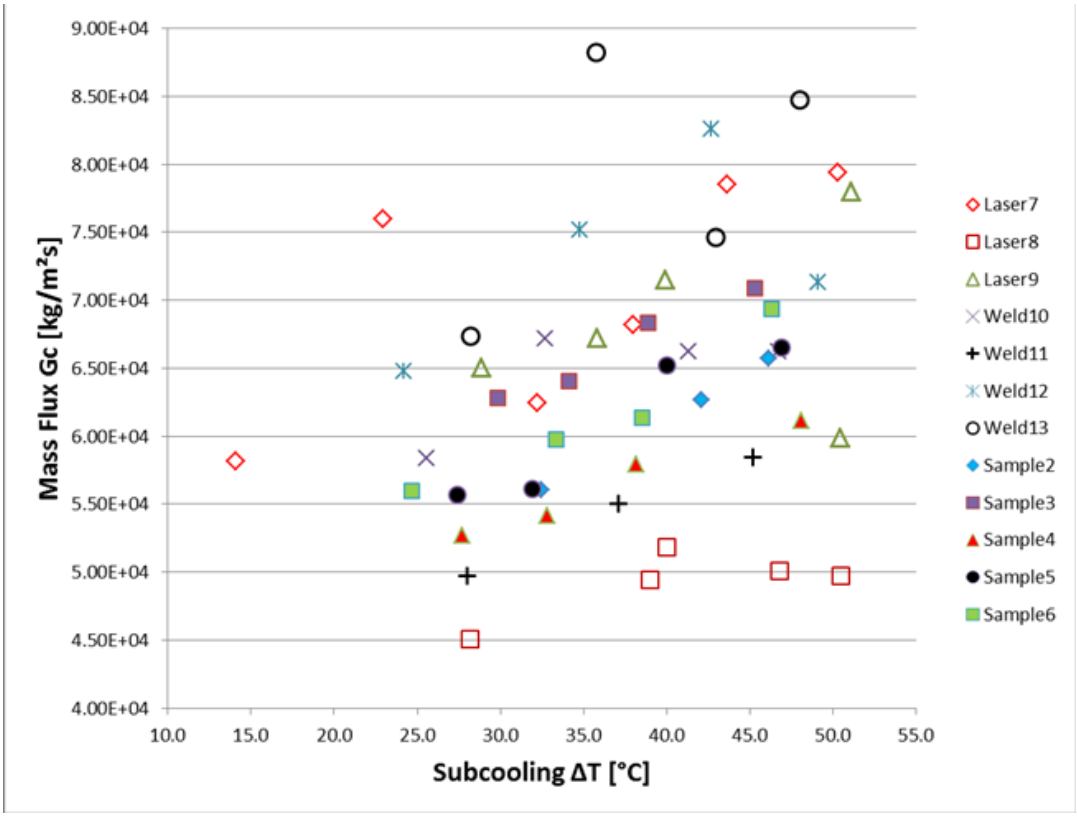

Figure 4.30 Choking mass flux for test specimen Batch 1 (Slit#2-6 referred as Sample2-6) compared with test specimen Batch 2 (Laser7-9 and Weld 10-13) for different subcooling.

Table 4.14: Subcooled Discharge Characteristics for Sample Laser8

Pressure Kpa	Temperature T [°C]	Subcooling ΔT [°C]	mass flow rate [kg/s]	G Mass Flux [kg/m²s]
6641	235.5	46.8	0.0289	5.0097E+04
6746	232.8	50.5	0.0287	4.9751E+04
6741	243.4	40.0	0.0299	5.1831E+04
6649	243.9	39.0	0.0285	4.9404E+04
6821	248.8	35.3	0.0312	5.4084E+04
6933	256.7	28.2	0.026	4.5070E+04
1518	171.7	27.1	0.015	2.6002E+04
3537	223.7	19.5	0.0199	3.4496E+04
5683	241.9	30.1	0.0263	4.5590E+04
6776	253.3	30.3	0.0316	5.4778E+04

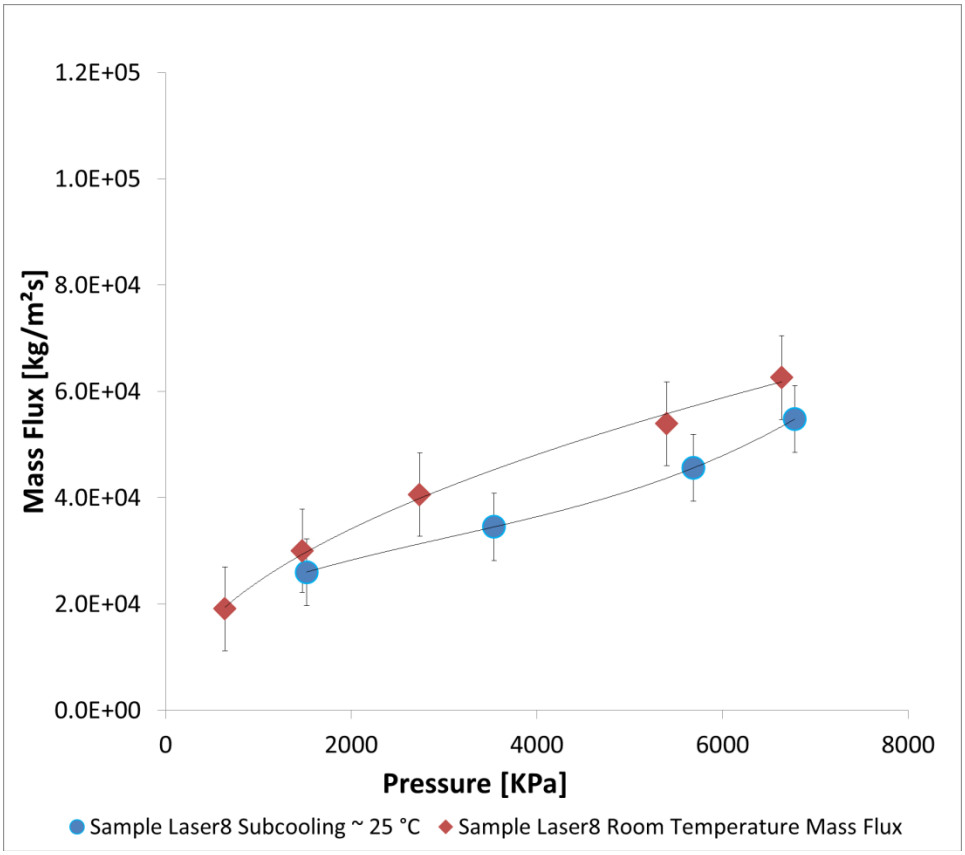

Figure 4.31: Subcooled Discharge Mass Flux compared with Cold Water Discharge for Sample Laser8

It should be noted that L/D for Slit#2 and Laser8 are 5.2 and 2.1 respectively. When Figures 4.28 and 4.31 are compared its shows that the difference between the cold water discharge flow rate and subcooled choking flow rate is lower for smaller L/D test specimen. This indicates that smaller L/D has high thermal non-equilibrium effect on the flashing flow.

Since the L/Ds being studied as a part of this research program are unique, it was decided to take samples from the studies conducted by Amos & Schrock, (1983) whose areas are similar to the samples studied. Studying data for similar pressures and degrees of subcooling will allow us to examine the effect of channel length L and the L/D ratio on mass flux. In Figure 4.32, the choking mass flux is plotted as function of L/D for various subcoolings. This data clearly demonstrate that increasing subcooling increases mass flux and lowering L/D also increases mass flux.

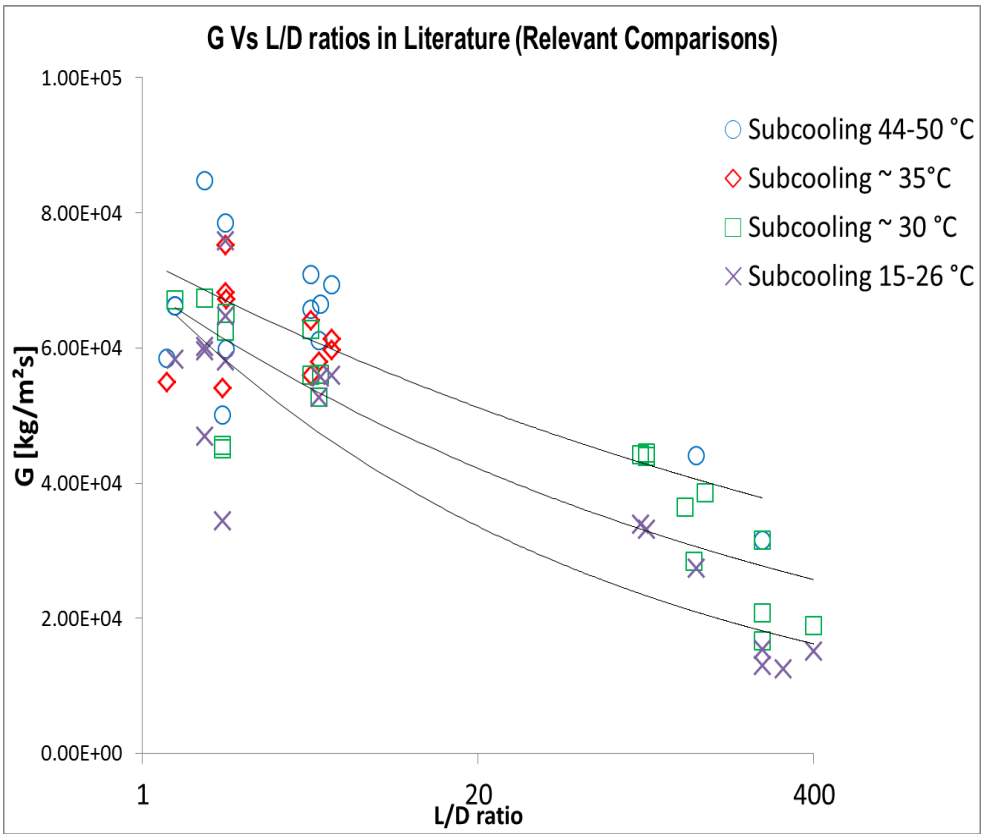

Figure 4.32 Plot of Mass Flux Vs L/D ratios for similar subcoolings clearly showing the effect of lowering L/D increases mass flux.

4.5 **Conclusions**

An experimental program is in place and being used to collect data for choking leak rates through simulated steam generator tube cracks. Laser cut slits are used to simulate the SG cracks. High definition optical microscopy was used to help determine the characteristics of the test specimens. The Length to Diameter ratio of the specimens ranges from 4.48 to 6.94 in Batch 1 and then from 1.1 to 2.1 in Batch 2, experiments on which is underway and is in a range in which there is very little experimental data, especially for short L. Using cold water discharge tests, the discharge coefficients for each specimen was determined. These discharge coefficients are different than 0.61 typically used for sharp edged orifice plates. Heated tests were performed for flashing choked flow at high pressures and temperatures. These tests showed the effect of subcooling on the discharge rate, as well as the effect of stagnation pressure. This data is useful in helping determine the characteristics of small L/D cracks that have developed in steam generator tubes in service. These data may also be useful in future modeling efforts in range of the tests conducted.

5. CHOKING FLOW MODEL

5.1 Introduction

In this chapter, experimental results are compared to theoretical models for two-phase critical flow. Only simple models will be considered, as the complexity of implementing a two-fluid model is not advantageous. Not only is it costly to apply a two-fluid model, but the interphase transfer terms have been mostly developed for flow in a much larger channel than considered in this work, and are largely dependent upon flow.

As was noted in Chapter 4, many different assumptions have previously been made in modeling such flow those are not necessarily justified. While the goal of two-phase critical flow models is to predict experimentally determined flow rates, agreement between model prediction and experiments does not prove the assumptions made are justified. For example, neglecting friction and assuming isentropic flow in a constant area channel is not physical.

The main focus of this chapter will be on the derivation and implementation of both homogeneous equilibrium and homogeneous non-equilibrium models.

5.2 Solution Procedure

A computer program is developed in MATLAB which performs the numerical calculations of the model equations described. Fluid stagnation state, channel geometry, entrance loss coefficient, and single phase Darcy friction factor are input quantities. An iterative solution technique is applied. An initial guess of the mass flow rate M is given to the program. Using a combination of bisection and interpolation algorithms, the program then finds the mass flux for which the flow is predicted to be critical at the exit plane of the channel. At each grid point the sound speed is calculated to check whether the flow is choked. If the initial guess of mass flow rate results in subcritical flow at the exit, the assumed flow rate is increased. After sequential increase in mass flow rates, eventually a value will be specified that causes choking upstream of the exit. This flow rate and the immediately preceding flow rate then bound the solution. The program then reduces the bounds until a mass flow rate is found that causes choking at the last grid point within a specified tolerance.

A similar technique is used if the first guess of mass flow rate predicts choking to occur before the exit.

Integration of the model equations was performed by ordinary differential equation solvers which are part of the MATLAB libraries. The single-phase fluid equations are solved using a 5th order Runge-Kutta scheme. The integration of the single-phase field equations is terminated once flashing occurs. The solution is then supplied to another routine which solves for the two-phase dependent variables using a multi-step Adams-Bashforth-Moulton predictor-corrector solver.

These routines allow for user defined 'events' to be analyzed at each time step and the integration is halted if the input function is zero. This allowed for termination of the single-phase integration at the flashing location by defining the flashing criteria as a function of the solution. The function employed for the flashing criteria for the homogeneous equilibrium model is:

$$C_{fl}(Y, z) = P - P_{sat}(T) \tag{5.1}$$

where Y is a vector of dependent variables and z is the location along the channel. For the homogeneous non-equilibrium model, C_{fl} was given by:

$$C_{fl}(Y, z) = P - P_{sat}(T) + P_{fl} \tag{5.2}$$

where P_{fl} is given by the Alamgir-Lienhard correlation as a function of P, T_l and u. Integration of the single-phase flow equations was terminated once the flashing criterion ($C_{fl} = 0$) was met.

Similarly, the integration of the two-phase flow equations was terminated when critical flow criteria was met. The form of the critical flow criteria was:

$$C_{Gc}(Y, z) = G_c(Y) - u\rho(Y) \tag{5.3}$$

Here, the critical mass flux, $G_c(Y)$, was calculated using the appropriate sound speed definition for the model being used. Supersonic choking was assumed to occur if

$$C_{Gc}(Y, z) < 0 \text{ at } z = z_{fl}. \tag{5.4}$$

In some instances, the two-phase pressure gradient becomes too large for integration to continue. As the pressure difference is the main driving force of the fluid, the point at which the pressure gradient becomes excessively large the fluid is accelerated greatly. Therefore, when the two-phase pressure gradient exceeds 10^{13} Pa/m integration is stopped and the flow is assumed to be choked.

As mentioned above, thermodynamic properties were coded into MATLAB using two different approximation techniques outlined by Ishimoto et al., (1972) and Garland et al., (1992). It is extremely important that the property values and their derivatives are approximated well otherwise the value of the predicted mass flux could be affected greatly. Two different property routines were coded in order to compare and check the coded approximations. The comparison of the two property routines for saturated water at a given pressure can be seen in Table 4.1. As can be seen, all the property values and their derivatives agree well and fall within 2% of each other. Subcooled water properties and their derivatives were calculated in a similar manner using a separate subroutine. These values were also calculated based on the approximations given by Garland et al. (1992). Superheated fluid properties were estimated by extrapolating the subcooled liquid properties into the superheated region.

In the case where friction factor is not known or well established, roughness values are used to determine an appropriate friction factor. In the case of rough pipe flow, the viscous sub layer thickness is small compared to the roughness height and therefore the flow is dominated by the roughness of the pipe wall and is independent of Reynold's number. This is consistent with flow through small rough passages such as those under investigation here. A friction factor correlation considering these effects was first derived by Von Karman and is adopted in this study with the following form (Schlichting, 1979):

$$f = \frac{1}{(2Log\frac{D}{2K} + 1.74)^2} \quad , \tag{5.5}$$

where D is the Hydraulic Diameter and K is the surface roughness factor.

Table 5.1: Comparison of saturated water properties coded in Matlab using two different approximations given by Ishimoto et al., (1972) and Garland et al., (1992).

Thermodynamic Properties and their Derivatives at P = 506500 Pa			
Property	**Ishimoto et. al.**	**Garland et. al.**	**% diff.**
VF	1.09E-03	1.10E-03	-0.62
DVFDP	8.38E-11	8.52E-11	-1.72
VG	3.70E-01	3.70E-01	0.01
DVGDP	-6.88E-07	-6.89E-07	-0.13
HF	6.42E+05	6.43E+05	-0.10
DHFDP	3.22E-01	3.23E-01	-0.09
HG	2.75E+06	2.75E+06	-0.05
DHGDP	8.65E-02	8.42E-02	2.65
SF	1.87E+03	1.87E+03	-0.09
DSFDP	7.55E-04	7.60E-04	-0.58
SG	6.81E+03	6.69E+03	1.89
DSGDP	-6.66E-04	-6.63E-04	0.47

5.3 **HEM Model Results**

The work done by Amos and Schrock (1983) is one of the first experimental and theoretical programs to study geometries of small slits. The length of their test section or channel is 6.35 cm. Because of the length of their channel, they were able to place pressure taps along the channel to see how the flow is developing from the pressure profiles. This data is useful in verifying the program being implemented in this work. A large portion of the data for slits with a nominal opening of 2.54E-4 m and 3.81E-4 m produced by Amos and Schrock (1983) was chosen to determine the effectiveness of the HEM model. Various runs were chosen over a range of pressures (4.271-15.747 MPa) and subcoolings (2.1-61.5^{o}C). Also, this data was chosen because the hydraulic diameters of the channels (Dh = 0.418 − 0.747mm) are in the range of those performed on SG cracks in this study (Dh = 0.586 − 0.709mm).

HEM model predictions from the current work are compared to those performed by Amos and Schrock (1983), under the same stagnation conditions and subcooling as shown in Table 5.2 and Table 5.3. The comparison between the two can be seen for both smaller and larger slit openings illustrates the value Gc is a comparison between the individual model calculated mass flux and the experimental value and is useful to test the effectiveness of the model. It is quite apparent from the model predictions that the HEM under predicts the data as expected. Only 3 of the 40 case runs resulted in an overprediction of the experimental mass flux, with one of these within experimental error. The model also, predicts the flashing location along the channel as given by the flashing

criteria, or when the fluid pressure equals the saturation pressure at the fluid temperature. These predictions are in close proximity to those predicted by Amos and Schrock (1983), however they tend to predict flashing further downstream than those observed experimentally. For example, in runs # 69 and # 71 the HEM predicted flashing to occur at 6.302 cm and 3.416 cm downstream of the entrance, while the flashing locations roughly determined experimentally were 4.8 and 3.3 cm respectively. This is somewhat counterintuitive, as flashing criteria of the HEM is expected to cause flashing further upstream. Also the difference in exit pressures predicted by the HEM model and experimental data is obvious. The difference of these exit pressures compared to the experimental data is a weakness of the HEM. In all cases presented here, the HEM overpredicts experimental exit pressures.

Figures 5.1 and 5.2 present the comparison of the current implementation of the HEM with the critical mass flux data of Amos and Schrock (1983) graphically. As was expected, mass flux is underpredicted by the HEM. The dotted lines represent a reference to a prediction equal to the experimental values of plus or minus 5% Gc. Horizontal lines on the data points represent a 5% error in the experimental mass flux. Amos and Schrock estimated a 5% error in their experimental mass flux data, however exact values of error for each run has not been well documented. For the smaller channel, 17 of the 23 mass flux data are underpredicted by over 5% with 10 of those 9% or more. The larger channel mass flux was underpredicted by more than 5% in 13 of 17 runs, with only 3 of those falling below more than 9%. From this limited study, a conclusion that as the channel area decreases, the difference between the HEM model prediction and the experimental data increases. A general trend of increasing underprediction by the HEM with increasing pressure and decreasing subcooling is also evidenced.

One of the key advantages of applying a one or multi-dimensional model to choking flow is the ability to theoretically observe the flow progression and possible compare this to actual data. The HEM model predicted pressure profiles against pressure tap data are lower than that observed experimentally, and therefore it underpredicts the entrance loss as well as the single-phase frictional pressure drops. It is difficult to narrow down the exact location of flashing for the experimental data; however it can be estimated as the point at which there is a non-linear deviation from the single-phase pressure drop. Since the quality of the single phase liquid is not a dependent variable of the model, it is assumed to be zero before flashing occurs. This allows one from a graphical point of view to estimate flashing the model flashing location as well as follow the progression of the two-phase mixture along the channel length. The HEM tends to over-estimate the quality of the mixture at the exit, when compared to the HNEM, which leads to a lower critical mass flux. As there are no experimentally determined values for the mixture quality, a comparison is not made.

$$G_c = \frac{G_c - G_{exp}}{G_{exp}} x100 \qquad (5.6)$$

The model implementation was carried over to the data from the current experimental program. Table 5.4 shows a comparison of the HEM predictions with experimental data for 5 different slit specimens all having a channel length of 0.3175 cm. Again, for the case of subcooled stagnation conditions and for a much smaller channel length as characteristic to the current tests the HEM significantly under-predicts the critical mass flux. Unfortunately, unlike previous studies on longer channels, it is not possible to place pressure taps along such a short channel to obtain pressure profile data or estimate the exit pressure along the channel. Also, there is not a large enough database as of yet, to

make formal conclusions about the effect of L on the model predictions, however from these limited data sets, the HEM predictions were worse than those with larger L of 6.35 cm. Only two of the 19 model runs were within -10% of the experimental data for simulated SG tube cracks, while 11 of the 19 showed under predictions of greater than 15%. As shown for the comparison with Amos data in tabular format, a graphical representation of the percent difference in the HEM prediction of critical mass flux to experimental data can be seen in Figure 5.3. Note that the dotted reference line is a 10% under-prediction.

Table 5.2: Comparison of HEM model implementation to Amos and Schrock (1983) experimental data for 2.54E-4 m nominal slit openings (L=6.35 cm)

Stagnation				Experiment		HEM Theory		
RUN	Pressure	Subcooling	Dh	Gc	Pex	Flashing location	ΔGc	Pex
#	[MPa]	[°C]	[mm]	[kg/m^2-s]	[kPa]	[cm]	[%]	[kPa]
68	4.289	59.6	0.464	3.500E+04	1210	Exit	-3.70	1412
70	4.320	30.7	0.464	2.849E+04	1820	Exit	-8.62	2513
69	4.281	14.9	0.464	2.160E+04	2229	6.302	-13.02	3215
71	4.272	4.8	0.464	1.687E+04	1909	3.416	-19.10	2606
23	7.117	61.2	0.502	4.271E+04	2016	Exit	8.28	2440
51	7.050	60.3	0.418	4.091E+04	2214	Exit	-3.28	2512
24	7.055	29.2	0.502	3.641E+04	1007	Exit	-3.99	4471
25	7.055	18.2	0.502	3.131E+04	748	Exit	-9.20	5392
26	7.000	3.3	0.502	2.027E+04	595	1.694	-11.79	3880
36	9.553	59.1	0.453	4.405E+04	3309	Exit	-4.40	3993
37	9.600	28.1	0.453	3.247E+04	4446	6.258	-7.64	6150
38	9.667	22.4	0.453	2.748E+04	4301	5.879	1.31	5834
55	9.602	3.9	0.418	2.198E+04	3098	1.337	-16.61	4469
98	9.774	58.0	0.502	4.883E+04	3239	Exit	-6.87	4109
52	11.728	59.9	0.418	4.924E+04	3994	Exit	-3.78	7697
39	11.601	54.9	0.453	4.413E+04	4187	Exit	-9.74	6955
54	11.696	30.0	0.418	3.852E+04	5065	6.285	-7.40	7414
95	12.420	61.5	0.502	5.137E+04	4039	Exit	-5.03	5002
96	11.642	26.4	0.502	3.901E+04	4636	6.153	-11.84	7464
93	11.838	12.9	0.502	3.224E+04	4070	4.398	-13.90	6879
72	15.601	54.2	0.464	5.019E+04	2605	Exit	6.53	7350
92	15.798	12.0	0.502	4.231E+04	—	3.893	-26.35	8310
97	15.747	12.0	0.502	3.703E+04	4838	3.848	-20.47	8600

Table 5.3: Comparison of HEM model implementation to Amos and Schrock (1983) experimental data for 3.81E-4 m nominal slit openings (L=6.35 cm)

Stagnation				Experiment		HEM Theory		
RUN	Pressure	Subcooling	Dh	Gc	Pex	Flashing location	ΔGc	Pex
#	[MPa]	[°C]	[mm]	[kg/m^2-s]	[kPa]	[cm]	[%]	[kPa]
59	4.271	59.3	0.747	4.0990E+04	1313	Exit	-5.34	1387
57	4.220	28	0.747	3.2560E+04	2047	Exit	-6.54	2564
58	4.187	13.9	0.747	2.5260E+04	2387	Exit	-14.99	3290
60	4.134	2.9	0.747	1.4330E+04	1791	1.436	-7.99	2369
30	7.093	59.6	0.748	5.7810E+04	1878	Exit	-2.34	2623
27	7.073	29.6	0.748	4.4160E+04	2970	Exit	-3.07	4431
28	7.077	15.6	0.748	3.3980E+04	3400	Exit	-7.31	5562
29	7.091	6.2	0.748	2.5220E+04	2886	3.162	-8.50	4764
41	9.595	59.4	0.708	5.7920E+04	3552	Exit	-1.96	3814
43	9.584	29.9	0.708	4.3940E+04	4820	Exit	-5.56	6155
44	9.619	15.1	0.708	3.3230E+04	5264	5.659	-7.62	6511
42	11.580	53.3	0.708	5.7830E+04	4478	Exit	-4.82	5277
45	11.608	28.6	0.708	4.4480E+04	5997	Exit	-6.18	7723
76	11.672	11.8	0.747	3.8600E+04	5905	4.572	-16.80	7356
79	11.672	2.1	0.747	3.0580E+04	4887	0	-15.98	6228
74	15.398	54.6	0.747	6.9690E+04	6135	Exit	-6.73	7194
78	15.452	26.5	0.747	5.2960E+04	7613	Exit	-8.45	10802

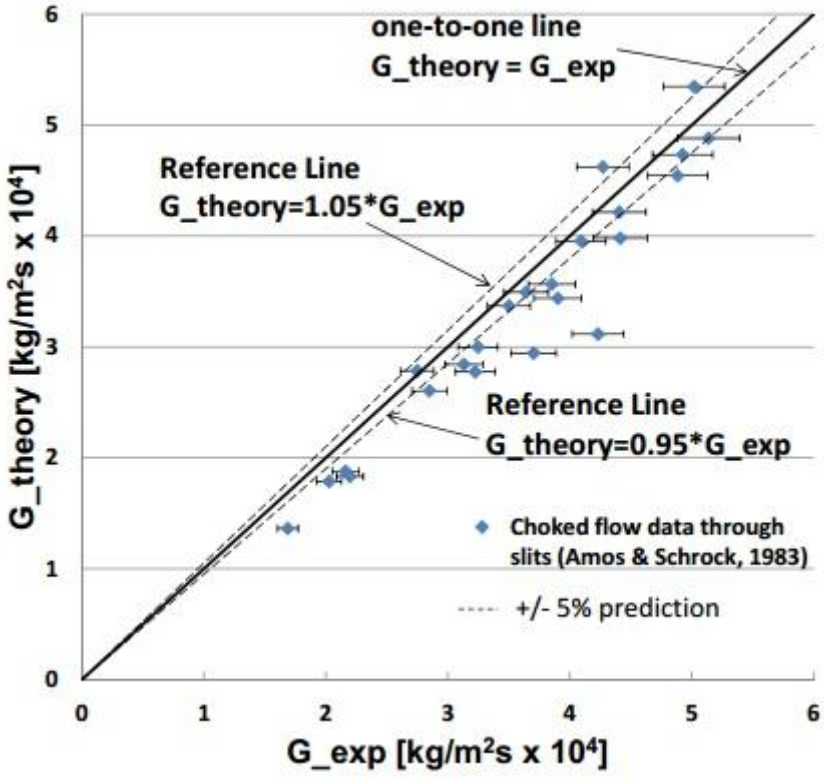

Figure 5.1: Current theoretical HEM implementation compared with Amos and Schrock (1983) choked flow data for 2.54E-4 m nominal slit openings (L=6.35 cm)

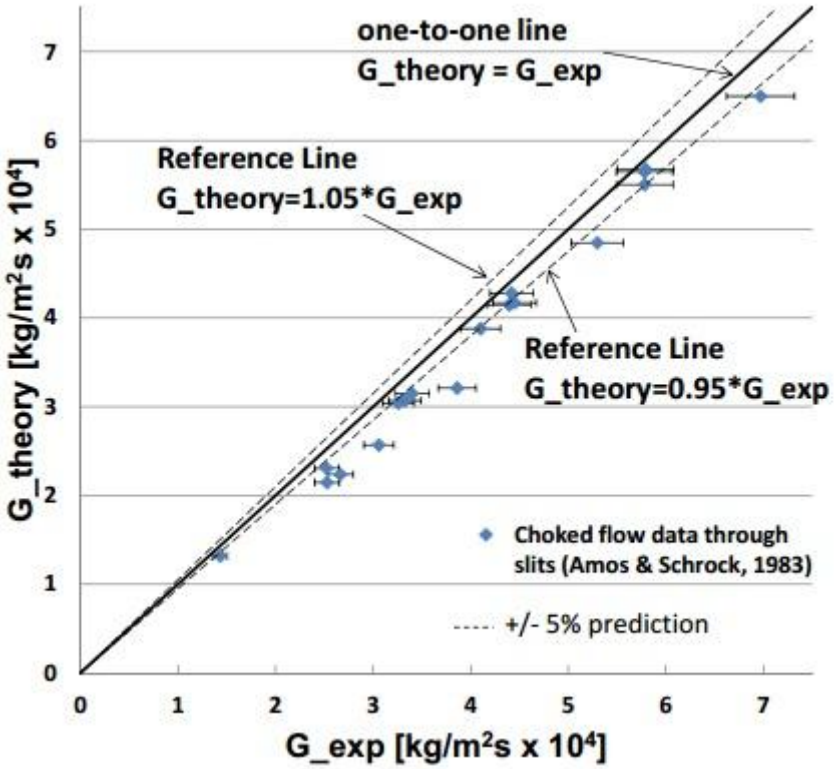

Figure 5.2: Current theoretical HEM implementation compared with Amos and Schrock (1983) choked flow data for 3.81E-4 m nominal slit openings (L=6.35 cm)

Table 5.4: Comparison of HEM model implementation to experimental data for simulated SG cracks obtained in this study (L=0.3175 cm)

	Stagnation			Experiment	HEM Theory	
Spec.	Pressure	Subcooling	Dh	Gc	Flashing location	ΔGc
#	[MPa]	[°C]	[mm]	[kg/m^2-s]	[cm]	[%]
2	6.728	46.1	0.709	6.571E+04	Exit	-13.90
	6.735	42.1	0.709	6.268E+04	Exit	-13.08
	6.874	32.5	0.709	5.603E+04	Exit	-12.22
3	6.735	45.3	0.700	7.090E+04	Exit	-20.90
	6.728	38.9	0.700	6.837E+04	Exit	-23.06
	6.758	34.1	0.700	6.406E+04	Exit	-22.22
	6.866	29.9	0.700	6.280E+04	Exit	-24.77
4	6.770	48.1	0.659	6.111E+04	Exit	-6.56
	6.776	38.2	0.659	5.795E+04	Exit	-10.47
	6.831	32.8	0.659	5.414E+04	Exit	-9.80
	6.818	27.7	0.659	5.268E+04	Exit	-14.14
5	6.698	46.9	0.647	6.652E+04	Exit	-15.56
	6.770	40.0	0.647	6.520E+04	Exit	-19.03
	6.786	31.9	0.647	5.615E+04	Exit	-14.50
	6.849	27.4	0.647	5.571E+04	Exit	-19.24
6	6.681	46.3	0.586	6.572E+04	Exit	-19.98
	6.597	38.5	0.586	5.814E+04	Exit	-16.53
	6.767	33.4	0.586	5.661E+04	Exit	-18.65
	6.737	24.7	0.586	5.307E+04	Exit	-20.10

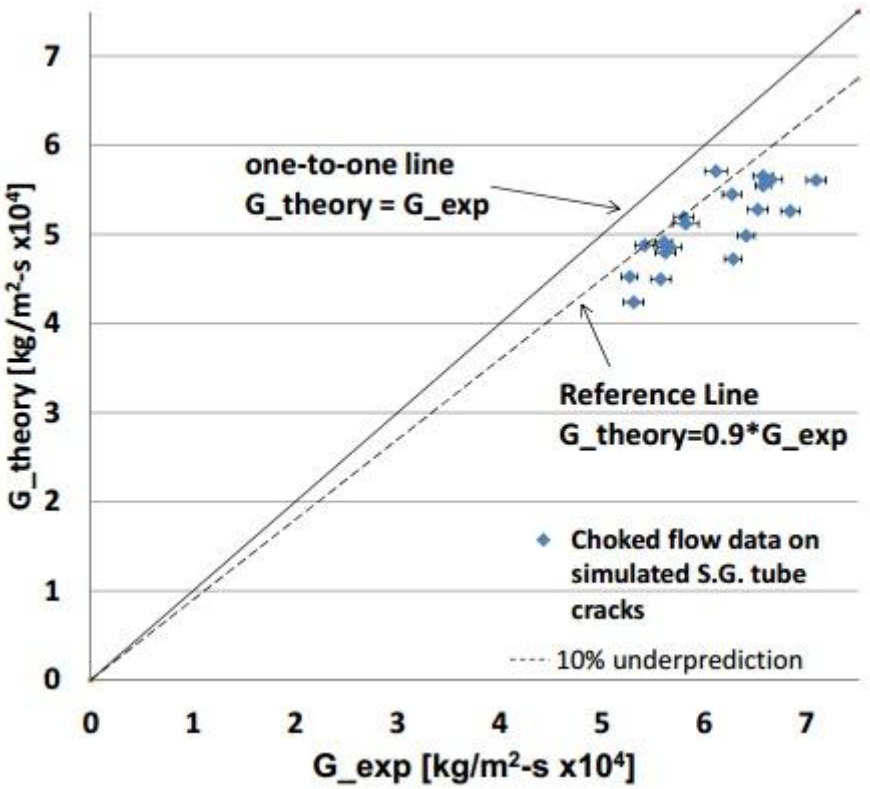

Figure 5.3: Current theoretical HEM implementation compared with experimental mass flux for simulated SG cracks obtained in this study (L=0.3175 cm)

5.4 **HNEM Model Results**

In this section, a comparison of the HNEM to that of the same data previously discussed is made. The comparison between the HNEM and Amos's data for 2.54E-4 m and 3.81E-4 m nominal slit openings can be seen in Tables 5.5 and 5.6 respectively. It is quite apparent that adding the thermal non-equilibrium assumption, allowing the fluid to become superheated before flashing greatly improved the HNEM critical mass flux predictions. The predicted mass flux for all but two of the data points for a channel length of 6.35 cm lie within 9% of their respective experimental values, with 26 of the 40 runs within 5%. The predicted exit pressure of the model also improved, however it still over predicts experimental exit pressures. For those runs, in which flashing occurred inside the channel, the predicted flashing location shifted downstream compared to that of the HEM, however again these seem to stray further downstream from the experimentally determined flashing locations. Figures 5.4 and 5.5 show the comparisons of Amos and Schrock data (1983) with HNEM predictions in a graphical form. The HNEM predicts the choking mass fluxes about within about 5% of the experimental values.

When comparing the HNEM with the simulated SG crack data, a large improvement is also evident as shown in Table 5.7 and Figure 5.6. In fact, compared to the HEM, the HNEM shows a much greater improvement for the shorter length channel when compared to the 6.35 cm length channels. On average, the predictions are 11.8% closer to the experimental values when compared the HEM predictions. This shows that applying thermal non-equilibrium assumptions increases as well as improves the critical mass flux pre-dictions for simulated SG cracks. It is impossible to compare the predicted exit pressures in the current study, however it is evident that thermal non-equilibrium delays flashing and increases the two-phase pressure drop, but still over predicts the exit pressure

when compared to experimental data. Also, with the shortened channel length in the present study, flashing is predicted to occur at the exit of the channel in all cases. While from a modeling perspective this was expected, the actual vaporization process in subcooled flashing flows through short narrow channels is up for debate.

It is noticed that the HNEM model better predicts the entrance losses as well as the single-phase frictional pressure drop when compared to the HEM. However, the model obviously predicts flashing to occur further downstream than the experimental estimate of flashing location. Neither model is able to capture the characteristics of the two-phase pressure drop. Both models over predict the exit pressures, however at the highest subcoolings where flashing occurs at the exit, the critical pressure ratio is well predicted. This observation implies that the single phase liquid region may in fact be well predicted in any model using the homogeneous mixture assumptions.

Table 5.5: Comparison of HNEM model implementation to Amos and Schrock (1983) experimental data for 2.54E-4 m nominal slit openings (L=6.35 cm).

	Stagnation			Experiment		HNEM Theory		
RUN	Pressure	Subcooling	Dh	Gc	Pex	Flashing location	ΔGc	Pex
#	[MPa]	[°C]	[mm]	[kg/m^2-s]	[kPa]	[cm]	[%]	[kPa]
68	4.289	59.6	0.464	3.500E+04	1210	Exit	-2.26	1309
70	4.32	30.7	0.464	2.849E+04	1820	Exit	-4.85	2362
69	4.281	14.9	0.464	2.160E+04	2229	Exit	-4.95	3127
71	4.272	4.8	0.464	1.687E+04	1909	4.859	-7.66	2773
23	7.117	61.2	0.502	4.271E+04	2016	Exit	9.53	2464
51	7.05	60.3	0.418	4.091E+04	2214	Exit	-1.66	2426
24	7.055	29.2	0.502	3.641E+04	1007	Exit	0.19	4226
25	7.055	18.2	0.502	3.131E+04	748	Exit	-0.20	5064
26	7	3.3	0.502	2.027E+04	595	3.335	2.65	3880
36	9.553	59.1	0.453	4.405E+04	3309	Exit	-2.61	3619
37	9.6	28.1	0.453	3.247E+04	4446	EXIT	-3.14	6047
38	9.667	22.4	0.453	2.748E+04	4301	6.095	6.26	5795
55	9.602	3.9	0.418	2.198E+04	3098	2.565	-4.39	4676
98	9.774	58.0	0.502	4.883E+04	3239	Exit	-5.28	3801
52	11.728	59.9	0.418	4.924E+04	3994	Exit	-2.31	4593
39	11.601	54.9	0.453	4.413E+04	4187	Exit	-5.08	4897
54	11.696	30.0	0.418	3.852E+04	5065	Exit	-3.54	7317
95	12.42	61.5	0.502	5.137E+04	4039	Exit	-3.65	4818
96	11.642	26.4	0.502	3.901E+04	4636	6.293	-8.35	7254
93	11.838	12.9	0.502	3.224E+04	4070	4.6877	-8.38	6596
72	15.601	54.2	0.464	5.019E+04	2605	Exit	7.68	7110

Table 5.6: Comparison of HNEM model implementation to Amos and Schrock (1983) experimental data for 3.81E-4 m nominal slit openings (L=6.35 cm)

Stagnation				Experiment		HNEM Theory		
RUN	Pressure	Subcooling	Dh	Gc	Pex	Flashing location	ΔGc	Pex
#	[MPa]	[°C]	[mm]	[kg/m^2-s]	[kPa]	[cm]	[%]	[kPa]
59	4.271	59.3	0.747	4.0990E+04	1313	Exit	-4.35	1316
57	4.220	28	0.747	3.2560E+04	2047	Exit	-3.17	2430
58	4.187	13.9	0.747	2.5260E+04	2387	Exit	-7.08	3115
60	4.134	2.9	0.747	1.4330E+04	1791	2.88	-0.08	2626
30	7.093	59.6	0.748	5.7810E+04	1878	Exit	-1.10	2517
27	7.073	29.6	0.748	4.4160E+04	2970	Exit	0.45	4239
28	7.077	15.6	0.748	3.3980E+04	3400	Exit	-0.17	5322
29	7.091	6.2	0.748	2.5220E+04	2886	4.78	1.31	5028
41	9.595	59.4	0.708	5.7920E+04	3552	Exit	-0.66	3674
43	9.584	29.9	0.708	4.3940E+04	4820	Exit	-2.13	5915
44	9.619	15.1	0.708	3.3230E+04	5264	6.10	0.11	6754
42	11.580	53.3	0.708	5.7830E+04	4478	Exit	-3.16	5101
45	11.608	28.6	0.708	4.4480E+04	5997	Exit	-2.87	7466
76	11.672	11.8	0.747	3.8600E+04	5905	5.13	-10.15	7631
79	11.672	2.1	0.747	3.0580E+04	4887	0.75	-14.82	6225
74	15.398	54.6	0.747	6.9690E+04	6135	Exit	-5.51	7071
78	15.452	26.5	0.747	5.2960E+04	7613	Exit	-6.00	10598

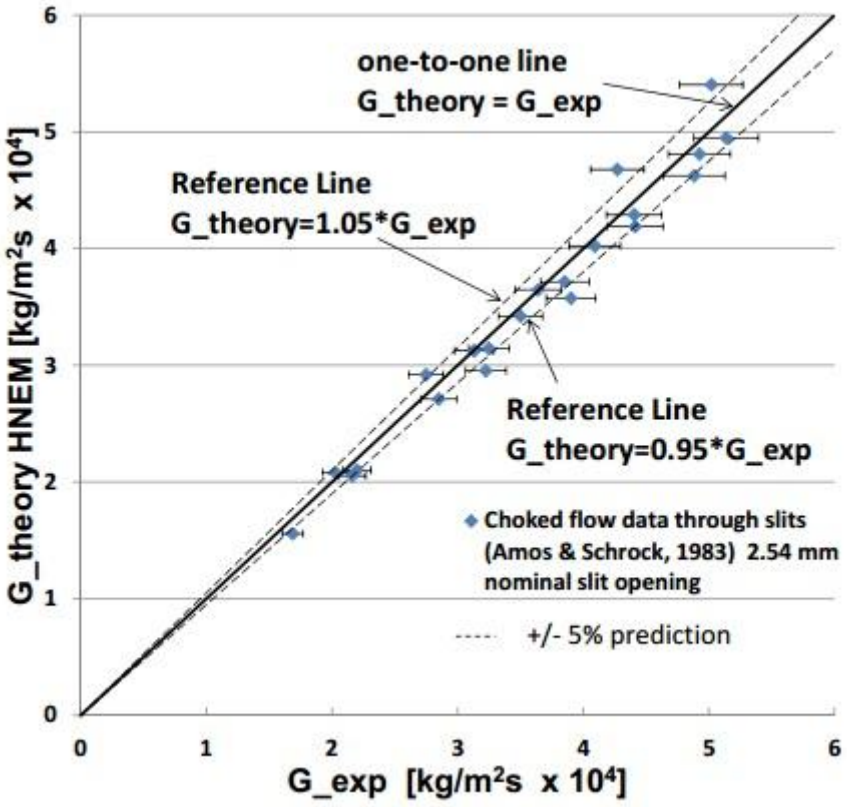

Figure 5.4: Current theoretical HNEM implementation compared with Amos and Schrock (1983) choked flow data for 2.54E-4 m nominal slit openings (L=6.35 cm)

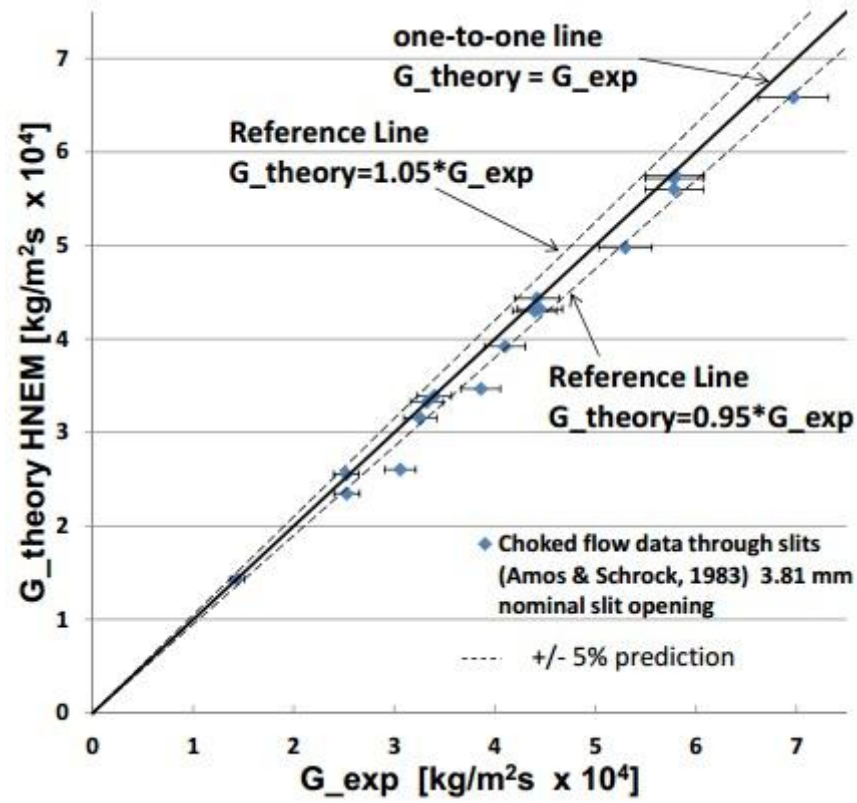

Figure 5.5: Current theoretical HNEM implementation compared with Amos and Schrock (1983) choked flow data for 3.81E-4 m nominal slit openings (L=6.35 cm)

Table 5.7: Comparison of HNEM model implementation to experimental data for simulated SG cracks obtained in this study (L=0.3175 cm)

	Stagnation			Experiment	HEM Theory	
Spec.	Pressure	Subcooling	Dh	Gc	Flashing location	ΔGc
#	[MPa]	[°C]	[mm]	[kg/m^2-s]	[cm]	[%]
2	6.728	46.1	0.709	6.571E+04	Exit	-1.90
	6.735	42.1	0.709	6.268E+04	Exit	0.12
	6.874	32.5	0.709	5.603E+04	Exit	4.35
3	6.735	45.3	0.700	7.090E+04	Exit	-9.61
	6.728	38.9	0.700	6.837E+04	Exit	-10.51
	6.758	34.1	0.700	6.406E+04	Exit	-8.24
	6.866	29.9	0.700	6.280E+04	Exit	-9.63
4	6.770	48.1	0.659	6.111E+04	Exit	6.35
	6.776	38.2	0.659	5.795E+04	Exit	4.76
	6.831	32.8	0.659	5.414E+04	Exit	7.39
	6.818	27.7	0.659	5.268E+04	Exit	4.15
5	6.698	46.9	0.647	6.652E+04	Exit	-3.68
	6.770	40.0	0.647	6.520E+04	Exit	-5.70
	6.786	31.9	0.647	5.615E+04	Exit	2.14
	6.849	27.4	0.647	5.571E+04	Exit	-1.76
6	6.681	46.3	0.586	6.572E+04	Exit	-3.43
	6.597	38.5	0.586	5.814E+04	Exit	2.79
	6.767	33.4	0.586	5.661E+04	Exit	2.14
	6.737	24.7	0.586	5.307E+04	Exit	-1.73

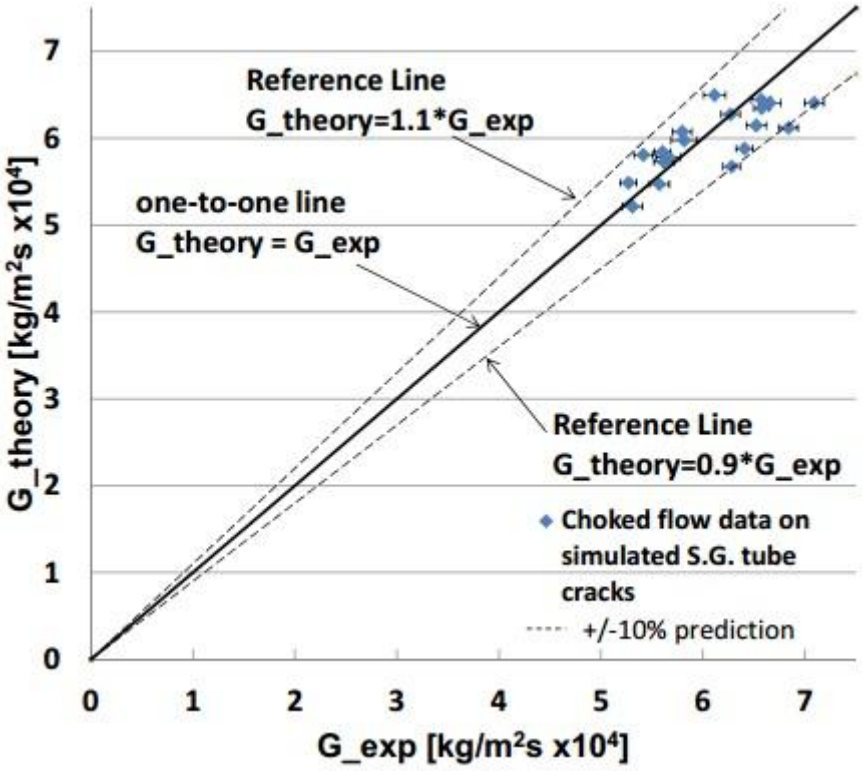

Figure 5.6: Current theoretical HNEM implementation compared with experimental data for simulated SG cracks obtained in this study (L=0.3175 cm)

5.5 **HNEM Sensitivity Analysis**

As with any model, the predictions it provides are based on a subset of input parameters which ultimately determine the solution. While great care should always be taken to provide input parameters based on the best physical evidence or correlations if required, there is always some uncertainty in every parameter. A simple sensitivity analysis was performed in order to check how the homogeneous non-equilibrium model performs based on perturbations to any one input parameter that it requires. The analysis has been limited to cases which relate to the experimental evidence found in this study; however it should be noted that a more extensive analysis should be performed if the length of the channel is different than that in this analysis. The length used it the same as the experimental test sections of 3.175 mm. The analysis was performed by taking base cases of inputs, an altering the individual inputs one at a time keeping the remaining inputs the same as the original case. The analysis has been restricted to the effects on the desired output parameter of critical mass flux (Gc). A sample set of results of the sensitivity of the HNEM to percent change of friction factor, subcooling, stagnation pressure, channel area and hydraulic diameter are given in Table 5.8.

Comparing a base case solution of the HNEM to a +/−10% change in friction factor shows that the model predicts a less than one percent change in the solution. The same is seen with a 10 percent change in the hydraulic diameter of the channel. The solution is more sensitive to the stagnation state of the fluid. A ten percent change in the subcooling or stagnation pressure results in an approximately 5% perturbation in the solution. The stagnation pressure and temperature greatly affect the solution due to the change in thermodynamic properties upon which the model is dependent. The greatest effect

however is that of the channel area. While the mass flow rate determined by the solution is completely independent of the channel area for a constant area duct, the mass flux is directly proportional to it. In other words, the magnitude of the change in area will be similar to the magnitude of change in the solution to mass flux. This provides a basis for determining the most important in-put parameters in the model solution. It is quite obvious that when determining the mass flux experimentally or through a modeling program, a good representation of the area is required. This was an expected result and prior to the first experiment in this study emphasis was placed on correctly measuring the area of the test specimens with the upmost precision possible as explained in Section 3.1

Table 5.8: Sensitivity of the HNEM model solution to selected input parameters for L=0.3175 cm

Modified Parameter	% change of parameter	ΔGc of solution to HNEM
Friction Factor	+10	-0.54
	-10	0.83
Subcooling	+10	3.38
	-10	-3.19
Stagnation Pressure	+10	5.23
	-10	-4.87
Channel Area	+10	-9.02
	-10	11.02
Hydraulic Diameter	+10	0.79
	-10	-0.41

5.6 **Conclusions**

A modeling program coded in MATLAB has been developed to calculate choking mass flow rate for steam-water flow through a user defined geometry. Incorporated into the code are single-phase fluid calculation routines as well as homogeneous two-phase mixture routines. The program was used to model existing data in literature produced by Amos and Schrock (1983) for slits with a channel length of 6.35 cm. The calculated mass flow rates were compared to both experimental data and existing theoretical calculations. The program was then used to predict the mass flow rate data that has been acquired in the current experimental program. As expected, the homogeneous equilibrium model under predicts the data. Also, the HEM predictions under predict the current flow rates seen in simulated SG cracks with length of 0.3175 cm more than slits with channel length of 6.35 cm.

The currently proposed theory suggest that non-equilibrium effects play an important role in modeling choking two-phase flow such as that seen in SG cracks. A second model was developed which incorporates thermal non-equilibrium to homogeneous flow. The HNEM was determined to better predict the choking mass flux, however, it fails to account for all characteristics of two-phase choking flow especially two-phase pressure drop when flashing occurs inside the channel. In the case of simulated steam generator tube cracks flashing and choking were predicted to occur at the exit plane. The HNEM

model is valid for prediction of the experimental choking mass flux within 10%. Amos and Schrock (1983) found that the HNEM was more successful for larger slits, and the results here further imply that the model is less successful for smaller slits. Prediction of the simulated crack mass flux by the HNEM improves with increasing subcooling and there is further evidence that the Alamgir-Lienhard correlation (equation 3.12) over predicts the pressure undershoot at flashing inception for steady state critical flow in slits. If in fact, flashing and choking occur at the exit plane in the current experimental studies with short channels, future experimental efforts should focus on the rapid vaporization process and possible effects of entrance phenomena such as vena contracta which may reduce the area occupied by the fluid.

6. ANALYSIS OF RELAP5 THERMO-HYDRAULIC CODE

6.1 **Introduction**

The goal of the work presented in this chapter is to assess the validity of using RELAP5, a one-dimensional thermal-hydraulic system code, for modeling of small L/D cracks and specifically small length channels. It is of interest to see how RELAP5 models fare in modeling choked flow in such geometries and to see if the models break down in anyway when the geometry changes, specifically when the length of the channel decreases.

The choking flow models in RELAP5/MOD3.3 were assessed in two ways. First, two choking flow models that are available in RELAP were assessed using two experimental runs by Amos and Schrock (1983). The runs were chosen based on the subcooling at two similar pressures of 4.272 MPa and 4.320 MPa. The subcooling for these two runs were 4.8 K and 30.7 K respectively. In the experiment conducted by Amos the channel length was 6.35 cm long and pressure profiles along the channel are available. This allows direct comparison of pressure profiles, and choking flow rate with RELAP5 models. Also, this allows for a starting point to assess how the models behave when the channel length is significantly shortened. The same two models in RELAP were then applied to current data in the case of a steam generator tube crack at similar pressures of approximately 3.54 MPa with a range of subcoolings between 19 and 40 K. This analysis, allowed the effect of subcooling at the stagnation condition to be assessed.

6.2 **RELAP5**

The MOD3.3 version of RELAP5 was used. In previous versions of RELAP5, the Ransom-Trapp (R-T) choked flow model (Ransom and Trapp 1980, Trapp and ransom 1981) was used. In MOD3.3, the current default choking model is the Henry-Fauske critical flow model. This change is due to two shortcomings that were observed with the Ransom-Trapp model. The first being, that the R-T model calculated values that were as much as an order of magnitude lower than that of the homogeneous equilibrium predictions if the slip ratio was not forced to be near 1, when two-phase critical flow at low pressures was intrinsic of the problem being solved. Since it is well known and excepted that the homogeneous equilibrium itself greatly under predicts choking flow rates, the R-T model being another order of magnitude lower is a great shortcoming. Also, for initially subcooled flow using thin orifice plates to model the break and liquid conditions near saturation, the R-T model predicted critical flow rates 40-50% less than those observed experimentally.

The R-T model under prediction at low pressures and low quality near the break are not of great concern in the case of steam generator tube cracks, because the differential pressure will be much greater than where the model breaks down at P ~ 0.2M P a. The case where the R-T model greatly under predicts choked flow under slightly subcooled conditions however is of much more interest. For these conditions, the model underestimates the amount of thermal non-equilibrium at the throat if the channel length is less than 10 mm long. In addition these shortcomings of the R-T model, the previous versions of RELAP5 showed discontinuous predictions of critical flow rates at the single-phase to two-phase transition (Wolf and Revankar, 2012).

The following subsections discuss the theoretical basis for the Henry-Fauske and Ransom-Trapp models and their application to subcooled critical flow.

6.2.1 **RELAP5 Choking Model and Criterion**

RELAP5 is a light water reactor thermohydraulic transient 1-Dimensional analysis code that was developed by the NRC to evaluate reactors. It is of interest to this study since it can calculate the critical flow rate for a pipe, junction, crack or other geometry by applying choked flow models.

The default model initially in use was developed by Ransom and Trapp (1980) and calculates the maximum flow rate through any geometry using time dependent differential equations and is a homogenous, thermal equilibrium, mechanical non-equilibrium (slip) model.

At the point of choking, there is no signal propagation upstream and the choked flow rate remains unaffected. The characteristic equation obtained by solving the mass, momentum and entropy conservation equations for two phase flows which are nonhomogeneous equilibrium in nature results in a characteristic equation (obtained by equating the void fraction, specific volume and quality change for each phase obtained in the equations) where the entropy and density of each phase is assumed to change with pressure and a virtual mass coefficient is used, thereby ensuring a smooth transition between the phases.

The solution to such a polynomial would result in roots with a real and imaginary part where the real part indicates flow velocity and imaginary portion indicating attenuation of the signal. Thus for choked flow, the real part of the signal would be zero (or very close to it) to ensure no signal is propagated upstream. Boundary conditions are established by invoking the speed of sound criterion whereby the Mach number is expressed as a function of void fraction, specific volume and virtual mass, thereby allowing the choking models to be applied to the roots of the characteristic equation obtained from the conservation equations (a similar approach was highlighted in the literature review chapter of this thesis).

While studying implementation of the boundary conditions however, it is important to note the effect of the virtual mass coefficients and the vapor fraction of the fluid on the velocity of sound (or the signal propagation in this case). The thermal equilibrium assumption results in a speed of sound variation in water with the following changes as vapor fraction changes (shown here for different Virtual masses at 7.5 MPa of pressure.

It is crucial to analyze this diagram and understand the phenomenon that is occurring. For a subcooled fluid, when applying the criteria for choking at the exit, the fluid undergoes a phase transition at this point. This could happen at the exit or slightly beyond it, or slightly before, depending on the friction loss along the channel, the entrance losses

and the length of the crack. The shorter the crack, the more likely it is that flashing will at or just beyond the exit for the same conditions of stagnation.

We can therefore draw the conclusion that as water (or any subcooled fluid) flows along a channel losing pressure till it reaches the exit of the channel or break where there is a very large pressure gradient over a negligible distance, vaporization will take place. This will result in the following:

i. The velocity of fluid in the subcooled region just upstream of flashing will be less than the speed of sound but accelerating

ii. The velocity of vapor just downstream of the point of flashing will greater than the speed of sound resulting in a further increase in velocity as the vapor moves downstream (supersonic fluid flow through a diverging area).

iii. This means that no pressure signal is propagated upstream and also that the pressure drops rapidly as the vapor expands downstream and accelerates.

The choking model in RELAP5 further simplifies this assumption at the cost of an error analysis of point of choking with comparison to error in mass flow rate by assuming that the narrowest point is the throat and choking occurs there and at this point, the fluid velocity is equal to the two-phase sound velocity.

The RT model then utilizes the pressure undershoot correlation of Alamgir & Lienhard, (1981) to account for the degree of superheat needed for flashing to occur. The final step is to apply the speed of sound criterion where velocity of fluid equals its local sound velocity. A problem to overcome here is that the sound velocity of a two-phase mixture and vapor is much smaller than the single phase sound velocity. This results in an instability that is overcome here by modeling the flashing zone as a transition region with a varying void fraction and specifying the upstream void fraction (to calculate single phase sound velocity) and the downstream sound velocity using the equation specified in (Nuclear Safety Analysis Division, Inc., 2003) which is dependent on the virtual mass coefficient, void fraction and phase densities as described earlier.

The MOD3.3 Version of RELAP5 utilizes the Henry-Fauske model described in the literature review chapter as its default. This is due to the tendency of the RT model to under predict mass flow rates for small geometry cracks with lengths less than 10 mm. The degree of under prediction increases as the subcooling reduces at higher pressures, which is more indicative of SG tube cracks thus making the model unreliable by at least an order of magnitude.

Unlike the RT model, which is a Nonhomogeneous Equilibrium model (NHEM), the HF model is a Homogeneous Non-Equilibrium model (HNEM). This is because it assumes there is no slip between the phases while accounting for temperature differences between phases and other interphase effects (Henry, 1970). This approach is justifiable if we assume that non-equilibrium effects are of greater importance for small geometries. At the same time, the crack geometry is so small that the conditions just prior to the choking plane can be considered equal to stagnation conditions.

For the geometries utilized in this study, it is not known how important wall friction, heat transfer effects and other two-phase and flow phenomenon that have been ignored by the HF model are, but it is doubtful there will be any significant length for flow development.

As discussed earlier, to account for the non-equilibrium effects, Henry and Fauske introduced a non-equilibrium parameter N to account for these thermal effects and it was represented in terms of the quality at the throat, which can be obtained by coupling the momentum and critical flow rate equations. To account for the quality after the choking plane however, the authors have assumed that the vapor follows the saturation curve and

this assumption, while simplifying calculation, may account for some of the interesting trends and observations discussed later in this chapter.

6.2.2 **RELAP5 Nodalization and Approach to modeling**

To analyze the data obtained in this study from the point of view of a widely used thermalhydraulics code, it was decided to examine RELAP5's predictive capabilities utilizing different models for choking and different approaches to modeling, resulting in the following methods of nodalization:

i. Treating the crack as a channel of 3.175 mm and 1.3 mm applying the Henry-Fauske model for choking

ii. Treating the crack as a channel of 3.175 and 1.3 mm applying the Ransom-Trapp model for choking

iii. Treating the crack as a junction applying choking models

iv. Treating (Amos & Schrock, 1983) cracks as junctions and applying choking models to compare results.

The nodalization involved establishing the stagnation conditions as recorded by instrumentation during the experiment and simulating flow upstream from the pressure vessel to the crack downstream. This involved modeling the 1 inch and ½ inch pipes leading to the crack channel/junction each as a channel split into a series of volumes (on the basis of hydraulic diameter). The justification for assuming the crack as a junction instead of a channel is due to the small geometry and flow channel length (1.3 mm) of the crack. This leaves very small length for the flow to develop and is standard practice in the United States to model such small geometries as junctions instead of cracks.

While applying the channel length approach, care must be taken to ensure that the ratio of volume length dx to the hydraulic diameter is always greater than 1. Combined with the constraint of the Courant Number, it became necessary to utilize only 2 control volumes across the channel, not allowing the author to view a pressure profile across the channel similar to what (Amos & Schrock, 1983) observed.

The Henry-Fauske and Ransom-Trapp (HF and RT models) models produce different results due to the nature of the models. The Ransom Trapp model has a tendency to under predict mass flow rate due to the assumption of thermal equilibrium which does not account for interfacial heat transfer and other effects while it was expected that the HF model would also under predict due to the assumption that the vapor formed follows the saturation curve thereby having a higher quality, but Wolf (Wolf and Revankar, 2012) noticed that the HF model over predicts his data (channel length 3.175 mm). Results obtained for the data in this study will be examined and comparisons made.

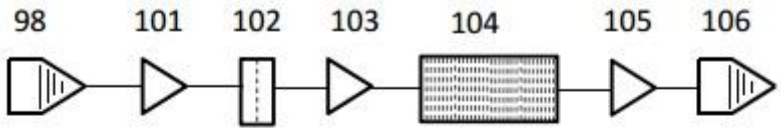

98 = P stagnation, time dependent
101= Pipe junction
102= Pipe (1 in. Dia., 2 in. long, 2 nodes)
103= Abrupt area change pipe junction
104= Crack length (63 or less nodes of 1mm)
105= Choking plane, pipe junction
106= Back Pressure, time dependent

Figure 6.1: RELAP5 Nodalization for the samples tested in this Study

6.3 **Model Comparison**

The choking flow models in RELAP5/MOD3.3 were assessed in two ways. First, two choking flow models that are available in RELAP were assessed using all experimental runs by Amos and Schrock (1983) for 2.54E-4 nominal slit openings. Two of the runs (#55 and #71) which have been discussed previously are again shown in this chapter. The subcooling for these two runs were 3.9 K and 4.8 K respectively. In the experiments conducted by Amos the channel length was 6.35 cm long and pressure profiles along the channel are available. This allows direct comparison of pressure profiles, and choking flow rate with RELAP5 models. Also, this allows for a starting point to assess how the models behave when the channel length is significantly shortened. The same two models in RELAP were then applied to current data in the case of a simulated steam generator tube crack.

The nodalization diagram used in these studies can be seen in Figure 7.1. As can be seen in the nodalization, a time dependent boundary condition (98) is set for the stagnation conditions. While the choking flow phenomena being considered is steady state, as the stagnation conditions are held constant, the use of a time dependent boundary condition allows the convergence to steady state to be plotted which can show if there is any oscillations in the final solution or not. The runs conducted here were over a period of 5 seconds and the solution converged to steady state in less than one second. A pipe of one inch in diameter and 2 inches long with 2 nodes is connected via a pipe junction 101 and 102. Pipe junction 103 is the beginning of the flow channel of interest. This junction has the abrupt area change option turned on, with a hydraulic diameter equal to that of the channel. The channel itself, pipe 104, is split into 63 nodes, 62 of which are 1 mm apart for a total channel length of 6.35 cm. For the simulated cracks, 5 equal sized nodes were used to model the channel length of 0.3175 cm. The end of the channel is connected to a pipe junction with the choking option turned on. This is the choking plane. The nodalization is then completed with a time dependent back pressure, which is again held constant.

Previous researchers have found that the wall roughness greatly influences the pressure drop and therefore the onset of flashing, void at the throat, and hence the critical mass flow rate when applying RELAP3D to flow through micro channels (Hassan and Frisani, 2009). In this study the wall roughness was found to be a particularly important input parameter to RELAP5. The Darcy friction factor is not an allowed input parameter to RELAP5 input decks. Friction factor instead is based on the Zigrang-Sylvester

approximation to the Colebrook-White correlation for turbulent Reynold's numbers (Sylveste and Zigrang, 1985). This approximation is given as a function of Reynold's number, diameter, and wall roughness as:

$$\frac{1}{\sqrt{f}} = -2log_{10}\left\{\frac{\epsilon}{3.7D} + \frac{2.51}{Re}\left[1.14 - 2log_{10}\left(\frac{\epsilon}{D} - \frac{21.25}{Re^{0.9}}\right)\right]\right\} \quad (6.1)$$

The advantage of using such a formulation in a large simulation code is that it is explicit. In the current study, an approximation of the wall roughness for the materials used in experimental studies under investigation was first applied. It was quickly determined that this was not a sufficient method of determining the correct friction factor. Typically, a much larger friction factor was approximated than that observed experimentally. For the following cases where comparisons are made to Amos and Schrock (1983) data, a wall roughness was solved for equation (6.1) using a general solver routine, where a roughness was found that matched the friction factor found experimentally. This was necessary to correctly predict the single phase pressure losses. In the studies performed for simulated crack geometries, the approximate wall roughness found from high resolution optical pictures was used. For obvious reasons, the wall roughness determines the slope of the single-phase pressure losses; however the upstream boundary condition of pressure is determined by the entrance loss. In all cases performed in this study, the default model used for entrance losses in RELAP5 is applied. The reasoning is simple, RELAP5 is used as a best estimate code and the fewer manual inputs used determines the effectiveness of the code as a general fluid solver. With this in mind, a summary of the results is shown below.

As can be seen in Figures 6.2 and 6.3, at stagnation conditions near saturation (4.8 and 3.9 K subcooling) it is expected that the fluid will flash somewhere along the channel length before the exit (choking) plane. It is evident from the experimental data that much larger pressure drop is seen after about 40 mm downstream of the entrance for case #71, indicative of two-phase pressure drop and flashing. The same is true for case #55 at approximately 10-20 mm along the channel. The exit pressure observed by Amos was 1909 kPa and 3098 kPa respectively. Both models over predict the exit pressure, and under predict the two-phase pressure drop. The Ransom-Trapp model provides a much better estimate of the single-phase pressure drop when com-pared to the H-F model. Note, that Amos did not actual observe or measure the flashing location in his experiments, it can only be approximated by the pressure measurements available.

One main advantage of using a well-developed code such as RELAP, is that many different parameters can be exported to help determine the flow characteristics. In this study, mixture and static quality were used to determine the flashing location. From the static qualities given in figures 6.4 and 6.5, it can be seen that vapor mass starts to develop far upstream of the experimentally determined values. It is more easily observed by looking at where the mixture qualities become positive in figures 6.6 and 6.7. For run #71 it is observed that flashing occurs further downstream using the R-T model than with the H-F model. This is indicative of the pressure undershoot model used by the R-T model. For case #55 however, it seems that the entrance loss is great enough to cause flashing at the entrance for both models. This indicates that while neither model provides a good estimate of the flashing locations, the entrance loss coefficient must be well known as well as roughness to improve the predictions of the models. The H-F model predicts a much larger void fraction and quality than the R-T model downstream of the flashing point. This could be indicative of the equilibrium flashing criteria at saturation

that the H-F model employs. The R-T model on the other hand is using a pressure undershoot which requires a larger drop in pressure to provide the superheat required for bubble growth, therefore the void fraction develops more gradually along the channel length.

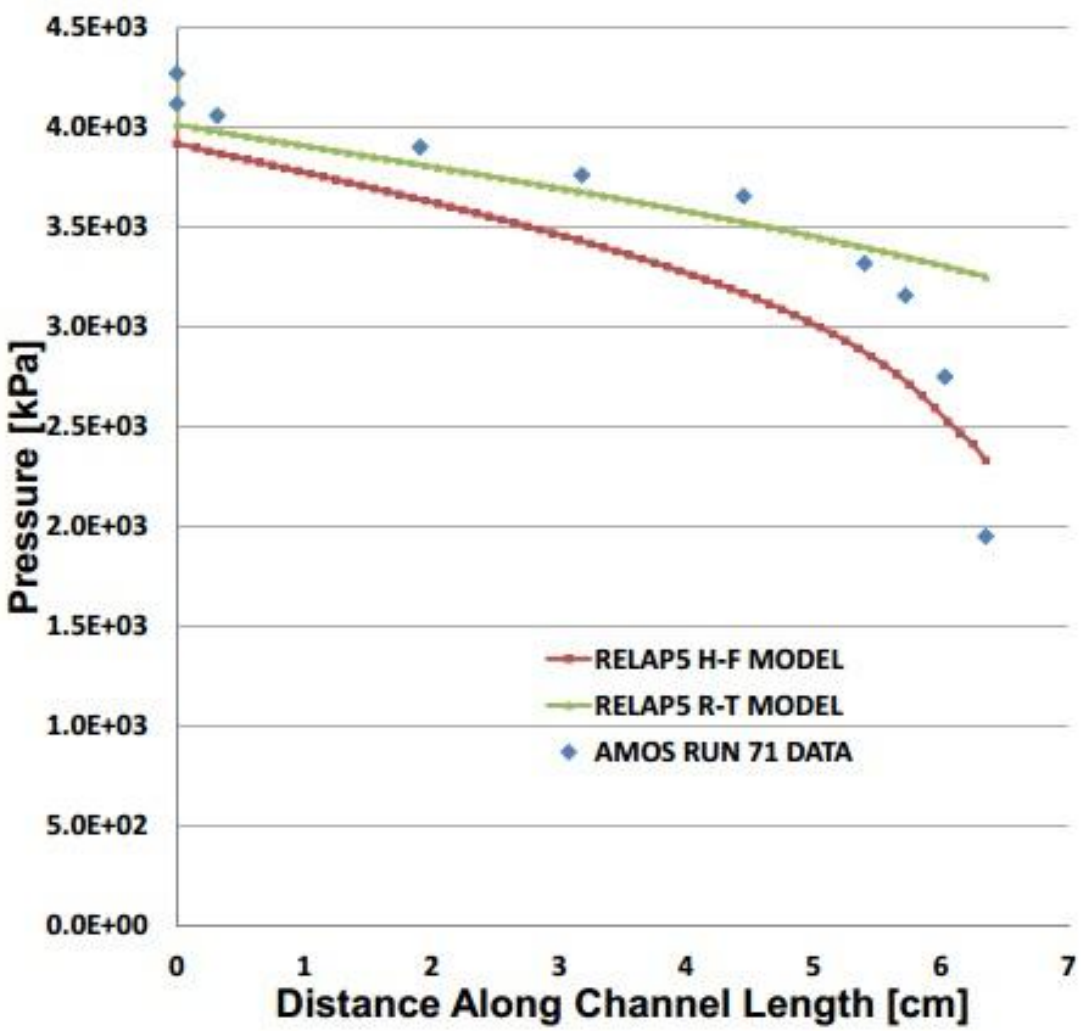

Figure 6.2: Pressure profile along channel length (L=6.35 cm) for Amos Run#71, with 4.8 K subcooling at 4.272 MPa, with H-F and R-T model predictions.

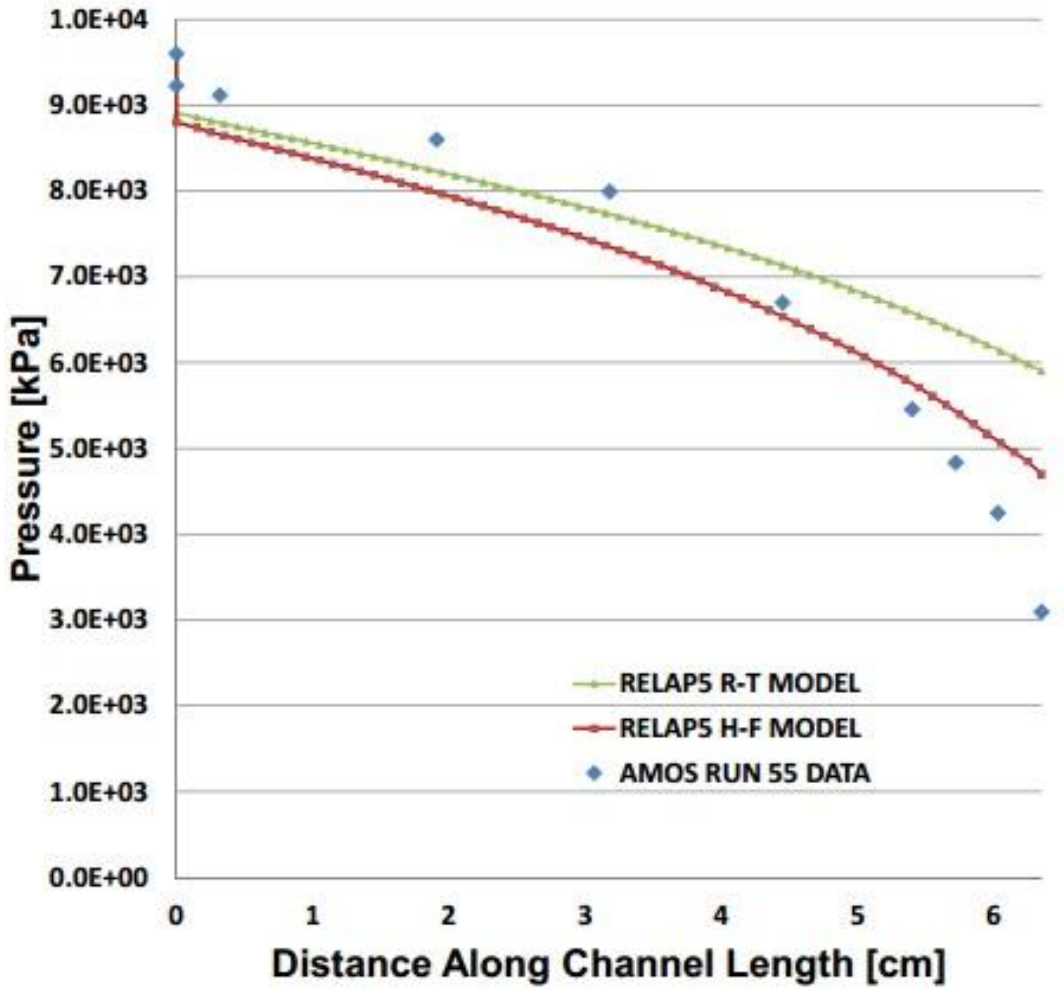

Figure 6.3: Pressure profile along channel length (L=6.35 cm) for Amos Run#55, with 3.9 K subcooling at 9.602 MPa, with H-F and R-T model predictions

In the case of higher subcooling at the inlet, it is expected that the liquid remains subcooled throughout the channel length and flashing and choking both occur at the exit plane. This is due to the fact that there is not enough pressure drop due to entrance losses and friction to reach the saturation point of liquid at the stagnation temperature. It is observed however that of the 23 runs studied that both the R-T and H-F models predict flashing to occur in all cases. The R-T model however, determined flashing to occur further downstream than that of the H-F model, again indicative of thermal non-equilibrium. For the highest subcoolings (Run #'s 68, 23, 36, 51 and 95), the flashing locations predicted by the R-T model were 61, 60, 59, 60 and 59 mm respectively. The H-F model predictions were much further upstream at 55, 51, 49, 52, 47 mm. In general this would lead one to believe that the H-F model would under predict the choking flow rates due to the higher qualities at the exit and the equilibrium assumption employed. This study however, found that this was not the case. Table, 6.1 lists a subset of the cases examined using RELAP5. As can be seen, the H-F model predicts higher critical mass flux in every case when compared

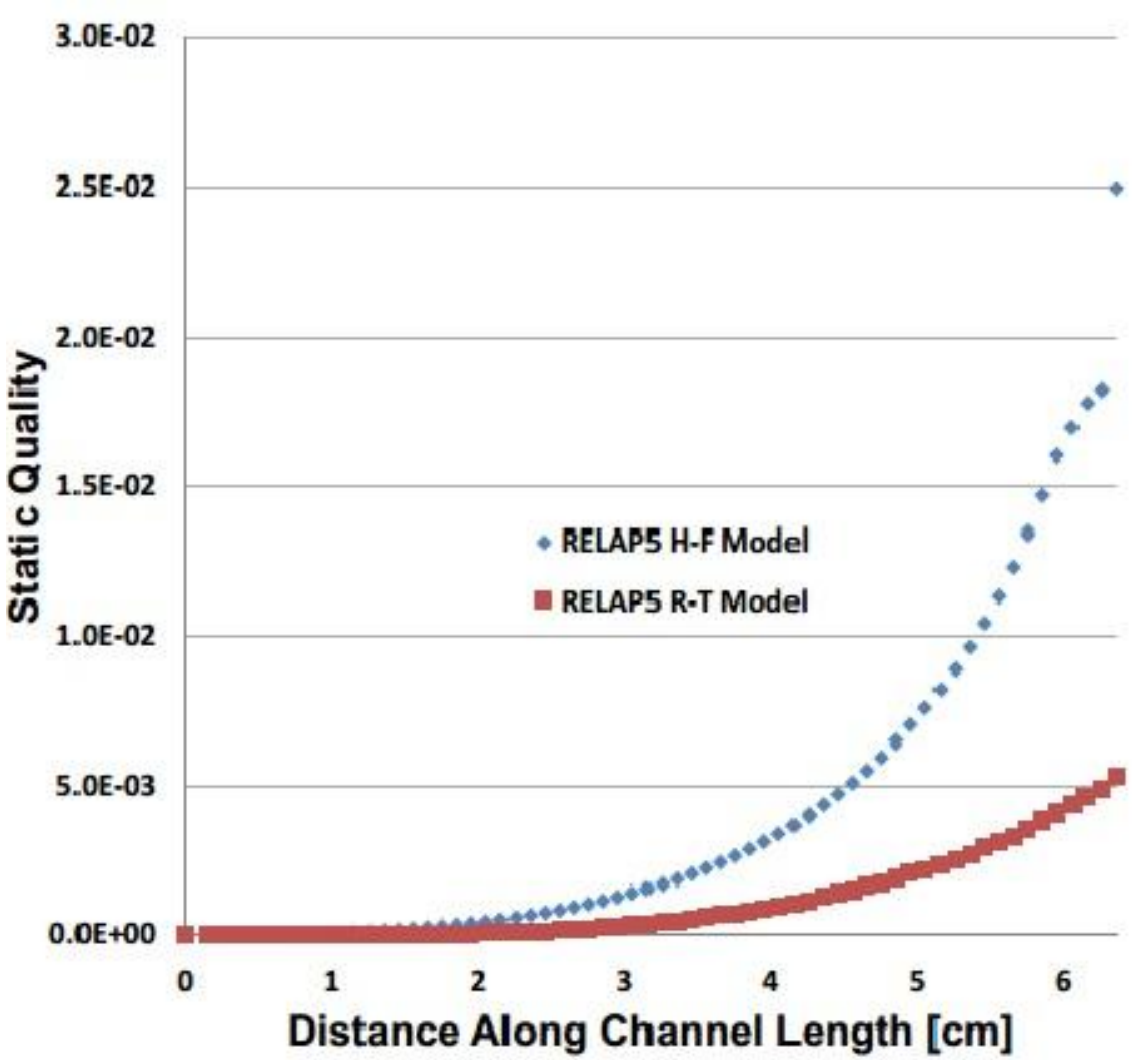

Figure 6.4: Static Quality versus channel length produced by the H-F and R-T models in RELAP5 using the stagnation conditions of Amos Run#71.

to the R-T model. It is hard to determine a relationship between subcooling and the model predictions, however at the lowest subcoolings the R-T model gives a better prediction to the critical mass flux. Also, in general the H-F model shows an over prediction of the mass flux. A better representation of these findings is shown in figure 6.8. The R-T model predicted the mass flux to within 6% for a majority of the cases, while the H-F model over predicted much of the data by as much as 37% in some cases. No absolute conclusion can be made from this study, however the R-T model is obviously a better choice in determining the choking mass flux from this geometry.

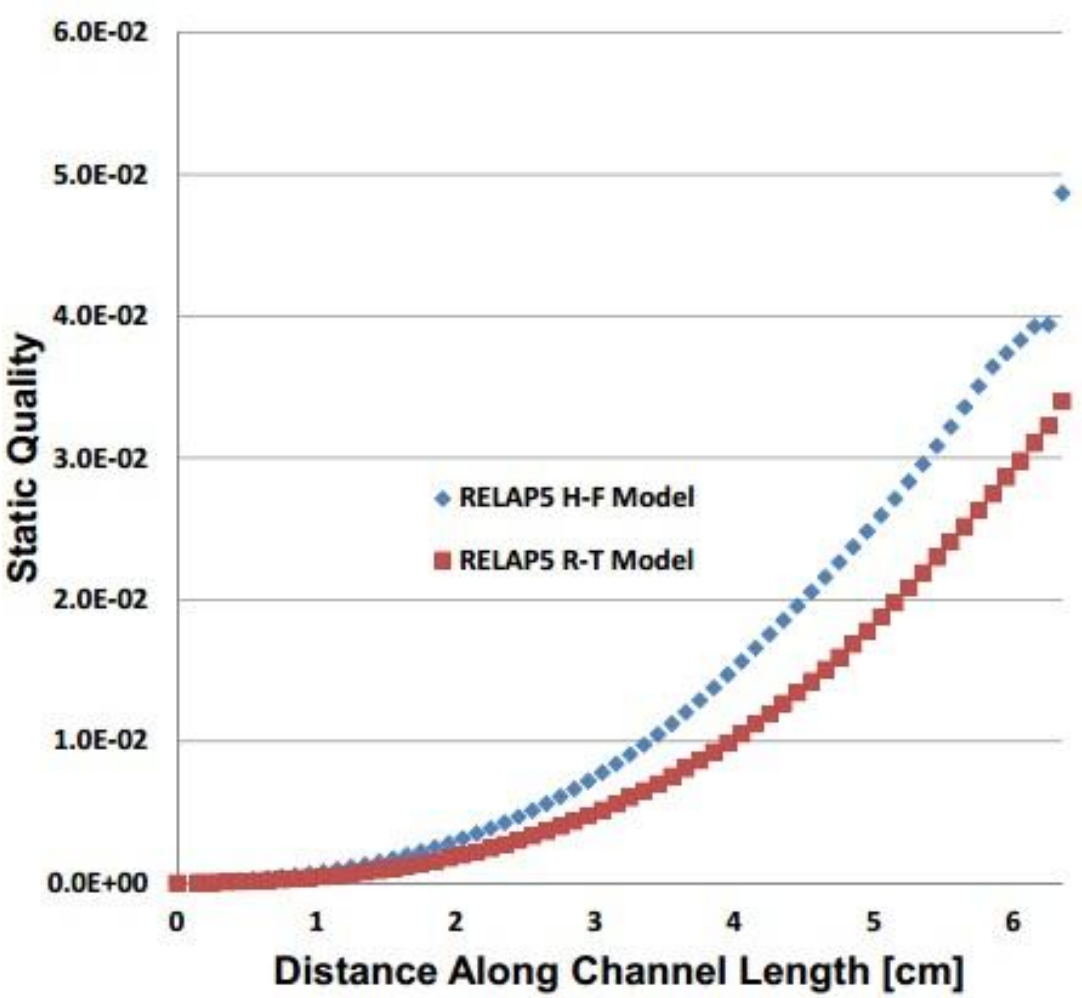

Figure 6.5: Static Quality versus channel length produced by the H-F and R-T models in RELAP5 using the stagnation conditions of Amos Run#55.

It was of interest to see how the two models behaved as the channel length was shortened from 63.5 mm to 1 mm and then even to simply a choking junction of zero dimension in RELAP5 at low subcooling. The models behaved somewhat as expected in that as the channel length is shortened for the same upstream condition, the predicted mass flux increases exponentially. The R-T model under predicts the H-F model in all cases except for when the channel is treated as a single junction with zero dimension as seen in Figure 6.9. When the choking plane is treated as a junction the void fraction just upstream of the choking condition is 0 for both cases as seen in Figure 6.10. As seen in Figure 6.9, the H-F model has a discontinuity in the mass flow calculation when the fluid just before the choking plane is of low void. This is due to the homogeneous assumptions employed in the model. The R-T model on the other hand has a smooth transition toward the point of zero void before the choking plane. It is interesting however that the two models predict void fraction in an entirely different manner as seen in Figure 6.11.

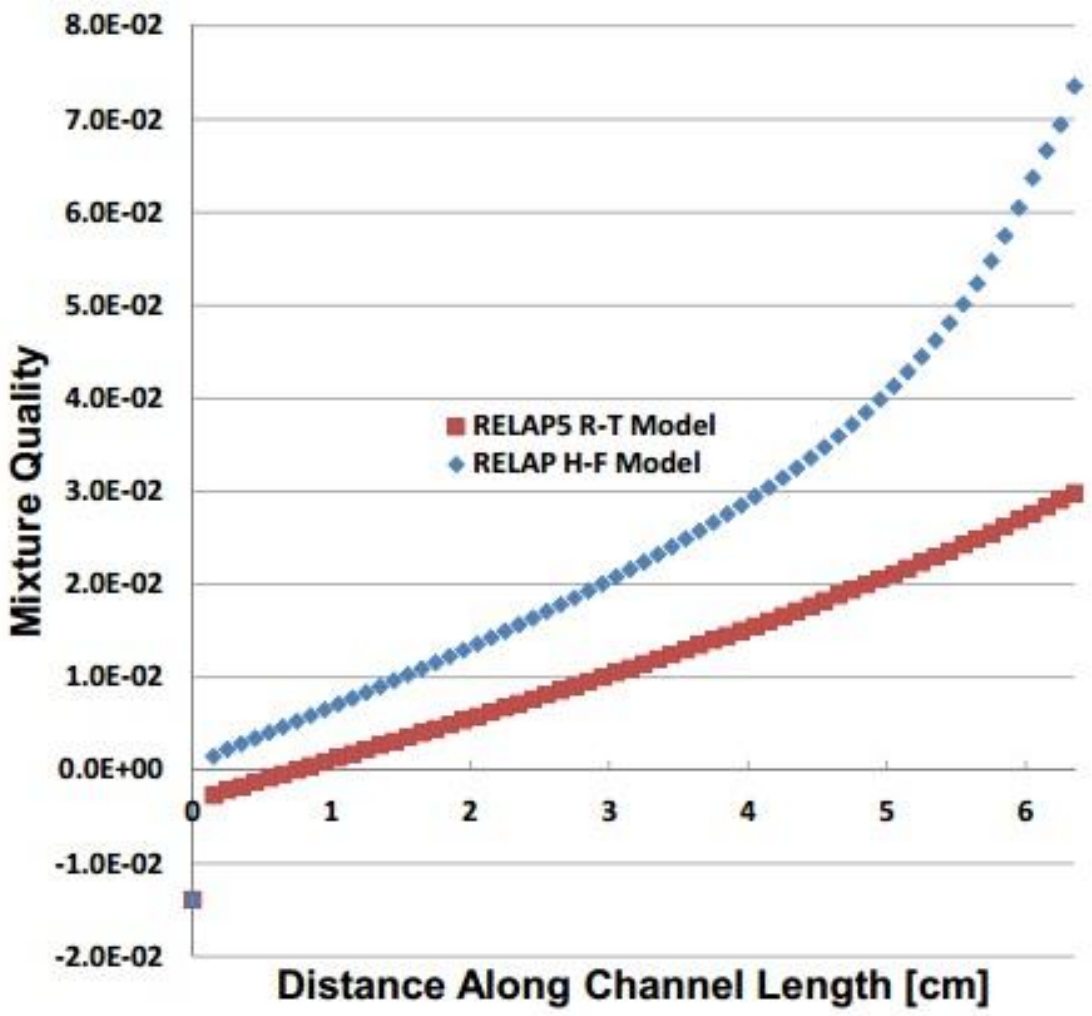

Figure 6.6: Mixture Quality versus channel length produced by the H-F and R-T models in RELAP5 using the stagnation conditions of Amos Run#71.

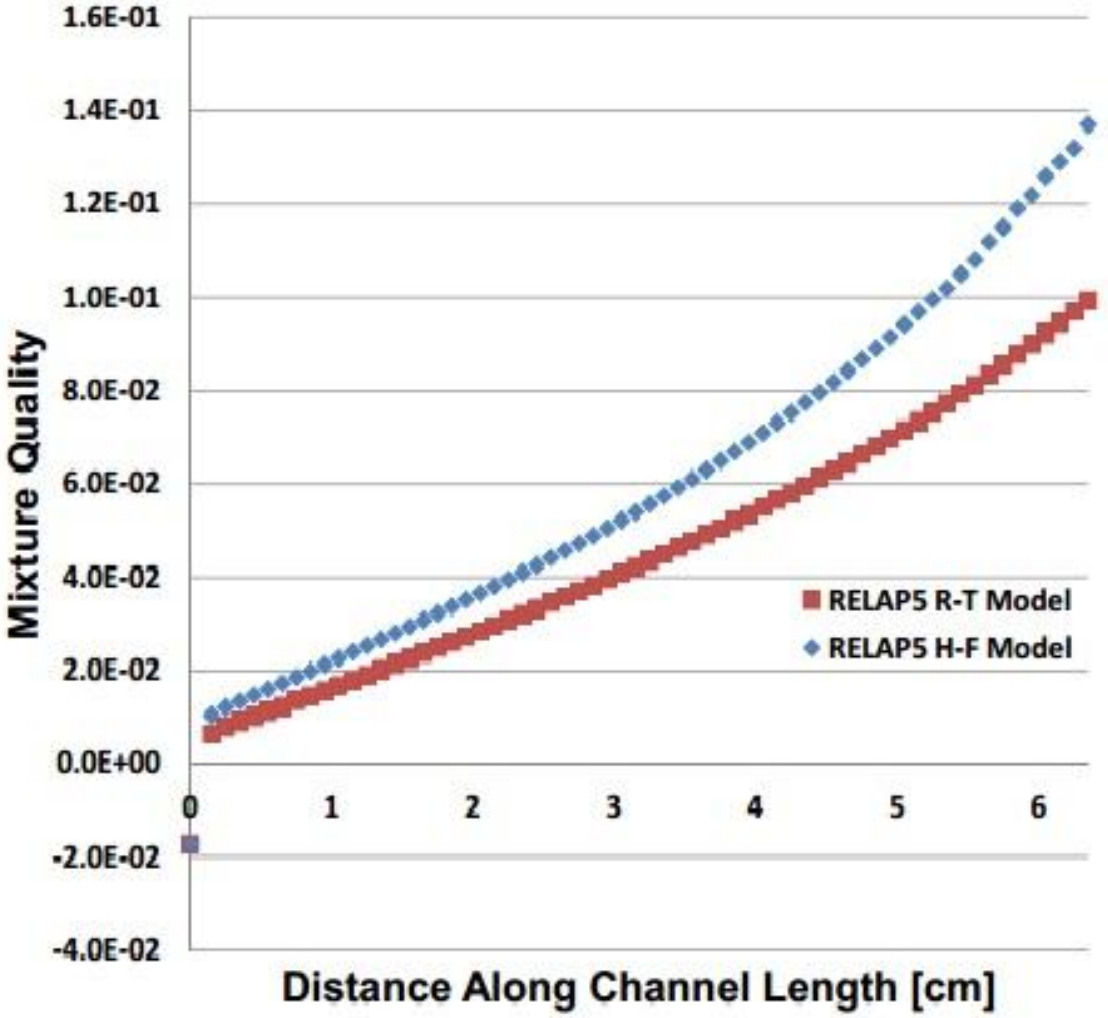

Figure 6.7: Mixture Quality versus channel length produced by the H-F and R- T models in RELAP5 using the stagnation conditions of Amos Run#55.

Table 6.1: Comparison of the H-F and R-T choked flow predictions to Amos and Schrock (1983) experimental data for 2.54E-4 m nominal slit openings (L=6.35 cm).

	Experiment			RELAP5 Henry-Fauske			RELAP5 Ransom-Trapp		
Run #	Pressure [Mpa]	ΔTsub	Gc [kg/m2 s]	Gc [kg/m2 s]	ΔGc %	Pexit [Mpa]	Gc [kg/m2 s]	ΔGc %	Pexit [Mpa]
68	4.289	59.6	3.500E+04	3.440E+04	-1.72	1.004	3.313E+04	-5.33	1.302
70	4.320	30.7	2.849E+04	2.914E+04	2.27	1.626	2.680E+04	-5.95	2.265
69	4.281	14.9	2.160E+04	2.435E+04	12.71	2.016	2.032E+04	-5.91	3.047
71	4.272	4.8	1.687E+04	2.052E+04	21.62	2.332	1.752E+04	3.86	3.254
23	7.117	61.2	4.271E+04	4.866E+04	13.93	1.695	4.626E+04	8.30	2.398
51	7.050	60.3	4.091E+04	4.109E+04	0.44	1.708	3.909E+04	-4.44	2.385
24	7.055	29.2	3.641E+04	4.007E+04	10.04	2.636	3.578E+04	-1.73	4.022
25	7.055	18.2	3.131E+04	3.543E+04	13.15	3.047	3.001E+04	-4.15	4.776
26	7.000	3.3	2.027E+04	2.788E+04	37.53	3.698	2.468E+04	21.77	5.018
36	9.553	59.1	4.405E+04	4.569E+04	3.73	2.300	4.279E+04	-2.85	3.525
37	9.600	28.1	3.247E+04	3.797E+04	16.93	3.412	3.256E+04	0.27	5.723
38	9.667	22.4	2.748E+04	3.733E+04	35.84	3.702	3.156E+04	14.83	6.149
55	9.602	3.9	2.198E+04	2.925E+04	33.07	4.700	2.705E+04	23.08	5.902
98	9.774	58.0	4.883E+04	4.912E+04	0.59	2.372	4.584E+04	-6.12	3.698
52	11.728	59.9	4.924E+04	5.110E+04	3.78	2.775	4.749E+04	-3.56	4.470
39	11.601	54.9	4.413E+04	4.394E+04	-0.43	2.844	4.025E+04	-8.79	4.733
54	11.696	30.0	3.852E+04	4.393E+04	14.03	3.984	3.736E+04	-3.01	6.935
95	12.420	61.5	5.137E+04	5.597E+04	8.96	2.781	5.180E+04	0.84	4.686
96	11.642	26.4	3.901E+04	4.495E+04	15.22	4.080	3.731E+04	-4.37	7.269
93	11.838	12.9	3.224E+04	4.011E+04	24.41	4.887	3.481E+04	7.97	7.480
72	15.601	54.2	5.019E+04	6.206E+04	23.64	3.597	5.563E+04	10.83	6.844
92	15.798	12.0	4.231E+04	4.579E+04	8.23	6.055	4.120E+04	-2.61	8.799
97	15.747	12.0	3.703E+04	4.354E+04	17.58	5.884	3.959E+04	6.91	8.452

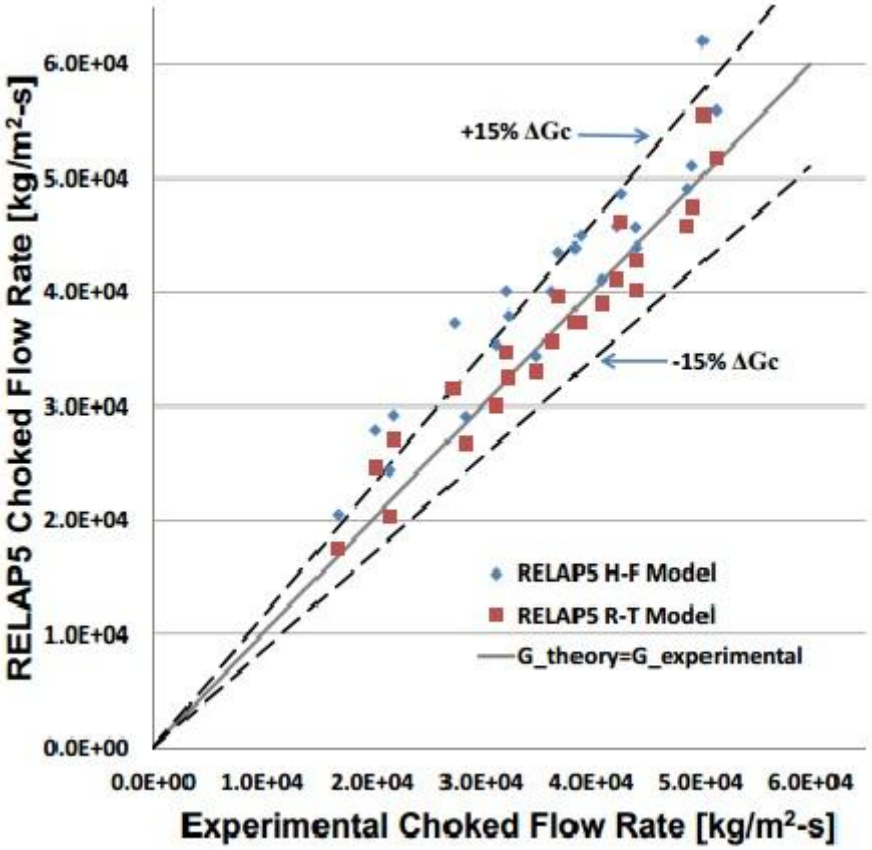

Figure 6.8: Comparison of the H-F and R-T choked flow predictions to Amos and Schrock (1983) experimental data for 2.54E-4 m nominal slit openings (L=6.35 cm)

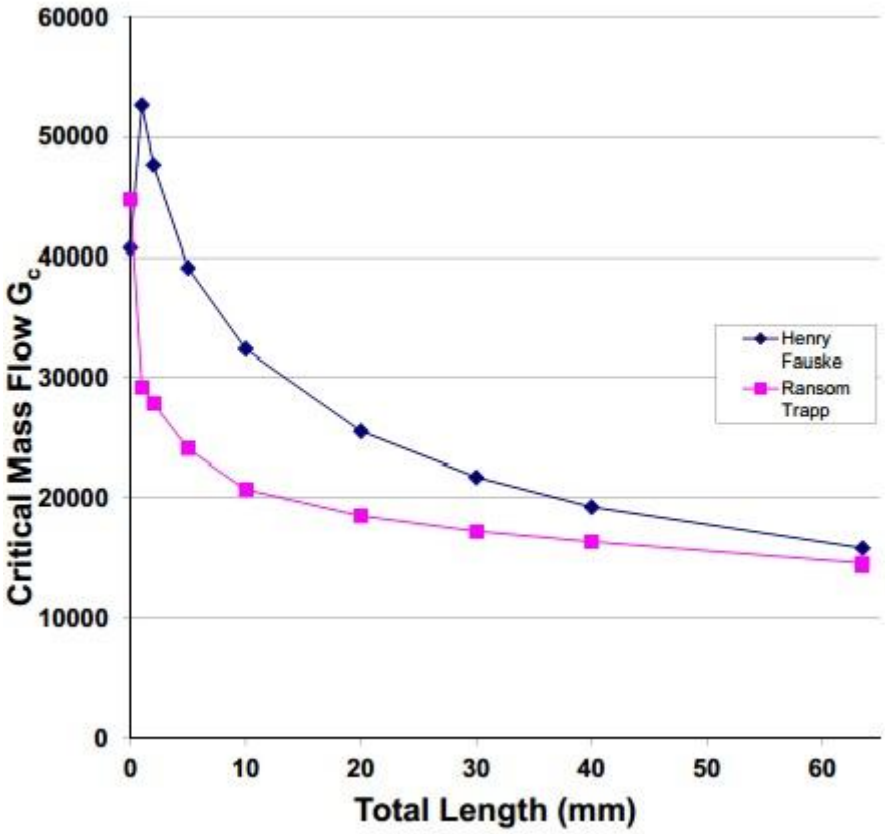

Figure 6.9: Critical mass flux at low subcooling for different total channel lengths

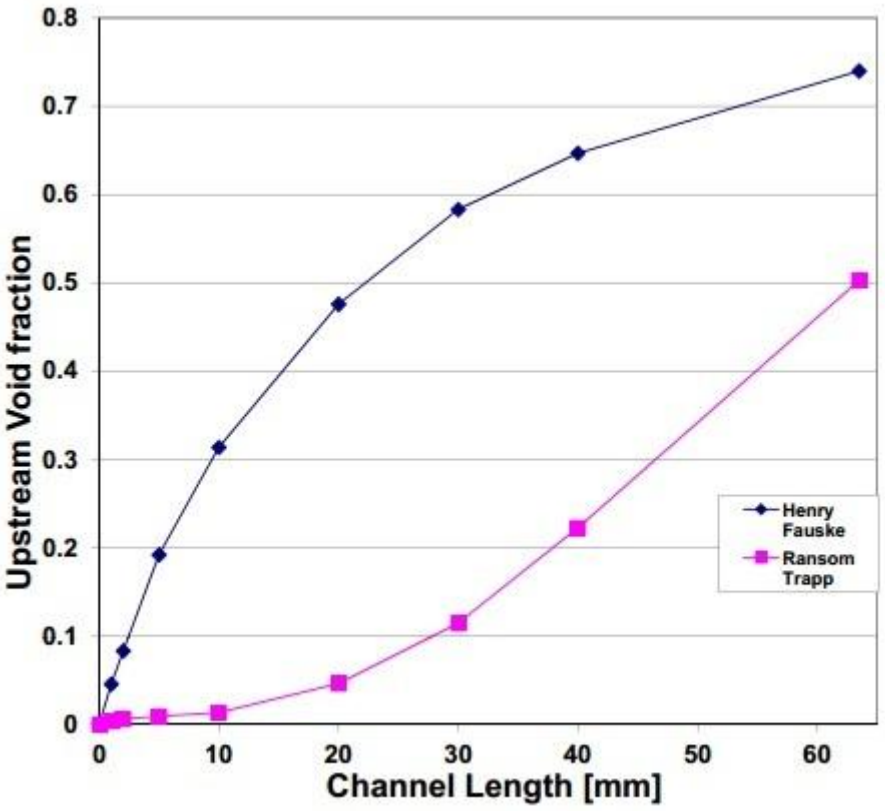

Figure 6.10: Void fraction just upstream of the choking plane for low subcooling for different channel lengths.

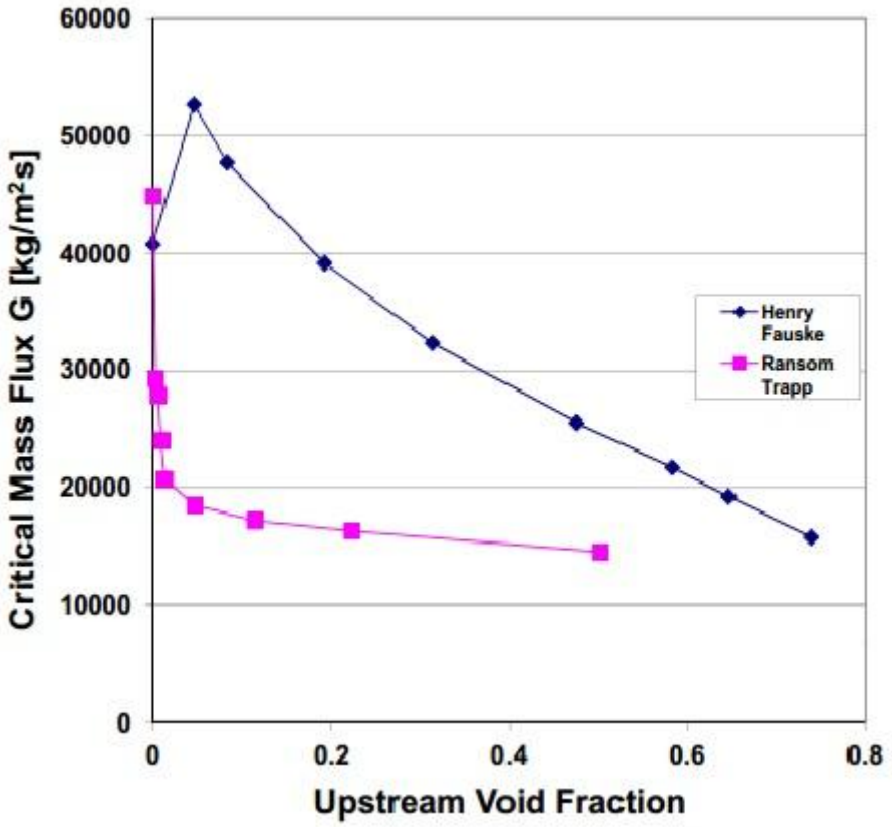

Figure 6.11: Critical mass flux versus upstream void fraction at low subcooling.

From these simple studies one can make assumptions as to how the model predictions will behave as the channel length is shortened. In the case of the simulated steam generator tube cracks in this study, the channel length are 3.175 mm and 1.3 mm. From figure 6.12 for cracks with channel length of 3.175 mm the critical mass flow rates predicted by the two models will diverge when compared to longer length channels. Also, the upstream void fractions will converge. This is indicative that the H-F model will further over predict the choking mass flux for the shortened channels, while the R-T model will either under predict remain the same with regards to percent difference of the prediction to experimental values. From these observations the analysis continues by applying the RELAP5 models to that of the data collected in this study.

It is advised in the RELAP manuals that a node size should be twice that of the hydraulic diameter. This allows for 5 nodes along the channel length to be used in this analysis. Tables 6.2 and 6.3 summarizes the predictions of both the H-F and R-T models versus the experimentally obtained values. In general, the models strayed further away from the data. The H-F model over predicts the mass flux in all but two runs, both of which Again, the choking mass flux data collected in this study had a channel length of 3.175 mm, with stagnation pressure near 6.8 MPa. The H-F and R-T models are both used to predict the experimentally obtained values a similar nodalization as previously discussed with the exception of the number of nodes used in the channel section were at high subcooling. The R-T model under predicts the data in every case.

Figure 6.13, shows comparison of model predictions with experimental data for simulated cracks with channel length 1.3 mm. As the channel length was shortened, the predictions by the R-T model strayed further away from that of the H-F models. There is a clear separation between the predictions. In this case, neither model can be chosen as a superior choice in modeling such flow. If there was such a case which required the use of RELAP5 to predict flows in very short channels, then a conservative point of view must be taken. In the choking flow analysis in nuclear reactors, a conservative point of view would be a greater loss of coolant inventory than expected. This would lead to a model choice which in general would over predict the flow rate exiting the reactor, or under predict the coolant inventory. If this were the determinant case, then the H-F model would be a better choice in predicting the choking mass flux through cracks or channels which exhibit similar characteristics as those in this study.

Table 6.2: Comparison of the H-F and R-T choked flow predictions to data collected in this study (L=3.175 mm)

Spec. #	Experiment			RELAP5 Henry-Fauske			RELAP5 Ransom-Trapp		
	Pressure [Mpa]	ΔTsub	Gc [kg/m2 s]	Gc [kg/m2 s]	ΔGc %	Pexit [Mpa]	Gc [kg/m2 s]	ΔGc %	Pexit [Mpa]
2	6.728	46.1	6.571E+04	7.008E+04	6.65	1.541	6.012E+04	-8.51	3.039
	6.735	42.1	6.268E+04	6.937E+04	10.66	1.589	5.838E+04	-6.86	3.230
	6.874	32.5	5.603E+04	6.866E+04	22.54	1.680	5.404E+04	-3.54	3.809
3	6.735	45.3	7.090E+04	6.980E+04	-1.55	1.561	5.970E+04	-15.80	3.079
	6.728	38.9	6.837E+04	6.862E+04	0.36	1.632	5.681E+04	-16.91	3.380
	6.758	34.1	6.406E+04	6.799E+04	6.13	1.684	5.449E+04	-14.94	3.649
	6.866	29.9	6.280E+04	6.806E+04	8.38	1.710	5.247E+04	-16.45	3.954
4	6.770	48.1	6.111E+04	6.965E+04	13.97	1.589	6.044E+04	-1.10	2.976
	6.776	38.2	5.795E+04	6.791E+04	17.19	1.696	5.614E+04	-3.12	3.445
	6.831	32.8	5.414E+04	6.733E+04	24.37	1.752	5.354E+04	-1.12	3.768
	6.818	27.7	5.268E+04	6.658E+04	26.39	1.784	5.060E+04	-3.95	4.054
5	6.698	46.9	6.652E+04	6.881E+04	3.43	1.609	5.958E+04	-10.44	2.989
	6.770	40.0	6.520E+04	6.795E+04	4.22	1.690	5.683E+04	-12.83	3.350
	6.786	31.9	5.615E+04	6.668E+04	18.75	1.775	5.286E+04	-5.86	3.782
	6.849	27.4	5.571E+04	6.645E+04	19.28	1.803	5.036E+04	-9.59	4.093
6	6.681	46.3	6.934E+04	6.661E+04	-3.93	1.793	5.830E+04	-15.91	3.014
	6.597	38.5	6.134E+04	6.510E+04	6.14	1.810	5.469E+04	-10.83	3.331
	6.767	33.4	5.973E+04	6.521E+04	9.18	1.862	5.265E+04	-11.84	3.702
	6.737	24.7	5.599E+04	6.383E+04	14.02	1.918	4.763E+04	-14.92	4.186

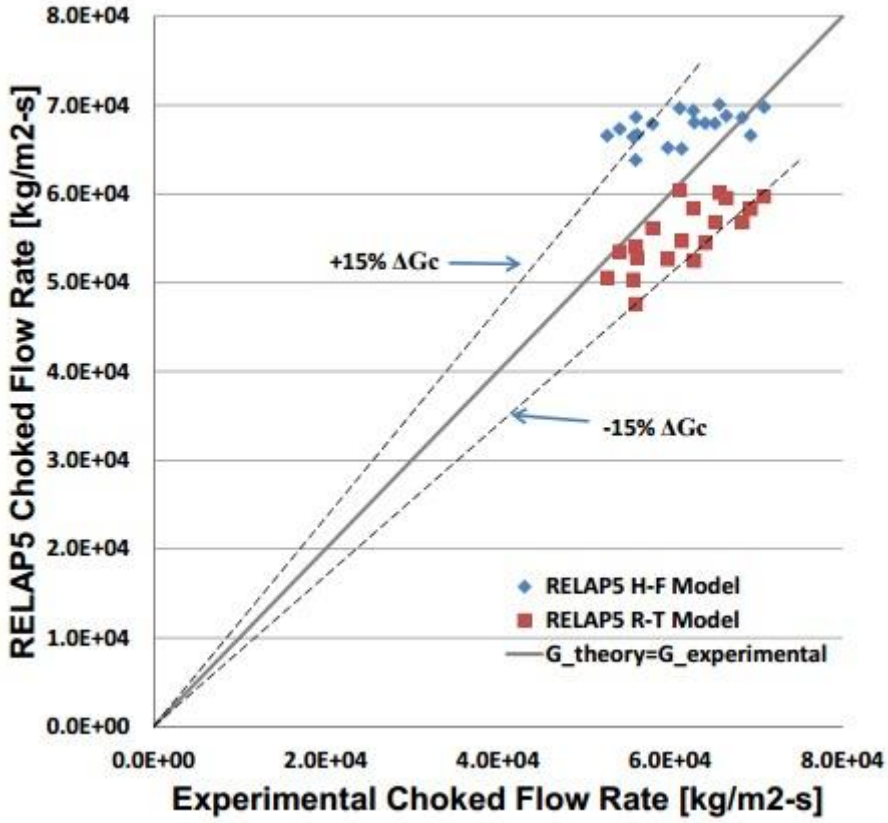

Figure 6.12: Comparison of the H-F and R-T choked flow predictions to data collected in this study (L=3.175 mm)

Table 6.3: Comparison of the H-F and R-T choked flow predictions to data collected in this study (L=1.3 mm)

Sample	Pressure	Subcooling	Exp Gc	Henry Fauske		Ransom Trapp		Junction	
	[kPa]	ΔT [° C]	[kg/m²s]	Gc [kg/m²s]	ΔGc [%]	Gc [kg/m²s]	ΔGc [%]	Gc [kg/m²s]	ΔGc [%]
Laser7	6756	43.6	7.848E+04	7.595E+04	3.2	6.206E+04	20.9	6.466E+04	17.6
Laser7	6877	50.3	7.936E+04	7.603E+04	4.2	6.217E+04	21.7	6.524E+04	17.8
Laser7	6764	38.0	6.821E+04	7.544E+04	-10.6	5.937E+04	13.0	6.437E+04	5.6
Laser7	6708	32.2	6.247E+04	7.432E+04	-19.0	5.610E+04	10.2	6.377E+04	-2.1
Laser7	6806	23.0	7.594E+04	7.350E+04	3.2	5.056E+04	33.4	6.356E+04	16.3
Laser7	6583	14.1	5.817E+04	7.072E+04	-21.6	4.325E+04	25.6	5.632E+04	3.2
Laser8	6641	46.8	5.010E+04	7.556E+04	-50.8	6.315E+04	-26.1	6.433E+04	-28.4
Laser8	6746	50.5	4.975E+04	7.594E+04	-52.6	6.510E+04	-30.8	6.499E+04	-30.6
Laser8	6741	40.0	5.183E+04	7.569E+04	-46.0	6.031E+04	-16.4	6.437E+04	-24.2
Laser8	6649	39.0	4.940E+04	7.498E+04	-51.8	5.932E+04	-20.1	6.389E+04	-29.3
Laser8	6821	35.3	5.408E+04	7.559E+04	-39.8	5.783E+04	-6.9	6.445E+04	-19.2
Laser8	6933	28.2	4.507E+04	7.523E+04	-66.9	5.459E+04	-21.1	6.449E+04	-43.1
Laser8	6776	30.3	5.478E+04	7.461E+04	-36.2	5.527E+04	-0.9	6.395E+04	-16.7
Laser9	6768	50.4	5.900E+04	7.471E+04	-26.6	6.508E+04	-10.3	6.509E+04	-10.3
Laser9	6761	51.1	7.683E+04	7.288E+04	5.1	6.535E+04	14.9	6.509E+04	15.3
Laser9	6845	39.9	7.046E+04	7.622E+04	-8.2	6.062E+04	14.0	6.482E+04	8.0
Laser9	6826	44.0	5.900E+04	7.651E+04	-29.7	6.251E+04	-6.0	6.498E+04	-10.1
Laser9	6787	35.8	6.622E+04	7.535E+04	-13.8	5.835E+04	11.9	6.433E+04	2.8
Laser9	6900	28.8	6.409E+04	7.509E+04	-17.1	5.492E+04	14.3	6.440E+04	-0.5
Weld10	6715	46.7	6.624E+04	7.858E+04	-18.6	6.490E+04	2.0	6.465E+04	2.4
Weld10	6853	41.3	6.624E+04	7.861E+04	-18.7	6.289E+04	5.1	6.494E+04	2.0
Weld10	6851	32.7	6.717E+04	7.727E+04	-15.0	5.828E+04	13.2	6.442E+04	4.1
Weld10	6852	25.5	5.841E+04	7.609E+04	-30.3	5.379E+04	7.9	6.396E+04	-9.5
Weld11	6847	28.0	4.970E+04	7.665E+04	-54.2	5.551E+04	-11.7	6.409E+04	-29.0
Weld11	6758	37.1	5.501E+04	7.761E+04	-41.1	6.055E+04	-10.1	6.427E+04	-16.8
Weld11	6702	45.2	5.845E+04	7.848E+04	-34.3	6.430E+04	-10.0	6.450E+04	-10.3
Weld12	6799	49.1	7.133E+04	7.609E+04	-6.7	6.458E+04	9.5	6.515E+04	8.7
Weld12	6932	42.7	8.259E+04	7.700E+04	6.8	6.224E+04	24.6	6.536E+04	20.9
Weld12	6856	34.8	7.520E+04	7.556E+04	-0.5	5.797E+04	22.9	6.456E+04	14.1
Weld12	6788	24.2	6.476E+04	7.358E+04	-13.6	5.135E+04	20.7	6.361E+04	1.8
Weld13	6798	48.0	8.477E+04	7.818E+04	7.8	6.490E+04	23.4	6.508E+04	23.2
Weld13	6853	42.9	7.463E+04	7.779E+04	-4.2	6.282E+04	15.8	6.503E+04	12.9
Weld13	6840	35.7	8.827E+04	7.666E+04	13.2	5.916E+04	33.0	6.455E+04	26.9
Weld13	6918	28.2	6.742E+04	7.591E+04	-12.6	5.499E+04	18.4	6.441E+04	4.5

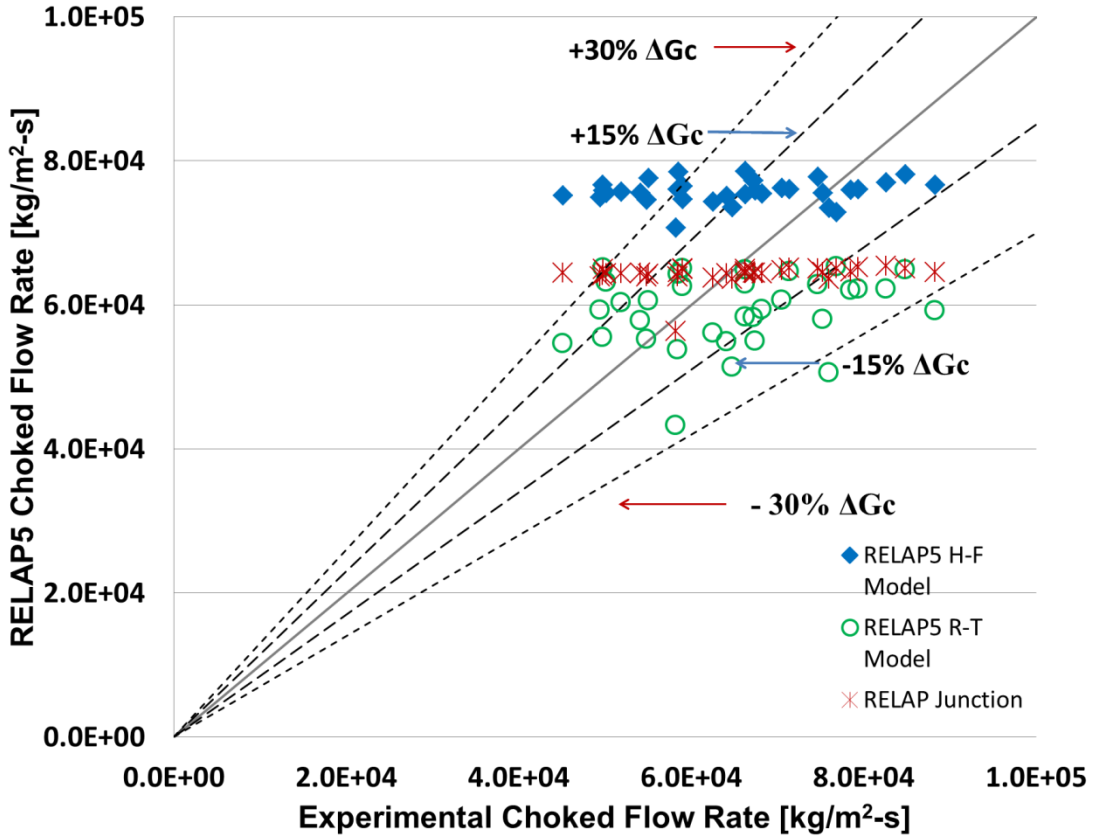

Figure 6.13: Comparison of the H-F and R-T choked flow predictions to data collected in this study (L=1.3 mm)

6.4 **Conclusions**

A limited analysis has been done to assess the validity of using RELAP5, a one-dimensional thermal-hydraulic system code, for modeling of small L/D cracks and specifically small length channels. Current implementation of RELAP5 has used imbedded models to predict flow parameters such as entrance loss coefficient however friction factor and entrance loss are found to play an important role in the choking predictions. A RELAP5 nodalization was created to model experimental data from literature as well as the current experimental program data. It is found that both the Henry-Fauske and Ransom-Trapp models better predict choking mass flux for longer channels. As the length of a channel decreases the H-F and R-T model predictions diverge from each other. While RELAP5 has been shown to predict choking flow in large scale geometries, it is not suited well for small channel lengths such as those in the current experimental program. In the case of a more conservative approach, where over prediction of mass flux through short channels is best, the H-F model would be most appropriate.

However, for the smallest channel length of 1.3 mm, both models predicted an almost constant value regardless of the obtained experimental value for similar conditions. This may be due to the limited nodalization options for such small geometries but leads to the conclusion that flashing is occurring beyond the exit of the channel

7. INTEGRAL MODEL FOR CHOKED FLOW

Modeling fluid flow has many different scales of complexity. In the previous chapter, a steady-state one-dimensional homogeneous model was developed, which would be considered the simplest form of a model that takes into account most aspects of the flow using conservation equations. One-dimensional flow models have been well established throughout the engineering community and have a proven track record for reliability and accuracy for simple flows. The complexity of a model will obviously increase as dimensions are added as well as the number of conservation equations. Multi-field models have recently gained much research interest, due to their promising ability to model complex transport phenomena. This approach applies conservation laws of mass, momentum, and energy to each phase and constitutive relations are used to close the system of equations. Some researchers have deemed the two-fluid model "ill-posed and mathematically complex, in the sense that the equation system is non-hyperbolic, non-linear, and non-conservative". Often times, the accuracy of the solution is questioned due to uncertainty in the constitutive relations, com-pounded by the presence of numerical errors. The next chapter will focus on modeling efforts using the state of the art two-fluid models available in the best estimate thermal-hydraulics code RELAP5.

7.1 Discharge Coefficient Models

In many instances, it is beneficial and required to make an estimate of a solution without the complexity of a multi-field model. An example of such would be the application of the discharge coefficient to approximate with great accuracy the flow rate through an orifice or nozzle. The discharge coefficient simply makes a correction to the ideal case. It is of interest in the case of choking flow through steam generator tube cracks to compare simple models, which have a low degree of difficulty in implementation. In fact, a discharge coefficient model has a direct relationship with the L/D, especially L in this study. For L/D = 0, experimental data shows that the critical mass flux can be shown by:

$$G_c = 0.61\sqrt{2\rho_f(p_0 - p_b)} \tag{7.1}$$

A similar expression has been found useful for 0 < L/D < 3, however it relies on experimental data or charts to define p_b. For 3 < L/D < 12 the flow is less than that predicted by these equations (Kazimi and Todreas, 1990). As stated in the introduction, data in this region is also greatly lacking. Generally, the prediction of two-phase critical flow remains unsolved. The results of one model predict an experimental data set well, but not others. This is affirmed by the many correlations for discharge coefficients for choking flow that have been proposed in the past.

The theoretical mass flow rate through a restriction can be easily derived from the Bernoulli equation. The actual flow rate can then be determined by multiplying the theoretical flow rate by the appropriate discharge coefficient. A final form of this equation is given by Fox & McDonald (Fox and McDonald, 1998) as:

$$\dot{m}_{actual} = C_d A_t \frac{\sqrt{2\rho(p_1 - p_2}}{\sqrt{1-\beta^4}} \tag{7.2}$$

where t specifies throat and 1 and 2 represent the upstream and downstream conditions. The factor β is given as a ratio of the throat diameter to the upstream diameter (Dt/D1). The discharge coefficient Cd is the parameter that is fitted to experimental data. This can take on many forms and is typically a function of Reynold's number and geometry of the restriction. For example, a correlating equation recommended for concentric orifices with corner taps is:

$$C_d = 0.5959 + 0.0312\beta^{2.1} - 0.184\beta^8 + \frac{91.71\beta^{2.5}}{Re_{D_1}^{0.75}} \tag{7.3}$$

7.1.1 **Burnell Model**

Of course, there are many other correlations for nozzles, venturis and other flow path interruptions. Typically, these correlations are limited to subcooled liquid flow. Few studies have been done on fluids with partial phase change. The researchers that studied two-phase flow through orifices simply multiplied the discharge coefficient by a so called 'expansion factor' (Romig, 1996). Similarly, Burnell (Burnell, 1946) made use of an empirical correlation for the critical pressure or throat pressure to correct for the delay caused in nucleation through an orifice (L/D < 1), which results in high flow rates through nozzles. The most beneficial aspect of his critical flux correlation is that it only requires knowledge of upstream stagnation conditions. The choking mass flux is given by:

$$G_c = \{2\rho_l(P - kP_{sat})\}^{0.5} \tag{7.4}$$

where k is an empirical correlation for the critical pressure given by Burnell (1947) as

$$k = 1 - 0.264\frac{\sigma(T_0)}{\sigma_{12.1\ bar}} \tag{7.5}$$

where σ is surface tension (Elias & Lellouche, 1994). Other researchers have studied flow of different fluids at different states for different L/D ratios. They each find a different correlation for the discharge coefficient that is only applicable in the range of their operating parameters. In light of this, data from this study is compared with simple choking flow models typically used for small tubes and slits, and a new correlation is developed to match the data using a modified Burnell model.

7.1.2 **Henry-Fauske Model**

In literature, many subcooled choking flow models for small tubes and slit geometries are primarily based on Henry and Fauske models (Henry & Fauske, 1971, Fauske 1985). In the code SQUIRT, which stands for "Seepage Quantification of Upsets In Reactor Tube", predications of crack geometry and critical flow through cracks in tubes are made using the Henry Fauske models (Henry & Fauske, 1971, Fauske 1985). The choking mass flux expression is given as:

$$G_c^2 = \left[\frac{x_o v_g}{nP} + (v_g - v_{fo})\left\{\frac{(1-x_o)\,N}{s_{gE} - s_{fE}}\frac{ds_{fE}}{dP} - \frac{x_o c_{pg}\,(1/n - 1/\gamma)}{P\,(s_{go} - s_{fo})}\right\}\right]_t^{-1} \tag{7.6}$$

where n is the polytropic exponent and N is an experimental parameter. If N equals unity, the prediction of the above equation is close to that of the homogeneous equilibrium model, and if N is zero the solution is the homogeneous frozen model. Therefore the quantity N describes the partial phase change occurring at the throat.

As a first order check the SQUIRT code is used to predict the choking flow through the slits. A sample set of results is shown in Table 5.1. The SQUIRT predictions are very poor for the choking flow through slits with small L/D, because the choking flow model in SQUIRT applies to large L/D, typically L/D > 12. In the present case of slits the L/D ratio is between 4 and 5.5. Here the liquid may not flash before the choking plane and the Henry and Fauske models which are based on long L/D does not apply.

Henry et al., (1975) developed a closed form choking mass flux relation for small L/D. This is given as:

$$G_c = 0.61\{2\rho_l P_0(1-\eta)\}^{0.5}$$

$$\left.\begin{aligned}\eta &= 0.1\,(\mathrm{L/D})\ \text{for}\ 0 < \mathrm{L/D} < 7\\ \eta &= 0.7\ \text{for}\ \mathrm{L/D} < 7\end{aligned}\right\} \tag{7.7}$$

The predicted mass flux with Burnell and Henry et al. (1975) models for similar upstream pressure of 6.8 MPa are shown in Table 7.1. The Burnell model over predicts the measured data. The Henry et al. model predicted lower values than those observed experimentally. Since the k value in the Burnell model uses surface tension values, a new relation is formulated to fit the experimental data. The coefficient k now depends on the upstream saturation and subcooled temperature conditions and is given as

$$k = 1 + 11.6\left(\frac{\Delta T_{sub}}{T_{sat}}\right)^{1.7} \tag{7.8}$$

A comparison between the data and predictions is shown in Figure 7.1. The new modified Burnell correlation agrees very well with the present experimental data.

Table 7.1: Predicted critical mass flux of various models

P [kPa]	Subcooling [°C]	G [kg/m²s]	SQUIRT Henry & Fauske Model (1970)	Henry et al. Model (1975)	Burnell Model (1942)	Modified Burnell
Slit #3						
6734.56	45.3	5.3123E+04	1.3394E+04	4.5327E+04	7.9909E+04	5.5077E+04
6727.95	38.9	5.1231E+04	1.3885E+04	4.5051E+04	7.5929E+04	5.2412E+04
6758.48	34.1	4.8000E+04	1.4423E+04	4.4939E+04	7.2721E+04	5.0335E+04
6865.94	29.8	4.7054E+04	1.4948E+04	4.5067E+04	6.9883E+04	4.8621E+04
Slit #4						
6769.78	48.1	5.6565E+04	1.1845E+04	4.5541E+04	8.1633E+04	5.6280E+04
6776.04	38.2	5.3640E+04	1.2944E+04	4.5165E+04	7.5645E+04	5.2264E+04
6831.01	32.8	5.0114E+04	1.3707E+04	4.5095E+04	7.2004E+04	4.9923E+04
6817.80	27.7	4.8763E+04	1.4369E+04	4.4829E+04	6.7977E+04	4.7310E+04

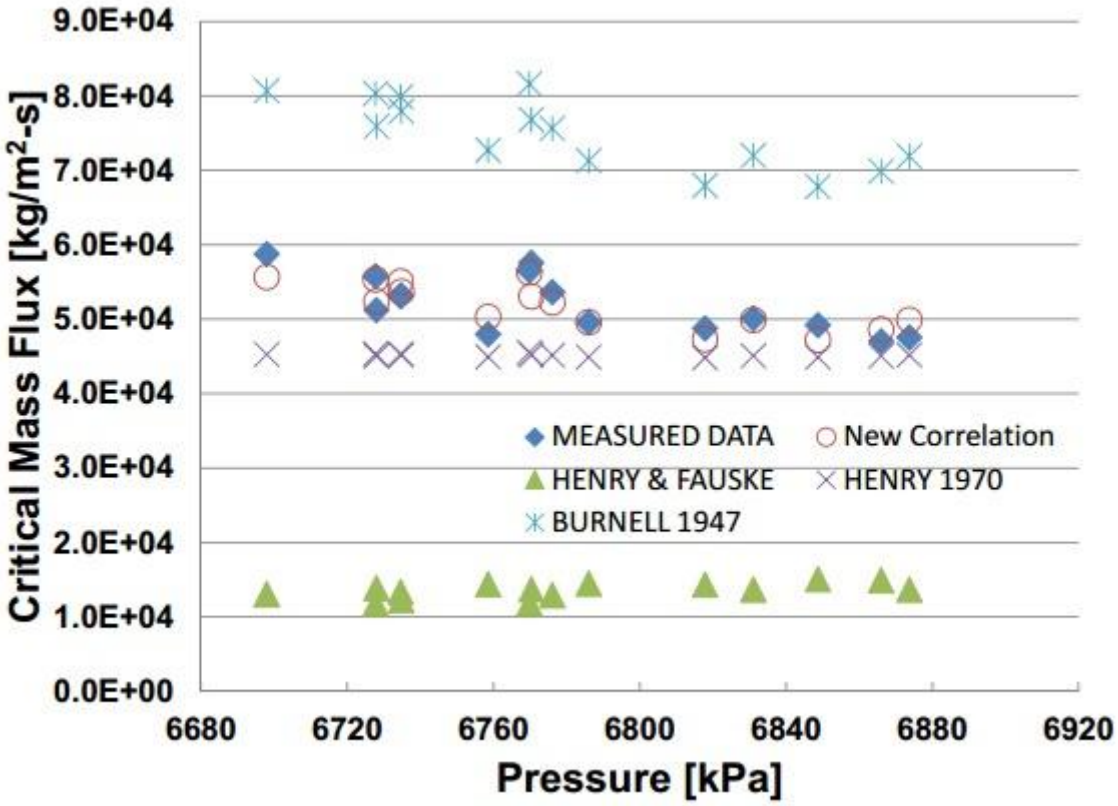

Figure 7.1: Choking mass flux data comparison with model predictions for slits near 7 MPa.

8. APPLICATION OF DATA TO PROTOTYPE CONDITIONS

8.1 Conditions

In general, choked flow is not directly scalable. This is due to the inherent nature of the phenomena and the dependence of the sound speed on pressure, temperature and fluid properties. If the model and prototype have the same pressure and temperature, then special flow area scaling for components which exhibit choked flow can be accomplished (Ransom et al., 1998). The conditions downstream of the choking plane do not affect the choking velocity unless the upstream pressure is reduced below twice the downstream pressure, in which an unchoked condition will exist. The unchoked condition will then be dominated by typical pipe flow characteristics. In the present study, experiments were conducted with the upstream pressure near 6.9 MPa, while the prototypic pressurized water reactor has a primary pressure of more than double, near 15.5 MPa. In this case the choking mass flux dependent properties will be significantly different. The saturation curve of pressure and temperature for water can be seen in Fig. 8.1, where red circles highlight pressure of 6.9 and 15.5 MPa. As can be seen, as pressure increases, the rate of change of saturation temperature decreases. The density for that of a subcooled inlet condition changes by 100kg/m3, while the subcooled liquid speed of sound changes by more than 250m/s between the two pressures.

In most instances, the stagnation conditions most significantly affect the two-phase choking by altering the point at which vaporization in the channel occurs and at what fluid quality the choking condition is met. The current experimental conditions are considered steady-state, which would be indicative of a steam generator tube leak at normal operating conditions. Due to the significant difference in the thermodynamic operating conditions of a PWR to that of the experiment, a new method is proposed on scaling the choking mass flux. This method is based on matching the potential of the fluid to flash between the prototype and the experiment. This is required due to the limited amount of data available on choking flow rates at high pressure and temperature for crack geometries. The non-dimensional subcooling number is used to describe the relative subcooling between the prototype and the experiment. The subcooling number is given as:

$$N_{sub} = \frac{h_f - h_i}{h_{fg}} \frac{\Delta\rho}{\rho_g} \tag{8.1}$$

where h is the enthalpy of the fluid at stagnation conditions.

This means that a fluid at higher pressures is required to have a larger subcooling than that of the same fluid at lower pressures to have a matching subcooling number. Since little experimental data exists, a modeling approach is adopted using a model which predicts the experimental data well. In this case, the HNEM model is used to predict the mass flux at both pressures for a range of subcooling number. In Figure 8.2 the critical mass flux are shown as function of subcooling for three pressure conditions: at 6.895 corresponding to the present experimental condition, at 11.14 MPa corresponding to typical CANDU reactor SG condition and at 13.79 MPa corresponding to typical PWR SG condition. The difference between the critical mass flux corresponding to pressure 6.895 MPa - 13.79 MPa and 6.89 MPA - 11.14 MPa is then plotted against the same non-dimensional number as seen in Fig. 8.3. A curve fit to this data can then be used to scale the lower pressure model results which fits well to data, to higher pressures such as 11.14 MPa CANDU reactor SG and 13.79 MPa PWR conditions.

In this example, the critical mass flux at PWR condition (13.79 MPa) is approximated by:

$$G_{c,\,13.79MPa} = (-5953.1N_{sub}^{2} + 31660\,N_{sub} + 3149) + G_{c,\,6.895MPa} \tag{8.2}$$

and for CANDRU reactor SG condition is approximated by

$$G_{c,\,11.14MPa} = (-3661.2N_{sub}^{2} + 19471\,N_{sub} + 1936.6) + G_{c,\,6.895MPa} \tag{8.3}$$

It must be noted, that this method should only be used for similar geometries.

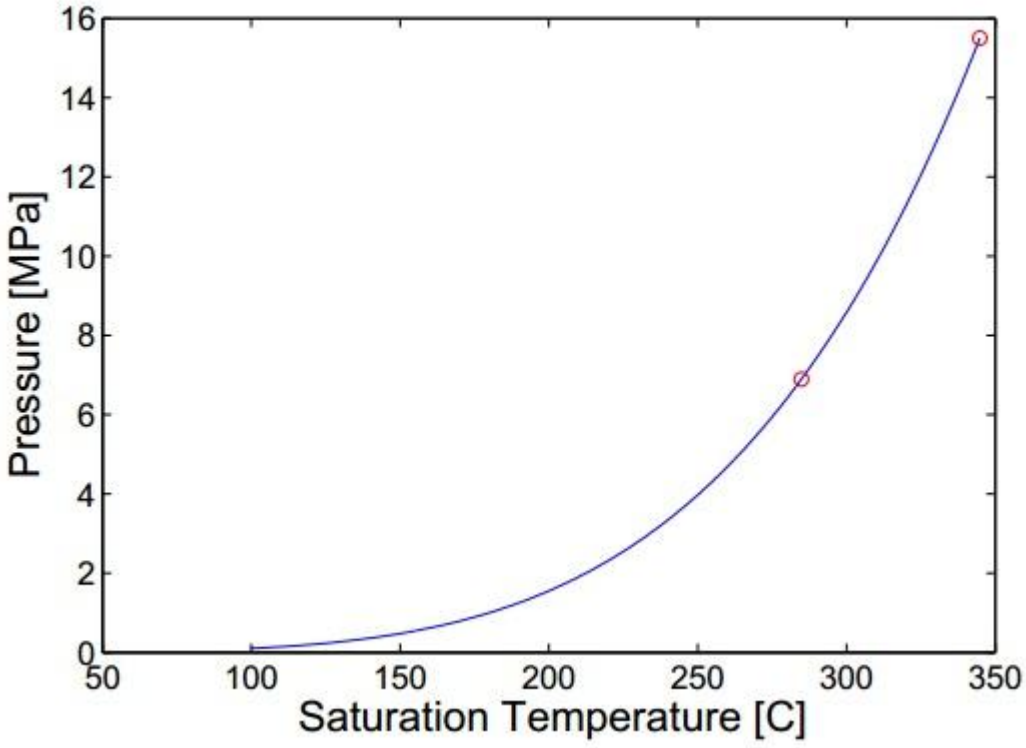

Figure 8.1: Saturation curve of water from 0.1 to 15.5 MPa.

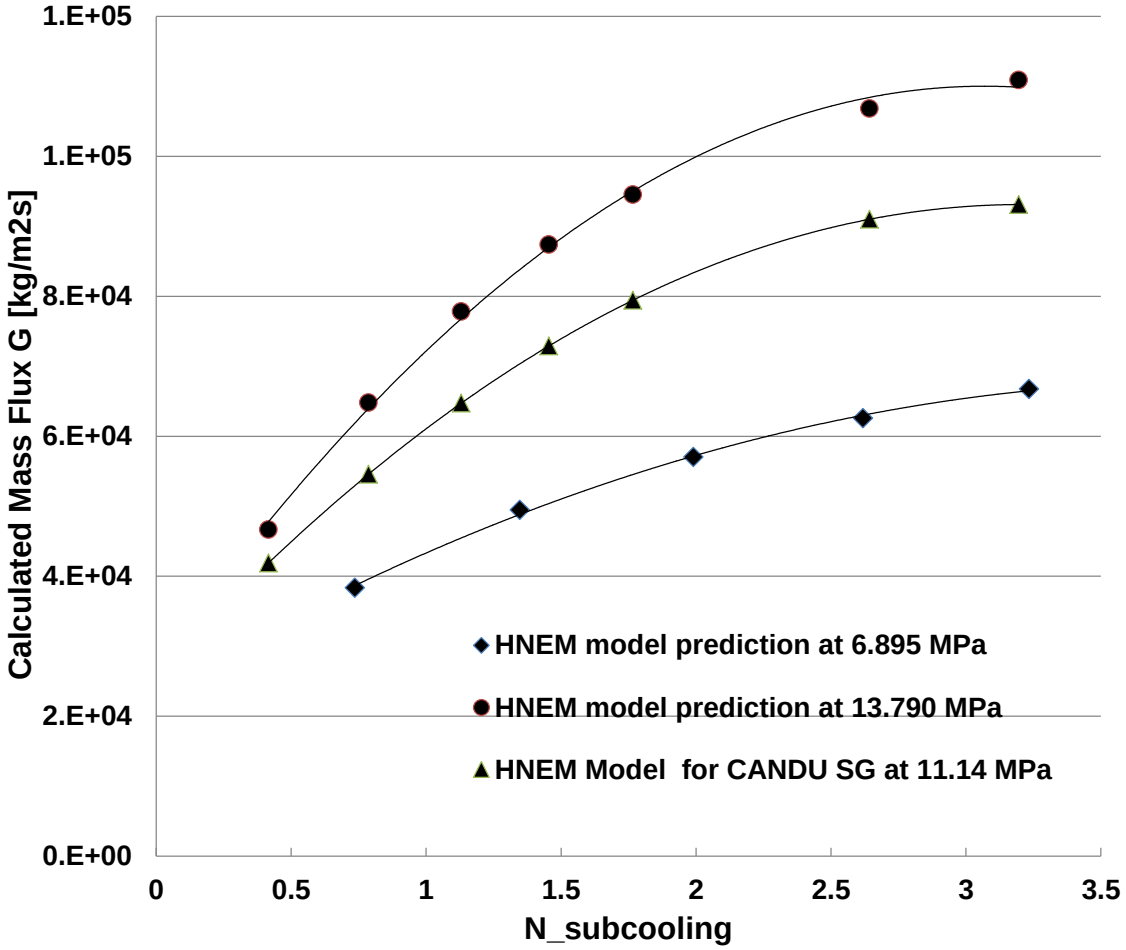

Figure 8.2: HNEM model mass flux predictions versus Non-dimensional subcooling number for pressures of 6.895 MPa (present experiments), 11.14 MPa (CANDU SG) and 13.79 MPa (PWR).

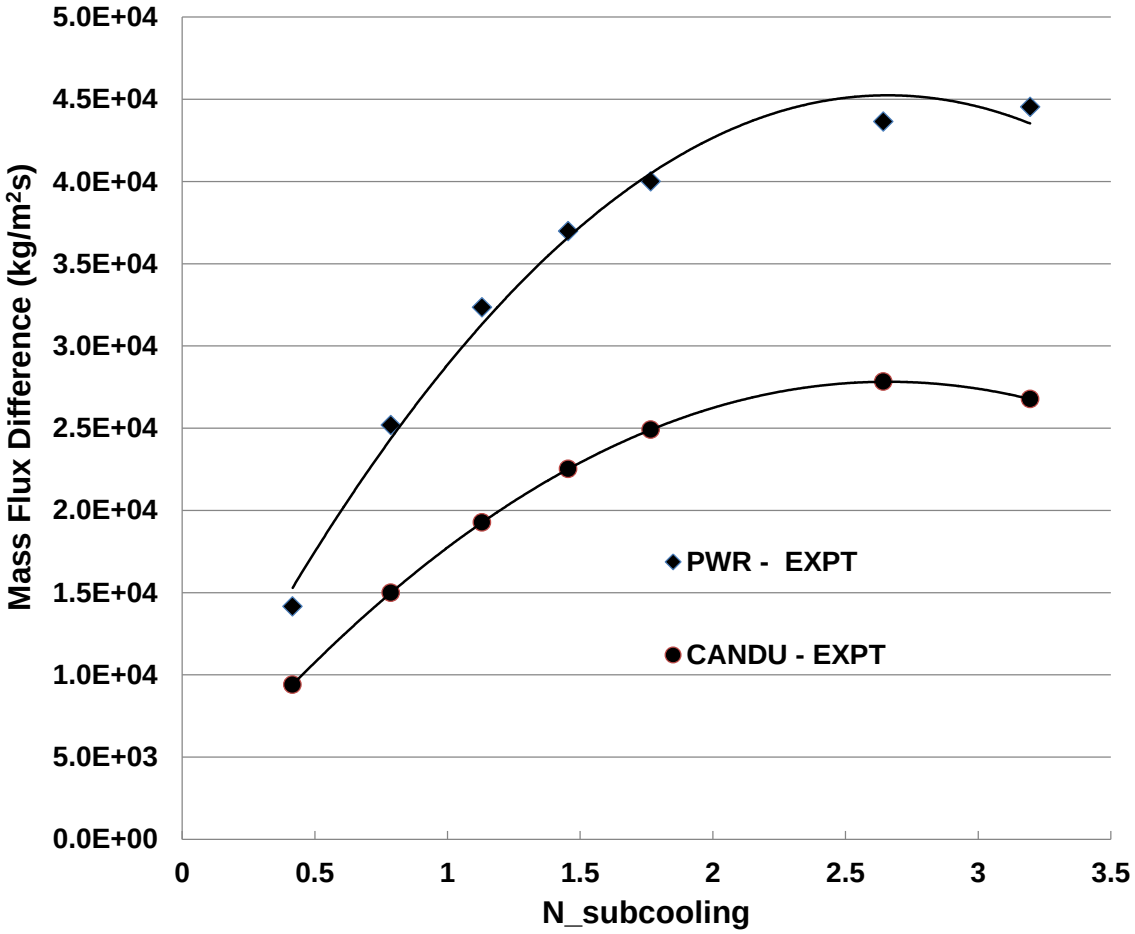

Figure 8.3: Deference between HNEM model mass flux predictions versus Non-dimensional subcooling number for pressures CANDU reactor (CANDU-EXPT) and PWR (PWR-EXPT).

9. CONCLUSIONS

9.1 Summary and Conclusions

9.1.1 Experiment

The experimental program provided new data on choked flow through simulated crack geometries relevant to CANDU steam generator tubes. The data is unique as it fills the needed data gap for low L/D range. In this regards a high pressure, high temperature test facility was built to measure subcooled flashing choked mass flow rates through small channels. The facility is modular and allows for many possible options of crack test specimens. Channels were manufactured to simulate cracks that form in steam generator tubes of operating pressurized water reactors with L/D ranging from 4.48 to 6.94. Data in literature on choked flow for small L/D is sparse. Actual cracked tube cuts that were removed from steam generator tubes in operation would be the ideal specimen to conduct experiments on; however these are difficult to obtain and work with (e.g., due to induced activity). Current research conducted on SG tubes with cracks is destructive and focused on the burst pressure (break) of the alloy tubes rather than the leak before break. Experiments on leak rates were conducted on laser cut simulated cracks with a channel length of 0.003175 m at pressures up to 6.9 MPa and temperatures of 259 ^{o}C. Also, an experiment to measure the dissolved gas present in the choking fluid was designed and conducted. This is atypical of previous work in literature.

Room temperature experiments were conducted at various pressures up to the limit of the test facility. These results show that the discharge coefficient of the simulated cracks are higher than the typical value seen for sharp edged orifice plates. Heated tests were also performed up to 6.9 MPa. The results of those experiments show that as subcooling increases, choking flow rates also increase for similar pressures. Similarly, at constant subcooling, the flow rates increase proportional to the square root of pressure across the channel. A new unique database of choking flow through simulated crack geometries has been created. A durable facility is in place to extend the database in the future.

9.1.2 **Modeling**

Three different approaches were used in modeling choking flow for SG cracks. The three approaches were based on the tools required to meet the needs and requirements of predicting choked flow rates. Developing a unique model and applying it is the most cumbersome approach, however it allows for specific model development to meet the objectives of theoretical ideas. A second approach to modeling choked flow is by use of so called integral models which are more simple and can easily be adapted to experimental data by simple modifications or discharge factors. This approach is used extensively in the valve industry, where data is plentiful. It allows for quick and accurate predictions of the mass flow, however it relies heavily on specific geometries and is highly empirical. The third approach is to use sophisticated tools that are already well established and adapt them to the geometry of choice. This method was investigated using the best estimate thermal hydraulics code RELAP5 in this study. RELAP's choked flow models have been tested extensively against large scale test data, however the limitations of the code as the geometry, especially channel length goes to zero has not been established.

The first approach in this study consisted of developing two one-dimensional models from conservation equations; a homogeneous equilibrium model as well as a homogeneous non-equilibrium model. Both models were used to predict the choking flow rates of data in literature as well as the data from this study. The homogeneous model behaved as expected resulting in gross underprediction of the choking flow data. It was theorized that slip would not be a factor in flows through such short channel lengths and that thermal non-equilibrium would be a dominant factor. The thermal non-equilibrium model developed used a correlation for pressure undershoot to ac-count for the effect of delayed flashing due to required superheat. It was found that while this model can be adjusted to successfully predict choking flow rates, it failed in predicting the two-phase pressure drop when flashing occurs inside the channel. It was determined that the HNEM in this study fairs better with longer channels. Never the less, a useful tool was developed in estimating the choking flow rates of subcooled water through simulated steam generator tube crack geometries within 10%. The failure of the model to provide more accurate predictions most likely is a product of many effects. In fact, it seems as if most choked flow models developed over history have focused on a few physical attributes which are theorized to have the most importance in two-phase choking flow such as slip and thermal non-equilibrium. No model to date is able to successfully predict all choking flow data in a mechanistic manner. Each model may have a number of shortcomings which are not yet recognized.

The next modeling approach consisted of testing numerous simple or integral type models which have been used extensively over the years. None of the models tested were accurate in their prediction of the mass flux data obtained in this study, however the Burnell model seemed to capture the trend of the data. A correlation was then developed to create a modified Burnell model which was able to accurately model the experimental data. This model shows the most accurate results, however it is most likely limited in its application to the content of this study. Unfortunately, to date there is not data in literature that this correlation can be tested against.

The third and final modeling approach consisted of testing the Ransom-Trapp and Henry-Fauske models available in the thermal-hydraulics code RELAP5 to data for short, small L/D geometries. It was again determined that the models work best for long channel

geometries. Also, it was observed that the behavior of the models as coded are extremely different for shortened channels. Apart from this, it is apparent that correctly modeling the entrance loss and frictional pressure drop is of upmost importance. From the data in this study, it was found that the H-F model overpredicts the data, while the R-T model underpredicts the data. It was concluded for crack geometries as modeled in RELAP for this study, neither model appears superior.

9.1.3 **Application of Data to Prototype Conditions**

While the phenomena of choking/critical flow cannot be fully scaled, previous research shows the effects of the change in mass flow rate can if the pressure and temperature of the prototype and model are similar. A method of scaling is pro-posed in this study which accounts for the potential of the fluid to flash using a non-dimensional subcooling number. It allows the possibility for choking mass flux to be scaled with pressure and temperature. This scaling method has not been tested. However, it provides a basis and opportunity for future developments in the area.

9.2 **Recommendations to Future Researchers**

This section has been included in order to provide insight to future researchers working in the area of choking flow, especially in small channels. The first and most important finding during the course of this work is the implications of poorly measured flow areas. Accurate measurement of flow area is important for various reasons. While the area of the specimen is not required to measure the mass flow rate during an experiment using the weigh tank method, the area directly effects the mass flux calculations. Therefore, the error in measured area will produce the same percent magnitude of error in the mass flux predictions.

Furthermore, it can be false leading to compare model results to experimentally obtained data without first addressing the accuracy of that data. While precision of the measurement may be addressed, the accuracy will ultimately determine how effective a model truly is. In this study it was found that to obtain the most accurate measurements of leak rates when comparing to data, three things are of most importance. First, as mentioned above, the area measurement must be accurate. Second, one must minimize error in mass flow rates. This was done in this study by using the weigh tank method. This method directly measures mass, and therefore, knowledge of flow areas, pressures, and more importantly temperatures must not be considered. Thirdly, the presentation of data and model results are highly influenced by the stagnation temperature or subcooling. It was found during the course of this study that any non-heated flow paths can greatly influence the stagnation temperature. While insulation will reduce the amount of heat loss to the environment, any unheated sections between the fluid and the insulation can absorb great amounts of energy, reducing the fluid temperature. It is therefore recommended to ensure that temperature of all flow channels or paths are close to the stagnation temperature desired for any given test.

9.3 **Suggestions for Future Efforts**

In review of the current study, there are many aspects of choking flow specifically related to steam generator tube defects which have not been addressed. It is difficult to obtain physical information about the dynamics of such flows, especially due to the high pressure and temperatures the experiments were conducted at. There are however some hypothetical, but highly possible mechanisms that could affect the choking flow rates. One such possibility is the effect of vena contracta, where fluid passing through a sharp edged orifice contracts and or converges and the flow separates from the edges of the flow channel. This would electively reduce the diameter of the flow area compared to the channel diameter, and hence increase the fluid velocity. There is also the possibility that the low pressure region near the edge of the flow channel will fill with vapor, leaving a liquid jet in the center. Another possible theoretical phenomena that may occur in subcooled choked flow, is a delay in the vaporization beyond the throat exit. As with many transport processes, there is a characteristic time which determines the rate at which the process can occur. If this were to occur, the mass flux exiting the throat may consist of only liquid, while the actual choking plane may exists just downstream of the throat exit where vaporization takes place.

The following work is suggested for further study:

i. Continue development of database on choking flow through small L/D configurations.

ii. Continue efforts on obtaining realistic steam generator tube crack specimens.

iii. Attempt to produce more test specimens that use acid etching to create more realistic longitudinal cracks. Actual SG tube samples made from Alloy 690 have been acquired, and are available for test specimen production.

iv. Perform low pressure two-phase choking experiments on crack geometries with varying channel length to provide a physical bases for the effects of vapor phase on choking in short channels, with small D_h.

v. Develop a new model based on experimental results using physical basis rather than strictly theory on choking flow phenomena.

vi. Perform a more thorough assessment of RELAP5 capabilities on modeling choking flow through SG crack geometries.

vii. Perform repeated tests in order to determine the reproducibility of data with a statistically backed analysis.

REFERENCES

Alamgir, M., & Lienhard, J. (1981). Correlation of pressure undershoot during hot water depressurization. *Transactions of ASME Journal of Heat Transfer, 103*, 52-73.

Amos, C. N., and Schrock, V. E. (1983). *Critical Discharge of Initially Subcooled Water Through Slits.* United States Nuclear Regulatory Commission, Division of Accident Evaluation, Office of Nuclear Regulatory Research & Lawrence Berkeley Laboratory. Washington, D.C. 20555: U.S. Nuclear Regulatory Commission NUREG-CR-3475.

Andresen, P., and Ford, F. (1988). Life prediction by mechanistic modeling and system monitoring of environmental cracking of iron and nickel alloys in aqueous systems. *Materials Science and Engineering: A, 103*(1), 167-184.

Argonne National Labs. (2010). *Steam Generator Tube Integrity Program, Light Water Reactors.* Retrieved January 17, 2013 from site: http://www.ne.anl.gov/capabilities/cmm/highlights/sgt_integrity_program.html.

Beckinsale, S., Mallinson, C., & Moore, H. (1921). The season-cracking of brass and other copper alloys. *J INST MET, 25*, 35-126.

Burnell, J. (1946). The flow of boiling water through nozzles, orifices and pipes. *Journal of Institute of Engineers, 18*, 41-48.

Electric Power Research Institute. (1994). *Steam Generator Progress Report.* EPRI, Palo Alto, CA: Research Project RP3580-06.

Electric Power Research Institute, (2006). *Steam Generator Integrity Assessment Guidelines.* Revision 2, EPRI report 1012987.

Elias, E., & Lellouche, G. (1994). Two-Phase Critical Flow. *International Journal of Multiphase Flow, 20*, 91-168.

Energy Information Administration, U. S. (2011). *US Reactor Operation Status Tables*. Retrieved January 17, 2013, from US Energy Information Administration: http://www.eia.gov/nuclear/reactors/stats_table1.html

Fauske, H. (1962). *Contribution to the theory of two-phase, one-component critical flow.* USDOE, Argonne National Lab. Argonne, Illinois: ANL.

Fauske, H. K. (1985). Flashing Flows or: Some Practical Guidelines for Emergency Releases. *Process Safety Progress, 4*(3), 132-134.

Frisani A. and Hassan, Y.A. and (2009). Analysis of leaks through microchannel cracks using RELAP5 3D. *Nuclear Technology, 167(2)* 304-312.

Galvele, J. R. (1987). A stress corrosion cracking mechanism based on surface mobility. *Corrosion Science, 27*(1), 1-33.

Garland W. J., Wilson R.J., Barkat J., Cizek J., Stasny M., and Zentrich I., (1992). Extension to the approximation functions for the fast calculation of saturated water properties. *Nuclear Engineering Design*, 381-388.

Henry, R. (1970). The two-phase critical discharge of initially saturated or subcooled liquid. *Nuclear Science and Engineering, 41*, 336-342.

Henry, R., & Fauske, H. (1971). The two-phase critical flow of one-component mixtures in nozzles, orifices and short tubes. *Transaction of ASME Journal of Heat Transfer, 93*, 179-187.

IAEA, (2007). *Assessment and Management of Ageing of Major Nuclear Power Plant Components Important to Safety: PWR Pressure Vessels 2007 Update,* International Atomic Energy Agency, Engineering Safety Section. Vienna: IAEA-TECDOC-1556.

IAEA, (2011). Assessment and Management of Ageing of Major Nuclear Power Plant Components Important to safety: Steam Generators, 2011 Update, International

Atomic Energy Agency, Engineering Safety Section. Vienna: IAEA-TECDOC-1668.

Ishimoto A., Uematsu M., Tanishita I., (1972). New Equations for the thermo-dynamic properties of saturated water and steam. *Bulletin of the JSME, 15,* 1278-1289.

Karwoski K.J., Makar G.L. and Yoder M.G. (2007). *U.S. operating experience with thermally-treated alloy 690 steam generator tubes.* Technical Report. NUREG-1841.

Kazimi M., Todreas N. (1990). *Nuclear Systems I; Thermal Hydraulic Fundamentals.* New York: Taylor and Franciis Group.

Kichirka P.J., M. Blaszkiewicz, W.A. Byers, G. Pierini,. (1997). *Oconee unit 2 steam generator tube examination.* EPRI. Electric Power Research Institute report TR-106863.

MacDonald, D. D., & Urquidi-MacDonald, M. (1991). A Coupled environment model for stress corrosion cracking in sensitized type 304 stainless steel in LWR environments. *Corrosion Science, 32*(1), 51-81.

Majumdar, S. (1999). Prediction of structural integrity of steam generator tubes under severe accident conditions. *Nuclear Engineering and Design, 194*(1), 31-55.

McDonald, R. F. (1998). *Introduction to Fluid Mechanics.* New York: John Wiley and Sons Inc.

Moody, F. (1965). Maximum flow rate of a single component two-phase mixture. *Journal of Heat Transfer, 87,* 134-142.

Norring, K., & Engstrom, J. (2008). Initiation of SCC in nickel base alloys in primary PWR environment: studies at Studsvik since mid 1980s. *Energy Materials: Materials Science and Engineering for Energy Systems, 3*(2), 113-118.

NSAD (2003) *RELAP5/MOD3.3 Code Manual Volume I: Code Structure, System Models & Solution Methods.* Nuclear Safety Analysis Division, Information Systems Laboratories, Inc. Office of Nuclear Regulatory Research, U.S. NRC, Division of Systems Research. Rockville, Maryland: .

Pagan, X. D. (2009). Characterization and structural integrity tests of ex-service steam generator tubes at ontario power generation. *Nuclear Engineering and Design, 239*, 477-483.

Rathbun H., (2009). Regulatory Perspective on US Steam Generator Replacement Activities. *IAEA Technical Mtg. on Heavy Component Replacement in Nuclear Power Plants.* Lynchburg, VA.

Ransom V.H. and Trapp J. A., (1980). The RELAP5 Choked Flow Model and Application to a Large Scale Flow Test," Proceedings of the ANS/ASME/NRD International Topical Meeting on Nuclear Reactor Thermal Hydraulics, NUREG/CP-0014, Vol. 2, p.799.

Ransom V.H, Wang W., and Ishii M.. (1998). Use of an ideal scaled model for scaling evaluation. *Nuclear Engineering and Design, 186,* 135-148.

Romig R.P., Rothfus. R., Kermode R.I.,. (1996). Partial vaporization in orifices and valves. *Industrial and Engineering Chemistry Process Design and Development*, 73-78.

Rebak, R. B, Szklarska-Smialowska, Z.. (1996). The mechanism of stress corrosion cracking of Alloy 600 in high temperature water. *Corrosion Science, 38*(6), 971-988.

Rios, R., Magnin, T., Noel, D., & De Bouvier, O. (1995). Critical analysis of alloy 600 stress corrosion cracking mechanisms in primary water. *Metallurgical and Materials Transactions A, 26*(4), 925-939.

Ru X, and Staehle, R. W., (2013). Historical Experience Providing Bases for Predicting corrosion and Stress Corrosion in Emerging Supercritical Water Nuclear Technology: Part 1 - Review. *Corrosion, 69*(3) 211-229.

Schlichting, H. (1979). *Boundary-Layer Theory.* New York: McGraw-Hill.

Schrock, V. (1992). Critical Flashing flow in pipes and cracks. *Dynamics of Two-Phase Flows*, 571.

Schrock, V., Revankar, S., Lee, S., & Wang, C. (1982). *Critical Flow Through Intergranular Stress Corrosion Crack in Pipes.* U.S. Nuclear Regulatory Commisison, Office of Nuclear Regulatory Research. Washington, D.C. 20555: Lawrence Berkeley Laboratory.

Staehle R.W., and Gorman J.A., (2003). Quantitative Assessment of Submodes of Stress Corrosion Cracking on the Secondary side of Steam generator Tubing in Pressurized Water Reactors: Part 1. *Corrosion, 59*(11), 931-994..

Staehle R. W., and Gorman J.A., (2004a) Quantitative Assessment of Submodes of Stress Corrosion Cracking on the Secondary Side of Steam Generator Tubing in Pressurized Water Reactors: Part 2, *Corrosion***,** 60(1), 5-63.

Staehle R. W., and Gorman J.A., (2004b) Quantitative Assessment of Submodes of Stress Corrosion Cracking on the Secondary Side of Steam Generator Tubing in Pressurized Water Reactors: Part 2, *Corrosion***,** 60(2),115-180.

Strang, G. (2007). *Computational Science and Engineering.* Wellesley, MA: Wellesley-Cambridge Press.

Sylveste, D. Z. (1985). A review of explicit friction factor equations. *Transactions of ASME, Journal of Energy Resrouces*, 280-283.

Trapp J.A. and . Ransom V.H., (1982). A Choked-Flow Calculation Criterion for Nonhomogeneous, Nonequilibrium, Two-Phase Flow, *Int. J. Multiphase Flow,* 8 (6) 669-681.

Turnbull, A., McCartney, L. N., & Zhou, S. (2006). A model to predict the evolution of pitting corrosion and the pit-to-crack transition incorporating statistically distributed input parameters. *Corrosion Science, 48*(8), 2084-2105.

Vadlamani, R.A and Revankar S.T. (2013). *An Experimental study of Subcooled choked flow through Steam Generator Tube Cracks.* Purdue University report NU/NE-13-15.

Vaia A.R., Prabhu P.J, and Stevens J.M. (2005). Laboratory examination of pulled mill annealed alloy 600 steam generator tube with free span axial ODSCC, Proceedings of the 12th International Conference on Environmental Degradation of Materials in Nuclear Power System – Water Reactors – *Edited by T.R. Allen, P.J. King, and L. Nelson TMS (The Minerals, Metals & Materials Society).*

Van Rooyen, D. (1975). Review of the stress corrosion cracking of Inconel 600. *Corrosion, 31*(9), 327-337.

Wallis, G. B. (1969). *One-dimensional two-phase flow.* McGraw-Hill.

Wallis, G. B. (1980). Critical Two-Phase Flow. *International Journal of Multiphase Flow, 6*, 97-112.

Wade, C. K. (1995). Steam Generator Degradation and Its Impact on Continued Operation of Pressurized Water Reactors in the United States. *Electric Power Monthly* August.

Was, G. S. (1990). Grain-Boundary Chemistry And Intergranular Fracture In Austenitic Nickel-Base Alloys - A Review. *Corrosion, 46*(4), 319-330.

Wolf, B. J., & Revankar, S. T. (2012). *Subcooled choked flow through steam generator tube cracks.* Purdue University Report, PU/NE-12-09.

APPENDIX A

Calibration of Load Cells

Two strain gauge type load cells are used to measure the weight of the suspended condensing tank. These load cells were calibrated by the manufacturer, and each can measure a load from 0-136.07 kg. An input voltage is required for their operation, which was chosen to be 10.00 V. The load cells output voltage in a mV range. Load cell #1 is calibrated from the manufacturer at 2.310 mV/V, and load cell #2 is 2.181 mV/V. A high precision instrument amplifier was built and used to amplify the output signal to meet the data acquisition system requirements. To ensure the manufacturer's calibration is correct and also to ensure the data acquisition system is operating properly, a simple calibration was done using Purdue's test section.

The calibration was done at room temperature, and all water used in the calibration was allowed to sit in open air until it reached room temperature. A gallon sized container was filled once in increments of 100 mL using a graduated cylinder. This allowed precise measure of the capacity of the container used which is 3.177 L. The condensing tank suspended from the load cells was then filled 3.177 L at a time, and a reading from each load cell was measured after each pour. A total of 66 container fills was used, which totaled to 209.682 L. The data can be seen below in Figure A.1

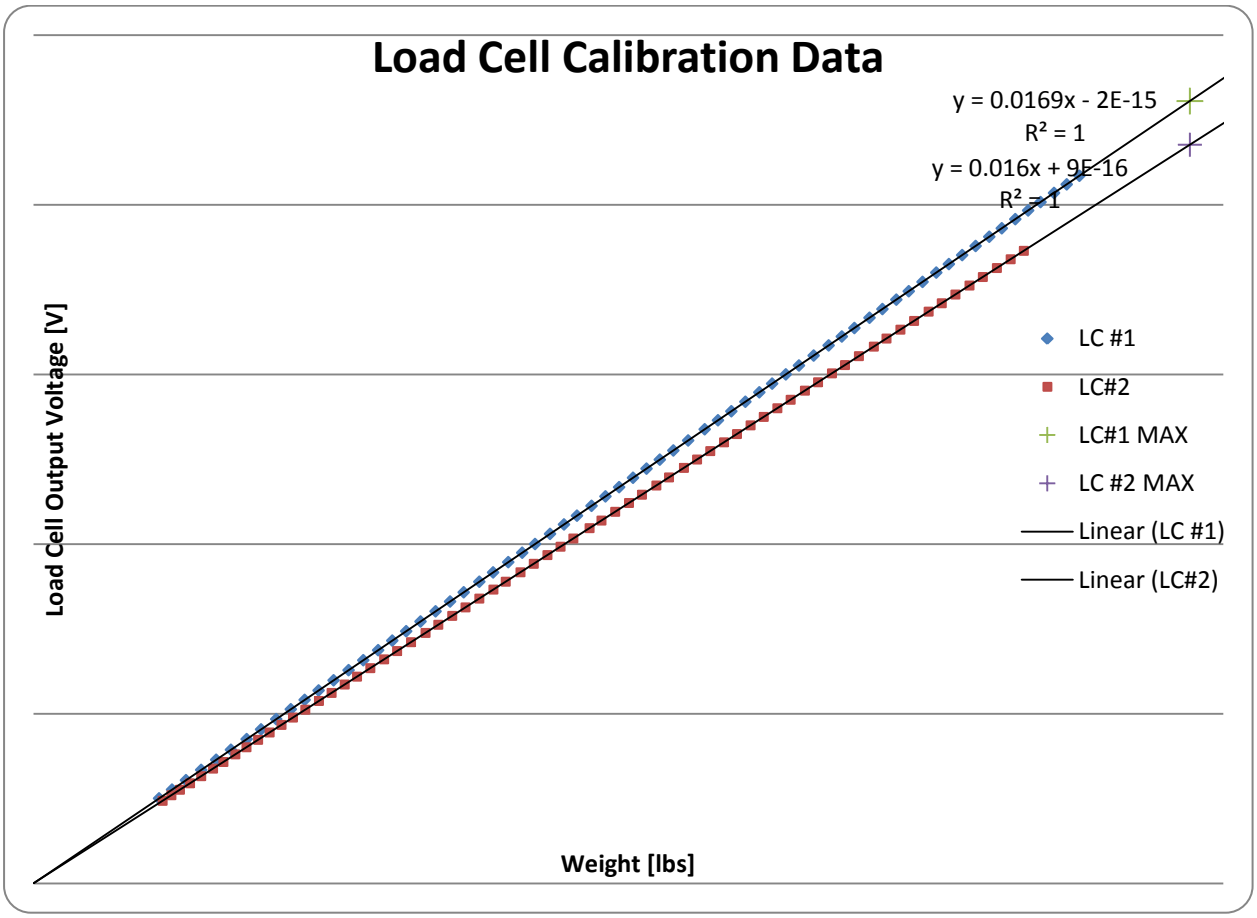

Figure A.1 Load cell calibration

A linear trend line was then fit to the data both producing an R^2 value of 1. As can be seen from the figure, data could not be taken near zero kg, because the weight of the

condensing tank itself is already being measured. Also, when the condensing tank is completely full, the total weight does not reach the maximum capacity of the load cells. However, these two data points are known, one being 0 and the other being 136.07 kg for each load cell, and are plotted separately. As can be seen the original calibrations data's trend line passes perfectly through each of these points. It can be concluded from this that each load cell is working properly to manufacture's specifications and that the data acquisition system is working in a precise manner.